

# MODELING AND CONTROL OF ALGAE HARVESTING, DEWATERING AND DRYING (HDD) SYSTEMS

by

FENGMING LI

Submitted in partial fulfillment of the requirements

For the degree of Doctor of Philosophy

Dissertation Advisor: Dr. Kenneth A. Loparo

Department of Electrical Engineering and Computer Science

Case Western Reserve University

May, 2012

Report Documentation Page				Form Approved OMB No. 0704-0188	
Public reporting burden for the collection of information is estimated to average 1 hour per response, including the time for reviewing instructions, searching existing data sources, gathering and maintaining the data needed, and completing and reviewing the collection of information. Send comments regarding this burden estimate or any other aspect of this collection of information, including suggestions for reducing this burden, to Washington Headquarters Services, Directorate for Information Operations and Reports, 1215 Jefferson Davis Highway, Suite 1204, Arlington VA 22202-4302. Respondents should be aware that notwithstanding any other provision of law, no person shall be subject to a penalty for failing to comply with a collection of information if it does not display a currently valid OMB control number.					
1. REPORT DATE <b>MAY 2012</b>		2. REPORT TYPE		3. DATES COVERED <b>00-00-2012 to 00-00-2012</b>	
4. TITLE AND SUBTITLE <b>Modeling and Control of Algae Harvesting, Dewatering and Drying (HDD) Systems</b>				5a. CONTRACT NUMBER	
				5b. GRANT NUMBER	
				5c. PROGRAM ELEMENT NUMBER	
6. AUTHOR(S)				5d. PROJECT NUMBER	
				5e. TASK NUMBER	
				5f. WORK UNIT NUMBER	
7. PERFORMING ORGANIZATION NAME(S) AND ADDRESS(ES) <b>Case Western Reserve University ,Department of Electrical Engineering and Computer Science,Cleveland,OH,44106</b>				8. PERFORMING ORGANIZATION REPORT NUMBER	
9. SPONSORING/MONITORING AGENCY NAME(S) AND ADDRESS(ES)				10. SPONSOR/MONITOR'S ACRONYM(S)	
				11. SPONSOR/MONITOR'S REPORT NUMBER(S)	
12. DISTRIBUTION/AVAILABILITY STATEMENT <b>Approved for public release; distribution unlimited</b>					
13. SUPPLEMENTARY NOTES					
14. ABSTRACT					
15. SUBJECT TERMS					
16. SECURITY CLASSIFICATION OF:			17. LIMITATION OF ABSTRACT <b>Same as Report (SAR)</b>	18. NUMBER OF PAGES <b>164</b>	19a. NAME OF RESPONSIBLE PERSON
a. REPORT <b>unclassified</b>	b. ABSTRACT <b>unclassified</b>	c. THIS PAGE <b>unclassified</b>			

CASE WESTERN RESERVE UNIVERSITY

SCHOOL OF GRADUATE STUDIES

We hereby approve the thesis/dissertation of

\_\_\_\_\_ Fengming Li \_\_\_\_\_

candidate for the \_\_\_\_\_ Doctor of Philosophy \_\_\_\_\_ degree \*.

(signed) \_\_\_\_\_ Kenneth A. Loparo (EECS) \_\_\_\_\_

(Chair of the Committee)

\_\_\_\_\_ Vira Chankong(EECS) \_\_\_\_\_

\_\_\_\_\_ Marc Buchner(EECS) \_\_\_\_\_

\_\_\_\_\_ Iwan Alexander(EMAE) \_\_\_\_\_

\_\_\_\_\_

\_\_\_\_\_

(Date) 26 March 2012

\* We also certify that written approval has been obtained for any proprietary permission contained therein.

## TABLE OF CONTENTS

TABLE OF CONTENTS.....	I
LIST OF FIGURES .....	V
LISTS OF TABLE.....	XII
ACKNOWLEDGEMENTS.....	XV
ABSTRACT.....	XVII
CHAPTER 1 INTRODUCTION .....	1
1.1 ENERGY CRISIS AND CLIMATE CHANGE .....	1
1.2 ALTERNATIVE ENERGY .....	3
1.3 ALGAE OIL EXTRACTION .....	5
1.3.1 Proposed HDD System.....	6
1.3.2 HDD Process.....	7
1.3.3 Laboratory System Performance .....	9
1.3.4 Objectives.....	14

1.3.5 Contributions.....	15
<b>CHAPTER 2 MATHEMATICAL MODELING OF THE HDD.....</b>	<b>17</b>
2.1 TRANSPORT EQUATION.....	17
2.2 DISCRETIZATION METHOD .....	18
2.2.1 Discretization of diffusive term .....	18
2.2.2 Discretization of the convective terms .....	20
2.2.3 Discretization of transient terms.....	22
2.2.4 Discretized equation of the system .....	24
2.3 MULTIPHASE MODEL.....	27
2.3.1 Mixture Model Theory .....	28
2.3.2 Volume of Fluid Model Theory .....	30
2.4 POROUS MEDIA CONDITIONS .....	32
2.5 MODELING SURFACE TENSION.....	33
2.6 PRESSURE CORRECTION.....	34

2.7 SOLVER FOR DISCRETIZATION EQUATIONS .....	37
2.7.1 Gauss-Siedel method.....	37
<b>CHAPTER 3 WEB TENSION CONTROL SYSTEM DESIGN .....</b>	<b>39</b>
3.1 WEB TRANSPORT SYSTEM .....	39
3.1.1 Wind/Unwind Transport System .....	39
3.1.2 HDD web transport system .....	47
3.2 CONTROL THEORY AND CONTROLLER DESIGN .....	51
3.2.1 Sliding Mode Control.....	52
3.2.2 Sliding Mode Controller.....	55
<b>CHAPTER 4 EXPERIMENTAL METHODS.....</b>	<b>60</b>
4.1 PERMEABILITY TEST .....	60
4.2 FREE FLOW TESTS AND CFD MODELING.....	72
<b>CHAPTER 5 RESULTS AND DISCUSSION .....</b>	<b>85</b>
5.1 CFD SIMULATION AND RESULTS.....	85

5.1.1 <i>Grid testing</i> .....	86
5.1.2 <i>Lookup table</i> .....	88
5.2 WEB TENSION CONTROL SYSTEM SIMULATION RESULTS .....	101
5.3 SIMULATION OF THE HDD SYSTEM .....	131
<b>CHAPTER 6 SUMMARY AND FUTURE WORK .....</b>	<b>136</b>
<b>BIBLIOGRAPHY .....</b>	<b>139</b>

## LIST OF FIGURES

Fig. 1.1 Simplification of the flows between space, the atmosphere, and the Earth's surface [2] .....	3
Fig. 1.2 Closed carbon cycle of algae .....	5
Fig. 1.3 Proposed HDD system schematic.....	9
Fig. 1.4 Dryer stage – Energy consumed when driving starting concentration to 5% water based on latent heat of vaporization.....	13
Fig. 1.5 Micrographs of dry algae filter adherence post AVS HDD (left) and Pressure Filtration (right) Magnification: Top-left 170x; -right 100x; Bottom-left 650x; -right 850x .....	14
Fig. 2.1 Two dimension cell structure .....	21
Fig. 3.1 Web tension control system.....	45
Fig.3.2 Simplified web tension system.....	46
Fig. 3.3 Unwind roll .....	46
Fig. 3.4 HDD web transport system.....	47



Fig. 4.1 Experiment method.....	62
Fig. 4.3 Flow rate v.s Pressure head for 15-9 filter.....	68
Fig. 4.4 Resistance v.s. Pressure head for 15-9 filter.....	68
Fig. 4.5 Observation of thickness changing over pressure head .....	69
Fig. 4.6 Vacuum filtration system setup.....	69
Fig. 4.7 Laser Profilometer .....	70
Fig. 4.8 Thickness of wet algae v.s. moisture content.....	70
Fig. 4.9 Temperature test for 15-9 filter.....	71
Fig. 4.10 Resistance v.s. Temperature for 15-9 filter.....	71
Fig. 4.11 Resistance v.s. Algae weight over deposit area .....	72
Fig. 4.12 Dynamic meshes.....	77
Fig.4.13 Simulated v.s. measured changing heights of free water test (1-2 filter).....	78
Fig. 4.14 Simulated v.s. measured changing heights of free water test (6-5 filter).....	78

Fig. 4.15 Simulated v.s. measured changing heights of free water test (7-2 filter).....	79
Fig. 4.16 Simulated v.s. measured changing heights of free water test 18-13 filter).....	79
Fig. 4.17 Simulated v.s. measured changing heights of free water test (25-20 filter) .....	80
Fig. 4.18 Simulated v.s. measured changing heights of free water test (6-3 filter).....	80
Fig. 4.19 Simulated results and measured data (0.01g/L, 1-2 filter) .....	81
Fig. 4.20 Simulated results and measured data (0.02g/L, 1-2 filter) .....	81
Fig. 4.21 Simulated results and measured data (0.04g/L, 1-2 filter) .....	82
Fig. 4.22 Simulated results and measured data (0.08g/L, 1-2 filter) .....	82
Fig. 4.23 Simulated results and measured data (0.01g/L, 7-2 filter) .....	83
Fig. 4.24 Simulated results and measured data (0.02g/L, 7-2 filter) .....	83
Fig. 4.25 Simulated results and measured data (0.04g/L, 7-2 filter) .....	84
Fig. 4.26 Simulated results and measured data (0.08g/L, 7-2 filter) .....	84

Fig 5.1 Grid test for 1g/L concentration fluid (flow rate).....	87
Fig 5.2 Grid test for 5g/L concentration fluid (flow rate).....	88
Fig 5.3 Grid test for 20g/L concentration fluid (flow rate).....	88
Fig. 5.4 Schematic for algae drying process .....	94
Fig. 5.5 Energy efficiency in different concentrations of input solution ....	101
Fig .5.6 Performance of Sliding mode controller (1 N tension, 1 in/min transporting velocity).....	105
Fig. 5.7 Performance of SMC_S (1 N tension, 1 in/min transporting velocity) .....	106
Fig. 5.8 Performance of SMC_AS (1 N tension, 1 in/min transporting velocity).....	107
Fig. 5.9 Performance of SMC (1 N tension, 10 in/min transporting velocity) .....	108
Fig. 5.10 Performance of SMC_S (1 N tension, 10 in/min transporting velocity).....	109
Fig. 5.11 Performance of SMC_AS (1 N tension, 10 in/min transporting velocity).....	110

Fig. 5.12 Performance of SMC (1 N tension, 20 in/min transporting velocity)	111
Fig. 5.13 Performance of SMC_S (1 N tension, 20 in/min transporting velocity)	112
Fig. 5.14 Performance of SMC_AS (1 N tension, 20 in/min transporting velocity)	113
Fig. 5.15 Performance of SMC (10 N tension, 1 in/min transporting velocity)	114
Fig. 5.16 Performance of SMC_S (10 N tension, 1 in/min transporting velocity)	115
Fig. 5.17 Performance of SMC_AS (10 N tension, 1 in/min transporting velocity)	116
Fig. 5.18 Performance of SMC (10 N tension, 10 in/min transporting velocity)	117
Fig. 5.19 Performance of SMC_S (10 N tension, 10 in/min transporting velocity)	118
Fig. 5.20 Performance of SMC_AS (10 N tension, 10 in/min transporting velocity)	119

Fig. 5.21 Performance of SMC (10 N tension, 20 in/min transporting velocity).....	120
Fig. 5.22 Performance of SMC_S (10 N tension, 20 in/min transporting velocity).....	121
Fig. 5.23 Performance of SMC_AS (10 N tension, 20 in/min transporting velocity).....	122
Fig. 5.24 Performance of SMC (20 N tension, 1 in/min transporting velocity) .....	123
Fig. 5.25 Performance of SMC_S (20 N tension, 1 in/min transporting velocity).....	124
Fig. 5.26 Performance of SMC_AS (20 N tension, 1 in/min transporting velocity).....	125
Fig. 5.27 Performance of SMC (20 N tension, 20 in/min transporting velocity).....	126
Fig. 5.28 Performance of SMC_S (20 N tension, 20 in/min transporting velocity).....	127
Fig. 5.29 Performance of SMC_AS (20 N tension, 20 in/min transporting velocity).....	128

Fig. 5.30 Performance of SMC_S controller with 30 db SNR (20 N tension, 20 in/min rewinding velocity) .....	129
Fig. 5.31 Performance of SMC_AS controller with 30 db SNR (20 N tension, 20 in/min rewinding velocity) .....	130
Fig. 5.32 System control module.....	133
Fig. 5.33 Simulation of HDD system (10 g/L, 10 N, 10 in/min, 15 db SNR)	133
Fig. 5.34 Simulation of HDD system (10 g/L, 10N, 20 in/min, 15 db SNR).	134
Fig. 5.35 Simulation of HDD system (10 g/L, 20N, 10 in/min, 15 db SNR).	134
Fig. 5.36 Simulation of HDD system (20 g/L, 20N, 10 in/min, 15 db SNR).	135

## LISTS OF TABLE

Table 1.1: HDD Laboratory System Performance. Data is presented as average across all runs. ....	13
Table 4.1 <i>Permeability</i> divided by L of each filter .....	73
Table 5.1 Expected draining Gravity flow rate ( $\text{m}^3/\text{s}$ ) .....	92
Table 5.2 Expected draining Capillary flow rate ( $\text{m}^3/\text{s}$ ).....	93
Table 5.3 Expected output algae mass flow rate ( $\text{kg}/\text{s}$ ) .....	93
Table 5.4 Expected water flow rate ( $\text{kg}/\text{s}$ ) in the output of capillary zone ..	94
Table 5.5 Required airflow for heater to dry algae ( $\text{klb}/\text{hr}$ ) .....	95
Table 5.6 Heating energy requirements for heating air ( $\text{kBtu}/\text{hr}$ ) .....	95
Table 5.7 Energy efficiency ( $\text{kBtu}/\text{lb}$ of dried algae) .....	96
Table 5.8 Expected draining Gravity flow rate ( $\text{m}^3/\text{s}$ ) for different web tension (1 g/L input solution) .....	96
Table 5.9 Expected draining Capillary flow rate ( $\text{m}^3/\text{s}$ ) for different web tension (1 g/L input solution) .....	96

Table 5.10 Expected output algae mass flow rate (kg/s) for different web tension (1 g/L input solution) .....	97
Table 5.11 Airflow (klb/hr) requirements for heater to dry algae for different web tension (1 g/L input solution).....	97
Table 5.12 Heating energy requirements for heating air (kBtu/hr) for different web tension (1 g/L input solution).....	97
Table 5.13 Energy efficiency (kBtu/lb of dried algae) for different web tension (1 g/L input solution) .....	97
Table 5.14 Expected draining Gravity flow rate ( $\text{m}^3/\text{s}$ ) for different web tension (10 g/L input solution) .....	98
Table 5.15 Expected draining Capillary flow rate ( $\text{m}^3/\text{s}$ ) for different web tension (10 g/L input solution) .....	98
Table 5.16 Expected output algae mass flow rate (kg/s) for different web tension (10 g/L input solution) .....	98
Table 5.17 Airflow (klb/hr) requirements for heater to dry algae for different web tension (10 g/L input solution).....	98
Table 5.18 Heating energy (kBtu/hr) requirements for heating air for different web tension (10 g/L input solution).....	99



Table 5.19 Energy efficiency (kBtu/lb of dried algae) for different web tension (10 g/L input solution) .....	99
Table 5.20 Expected draining Gravity flow rate ( $\text{m}^3/\text{s}$ ) for different web tension (20 g/L input solution) .....	99
Table 5.21 Expected draining Capillary flow rate ( $\text{m}^3/\text{s}$ ) for different web tension (20 g/L input solution) .....	99
Table 5.22 Expected output algae mass flow rate (kg/s) for different web tension (20 g/L input solution) .....	100
Table 5.23 Airflow (klb/hr) requirements for heater to dry algae for different web tension (20 g/L input solution).....	100
Table 5.24 Heating energy (kBtu/hr) requirements for heating air for different web tension (20 g/L input solution).....	100
Table 5.25 Energy efficiency (kBtu/lb of dried algae) for different web tension (20 g/L input solution) .....	100
Table 5.26 Pre-set parameters of the web tension control system .....	104
Table 5.27 Control Parameters.....	104
Table 5.28 Simulation cases .....	132

## **Acknowledgements**

I would like to express my deepest gratitude to my advisor, Professor Kenneth A. Loparo, for his advice, assistance, and patience throughout my graduate work and research at CWRU. I also want to thank my committee members: Prof. Chankong, Prof. Buchner, and Prof. Alexander, for their time and advice.

I also want to thank to all my colleagues, Yelei, Kevin, Wanchat, and Andy, for providing me insight through our discussion and conversation. I will always cherish the time we studied and had fun together.

I'd like to thank all my friends. I can't have more fun in my graduate career without them. I also want to take this opportunity to thank my parents and my brother. With their support and love, any obstacles I face in my life can be ride through.

Financial support for this work was provided by ARPA-E. DE-AR000037. I am heartily thankful to them.

Finally, I'd like to acknowledge my lovely wife, Yingping. She has provided a lot of support, encouragement, enthusiasm, and inspiration. I also want to thank her to take a very good care of my adorable daughter. Thank you.

# **MODELING AND CONTROL OF ALGAE HARVESTING, DEWATERING AND DRYING (HDD) SYSTEMS**

## **Abstract**

**By**

**FENGMING LI**

Alternative energy is a very important topic since there are some issues with the continued use of fossil fuel as a major source of energy. The alternative energy studied in this research is algae, which has received a lot of attention because it is easy to cultivate, the harvest cycle is only around 10 days, the yield is 5000~10000 gallons per year per acre, the oil extracted can be used directly in a variety of applications, and there is no further investment required in building transportation facilities. The key barrier to making algae oil a commercial success in the fuel market is the cost of production. One of the major costs of extracting oil from algae is the drying process, which is about 30~50 % of the total processing cost. In this research, experiments are conducted and a predictive model that can be used to develop optimal operating strategies for HDD systems, which provide the most efficient

method for dewatering algae. The predictive model is developed using fluid dynamics principles, and the dynamic aspects of the web transportation system. Simulation results show that the predictive model can be effectively used to operate the HDD system in different situations.

# **Chapter 1 Introduction**

## **1.1 Energy Crisis and Climate Change**

A major turning point occurred in the mid-1700s during the industrial revolution. The industrial revolution did not only change the way people live, but also had an effect on the Earth's ecology. Fossil fuels became a major source for power, and it has been widely used since then. There is no doubt that fossil fuels played an important role in industrialization, but they also had some adverse effects on the environment. According to IEA's report [1], around 81.4% of the world's energy was generated from fossil oil in 2007. In other words, fossil fuels dominate the energy supply. With the rising population and increasing demand of energy, fossil fuels will be depleted since it is a finite, nonrenewable, resource.

Another issue created by fossil fuel is the greenhouse effect, where the balance between radiation entering and leaving the earth has been disrupted. Figure 1.1 shows a representation of the exchange of energy between the Sun, the Earth's surface, the Earth's atmosphere, and outer space [2]. Extra

greenhouse gas has been introduced into the system over the years since fossil fuels were used broadly. It leads to an increase of radiation absorbed by greenhouse gas, and the original balance is disturbed. As a matter of fact, according to the report [3] from the Intergovernmental Panel on Climate Change (IPCC), the levels of Carbon Dioxide, Methane, and Nitrous Oxide have risen considerably since the Industrial Revolution. Another report [4] issued by the IPCC demonstrated that the increase of global average temperature, the increase of global average sea level, and the decrease of northern hemisphere snow cover may be related to the greenhouse effect. The report also shows the upward tendency of the global average surface temperature and global average sea level seem to match the upward swing of greenhouse gases. If that is true, it will be difficult to reverse the trend of increasing global average surface temperature and sea level unless we reduce the use fossil fuels. Besides, report provided by IPCC [4] illustrates the impact of the global average temperature change in the period 1980-1999. It shows the impacts are all-round us, and the result will be fatal if we don't respond quickly.

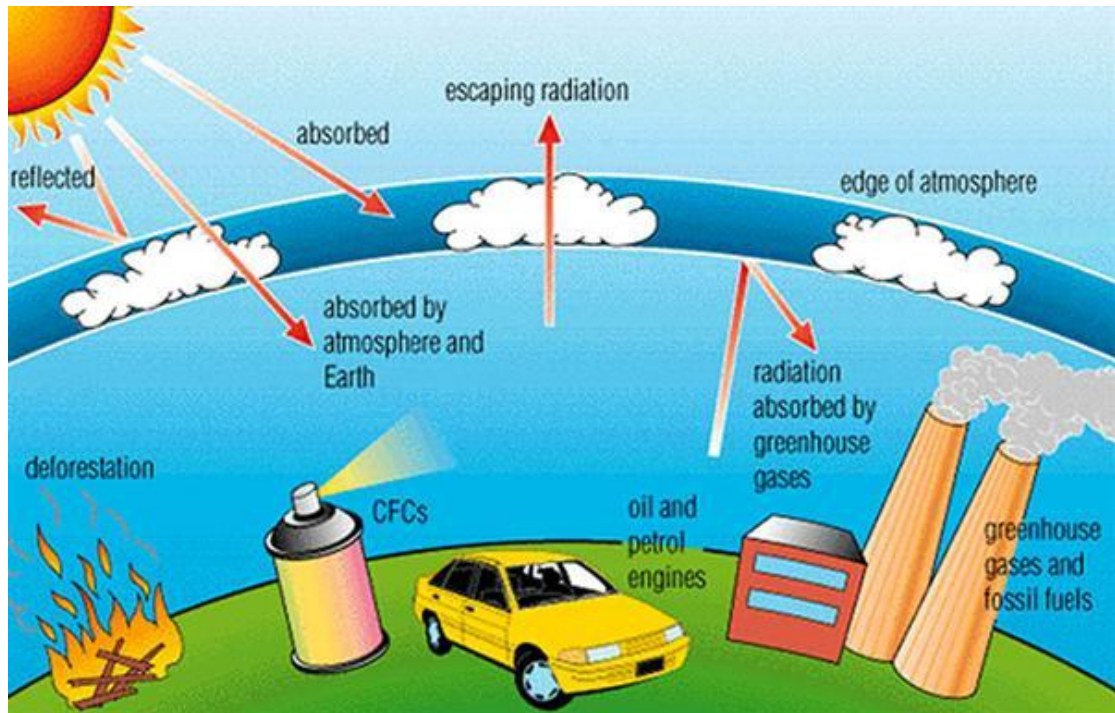


Fig. 1.1 Simplification of the flows between space, the atmosphere, and the Earth's surface [2]

## 1.2 Alternative Energy

Because of the energy crisis, and the fatal side effects of fossil energy, searching for reliable and never-depleting alternative energy is an important and urgent issue nowadays. There are some common types of alternative energy, such as solar, wave, biomass, tidal, and wind power, discussed in the past decades. Among them, bio-fuel is one of the most popular alternative energy resources for the following reasons. First, major modifications are not



necessary to switch to the use of bio-fuel. Second, it can reduce greenhouse gas emissions, and sustain longer than traditional fuel. Third, it is a renewable source. Fourth, bio-fuels are easily available from common biomass sources, environmentally friendly, and biodegradable [5][6].

Among all kind of biomasses, algae is one of the most potential species and it is arising scientific and public attention due to the reason that it is low-input, high-yield, up to 30 times more energy per acre than land crop be produced is claimed based on the experiment, to produce bio-fuels, it allows solar energy to be stored, and it can be used in today's engine and transport infrastructure just like other bio-fuel. Moreover, unlike other renewable energy resources such as wind, tidal, and solar power, algae can be cultivated and harvested systematically. After dewatering, oil in algae can be extracted to produce bio-diesel, and the residue can be used as additives in animal feed or used as feedstock in fast-pyrolysis process to produce bio-oil. Besides, algae are capable of making CO<sub>2</sub> as a carbon source just like other plants. Figure 1.2 shows the process of closed carbon cycle of algae. Besides, they are one of the most photosynthetically efficient plants on the earth, and they use photosynthesis to convert solar energy to chemical energy. The energy is storied in

the form of oils, proteins and the others. The algae oils can be made into biodiesel, and biodiesel is gaining public and scientific attention since it is competitive with traditional petroleum diesel fuel technically [7]. Algae also have some other advantages. They can be cultivated in either marine or fresh waters so that the occupancy of land can be avoided. And as you may know, over 70% of the surface of the earth is water. In other words, algae have plenty of places to grow. Moreover, the harvesting cycle of algae is about 1-10 days. It is way beyond fast to collect bio-oil. In short, algae have a lot of potential to be substitute for fossil fuel. Therefore, algae can be expected to be the major fuel source in the future.

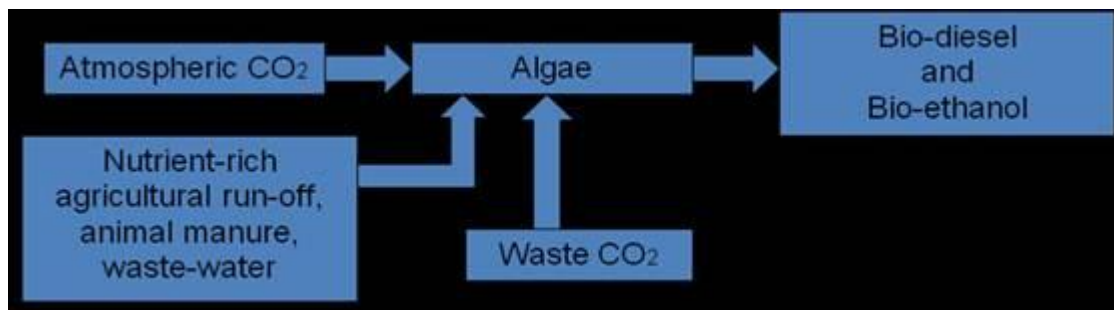


Fig. 1.2 Closed carbon cycle of algae

### 1.3 Algae oil extraction

There are a lot of reasons to develop algae oil technology. However, some technique issues still need to be overcome. One of the issues is that algae oil

extraction is a very costly process. Hence, further research on how to efficiently extract oils from algae is necessary. In this study, a new algae harvesting system will be proposed, with a focus on mathematically modeling and control the system.

### ***1.3.1 Proposed HDD System***

ARPA-E provided funding to a team lead by Univenture / Algaeventure Systems (AVS) to develop an innovative technology for removing the water from suspended algae with dramatically reduced energy consumption by utilizing surface physics and capillary action to more effectively harvest, dewater, and dry algae (HDD). Highly efficient HDD offers the potential to transform the economics of algae-based bio-fuel production, removing the major barrier to large-scale commercialization of this renewable alternative fuel source. A lab-scale prototype system at AVS has demonstrated 95% energy reduction in comparison to conventional centrifuge methods. Based on surface physics of materials, it uses several interacting web surfaces to continually extract algae from very low algae-water concentrations and dry it to less than 5% moisture content.

Harvesting and dewatering algae has long been cited as the major hurdle to making algae a commercially viable feedstock for bio-fuels production. Industry expert John Benemann noted the logistical difficulties associated with algae harvesting and dewatering as early as 1982, and recently (2008) re-asserted that “at present, there are no low-cost harvesting technologies available”. This remains a serious deficiency in commercial systems today. Dewatering processes are important, because as the sludge becomes drier, the lipid extraction process becomes more efficient. Transforming raw solution to a dense sludge sufficient for lipid extraction has historically been a multistage energy inefficient process consuming 30% - 50% of the total cost of algae cultivation.

### ***1.3.2 HDD Process***

The proposed HDD (harvesting, dewatering, and drying) process takes advantage of water surface characteristics, wherein water adhesion and capillary action is used to efficiently separate the sparse algae colonies into a dry cake-like biomass with extremely low moisture content that can be directly processed for oil extraction. The proposed HDD Laboratory System (Figure 1.3)

consists of an input load well that accepts a steady flow of water containing low-to-moderate concentrations (0.3 to 40 g/L) of algae biomass. A thin film of algae is collected on a porous filter web that passes under the input load well. Gravity causes a portion of the water to drain through the porous filter while the filter pore size is small enough to trap algae and transport it to contact the capillary action web traveling in the opposite direction. The parallel moving capillary belt will cause water to wick away from the algae using capillary action where water contacts the hydrophilic surface. This unique capillary action provides excellent water removal without differential pressure that could embed the algae into the filter and lead to filter pore fouling. A final drying stage is typically an evaporative approach, and the lab model consists of an electrically heated plate that is in close contact with the filter membrane to remove residual surface moisture. Water draining from the system may be reused as culture media or used for other downstream processing steps.

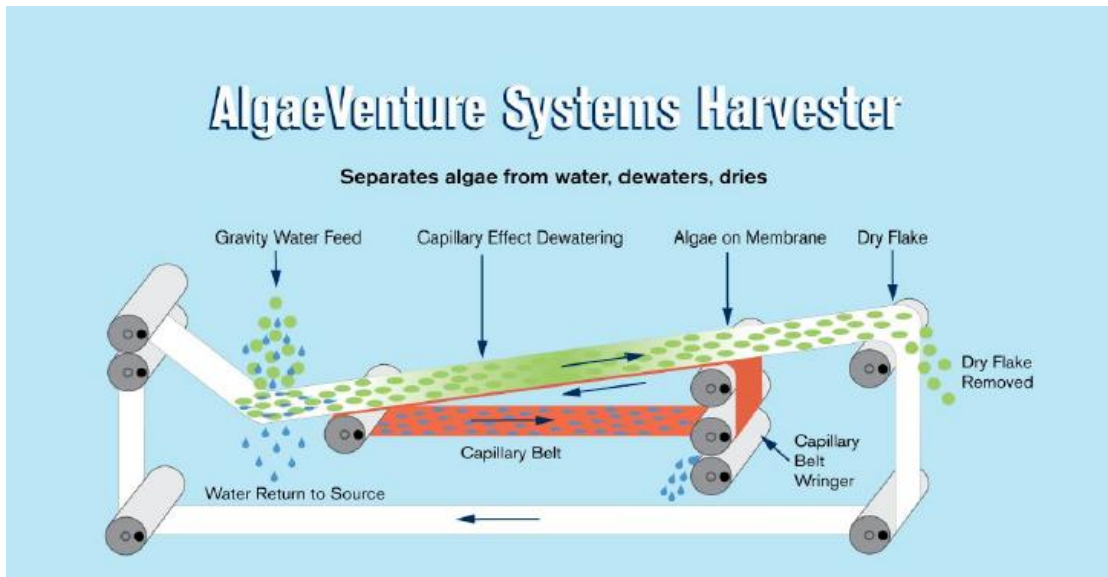


Fig. 1.3 Proposed HDD system schematic

### ***1.3.3 Laboratory System Performance***

Compared with other dewatering systems, the HDD device does not put energy into the system such as to maintain differential pressure, operate a centrifuge or bubble air through the solution for subsequent skimming, or pressure/flow based filtering. The only energy needed is to operate a low-drag transport belt and a final stage heater, providing transformational production cost savings when compared with conventional methods (i.e. centrifuge). System performance has been tested under controlled conditions for a representative set of Algae (Table 1.1).

Process runs were performed over a fixed processing time (10 minutes), belt rate, and heating under the following constraints and limitations:

- System performance requires a thin layer of solids (the filter cake) to be “painted” onto the filter belt to facilitate filtration and subsequent drying.
- Raw effluent throughput is limited to a flow rate that maintains filter cake consistency.
- Suboptimal “Off the Shelf” filters were tested.

Results showed that the energy needed to dewater to 20% solids was 6.7 Whrs in 10 minutes based on motor current, while the energy needed to dewater and dry to <5% moisture was 206 Whrs in 10 minutes based on motor/heater current. Furthermore, the AVS HDD Lab System running at 500 L/hr for a 3 g/L algae concentration used only 40 watts-hrs for dewatering 1498 g algae (dry weight). The resulting energy consumption, 0.0267 Whr/g, is 94.7% less than the best post flocculation centrifugal dewaterer (0.5 Whr/g) while doubling the solids concentration (20% for the proposed HDD vs. 10% for the centrifuge). Beyond the energy cost savings for the dewatering stage of

processing, this methodology also provides the opportunity for improvements in overall process performance:


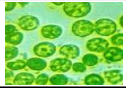

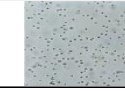

- Less drying (Figure 1.4): The doubling of the algae solids concentration during dewatering reduces the amount of energy needed by the heating stage. Indeed, when optimized, we believe the HDD can achieve 25% solids by weight from the dewatering stage alone. Based on a latent heat of vaporization model and conservatively assuming  $L_{\text{water}} = 800 \text{ kcal/kg}$ , 3.5 Wh/g will be needed by the AVS HDD to drive 75% water (250 g/L algae concentration) down to 5% water (950 g/L algae), while the centrifuge system will need 8.32 Wh/g starting at 80% water (200 g/L algae). This represents a 56% savings in the drying stage! Combining both dewatering and drying, the energy savings is approximately 58% (3.7 Wh/g AVS HDD vs. 8.82 Centrifuge). Because harvesting, dewatering, and drying are estimated to consume 30% to 50% of total algae oil production costs, the proposed HDD may represent a savings of between 17% and 29% of total algae oil production costs. However, these numbers represent theoretical savings.
- Facilitates drying: Thin “painted on” belt algae maximizes the



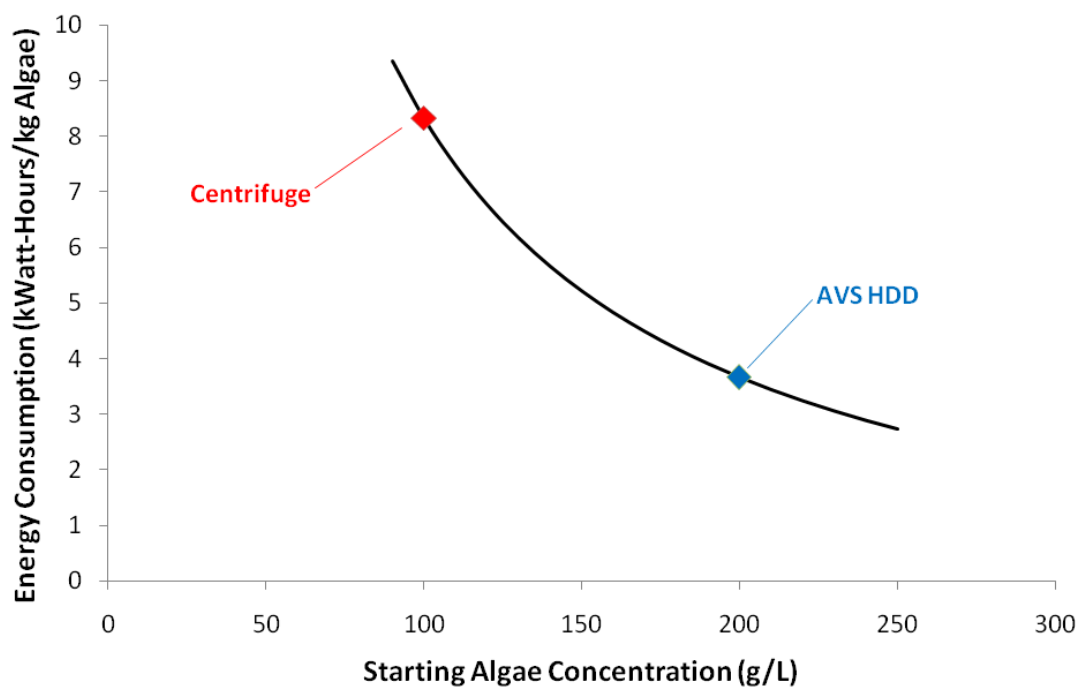
surface area to volume ratio facilitating downstream drying, including the possibility of minimizing/omitting the heating element.

- Minimizes cell analysis: Pressurized belt filtration system analyses algal cells releasing valuable oil, which will escape with the water. A low pressure HDD design would eliminate this issue.
- Increased filter belt life expectancy: Beyond the benefits of minimized fouling, vendor feedback indicates low-pressure design extends belt life due to reduced stretching.

**Table 1.1: AVS HDD Laboratory System Performance. Data is presented as average across all runs.**

Algae	Botryococcus braunii	Chlorella vulgaris	Euglena gracilis	Nannochlorops is salina	Pond Water Marysville, OH
Image					
Size Range (µm)	15-35	2-10	15-40	0.5-2	0.5-40
Density (g/L)	2	2.8	3.1	40.2	1
Algae Energy Content (Watt-hrs/gram Algae)	7.2	5.2	5.6	6.8	4.6
# of Process Runs	2	18	12	39	53
Flow rate (L/hr)	456	342	342	60	510
Escaped Algae (%)*	0.5	8	1	35	3
Residual Water in Dry Flake (%)	1.2	0.5	1.4	0.4	1.0
Dry Solids Yield (g)	152	147	175	261.3	83

Escaped Algae are the percentage of Algae that transferred with the water through the filter.



**Fig. 1.4 Dryer stage – Energy consumed when driving starting concentration to 5% water based on latent heat of vaporization**

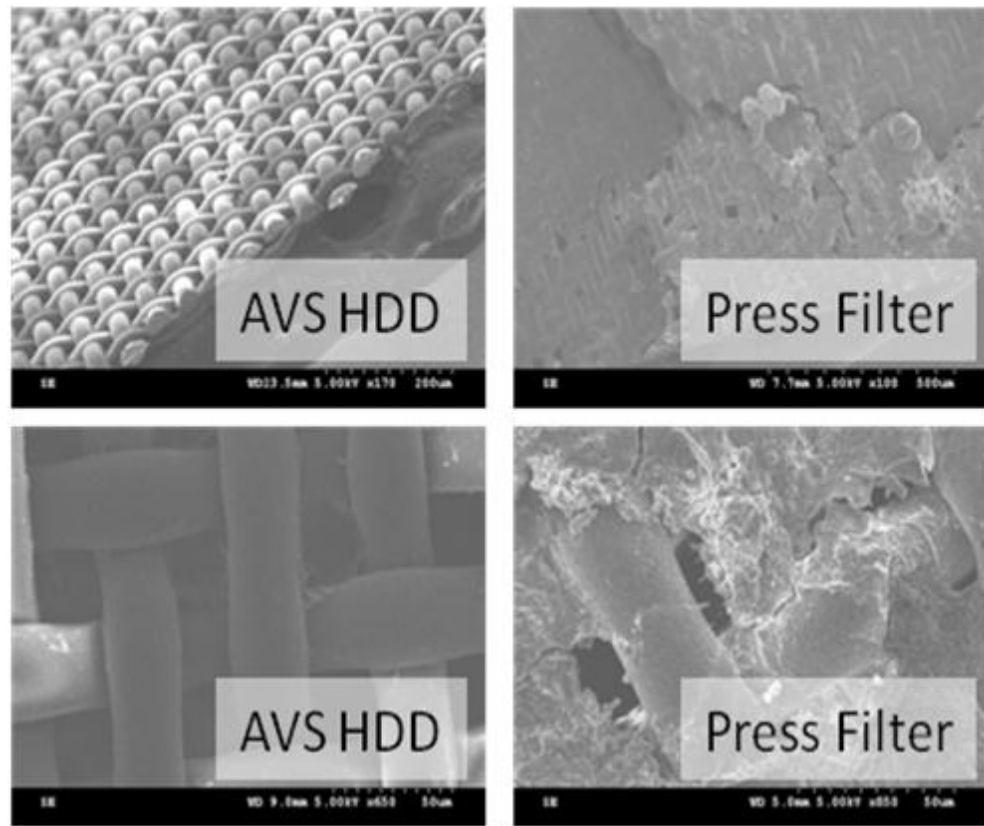


Fig. 1.5 Micrographs of dry algae filter adherence post AVS HDD (left) and Pressure Filtration (right) Magnification: Top-left 170x; -right 100x; Bottom-left 650x; -right 850x

### ***1.3.4 Objectives***

A prototype of the proposed HDD system was constructed. Dynamic models of the HDD process will be developed to capture the fundamental physics that are core to the operation of HDD. Physical models of core phenomenon such as filtering, capillary action, drying, and water cohesion (e.g. surface tension) will be established with suitable fidelity to permit combining

these models into a cohesive integrated functional model. Analytic models will be developed to enhance ease of use and form the foundation for an integrated approach to system and control design.

The laboratory HDD system will be used to develop both a parametric model of equipment operation and a first order analytic model of the drying process. The two models will be combined to predict the moisture content of the dried algae output. The thesis is organized as follows: introduction in chapter 1, mathematical formulation and CFD method in chapter 2, web modeling and tension control in chapter 3, experimental methods in chapter 4, results and discussion in chapter 5, and future work in chapter 6.

### ***1.3.5 Contributions***

In this research, a predictive model that can be used to operate the HDD system is developed. Using the model, operators can predict the fluid dynamics in the system, and decide on the “optimal” operating settings for both the web transport system, and the heater to reduce the overall operating cost. Moreover, the methods used in this research can also be adopted to simulate the scaled-up

system and can be applied to different geometries, filters, and different kinds of algae. Hence, the cost of trial-and-error experiments and the development time for the system can be reduced. Overall, not only does this research have the potential to reduce operating costs save and time but also offers a new approach to the study of HDD systems.

## Chapter 2 Mathematical Modeling of the HDD

According to observation and experimental data, some important physical processes involved in the HDD are studied. The objective of this chapter is to establish the governing equations and create a simulation model for each part of HDD system based on the physical laws.

### 2.1 Transport equation

Generally, the scalar transport equation can be stated as follows:

$$\int_{c.v.} \frac{\partial}{\partial t} (\rho\eta) dV + \oint \rho\eta \vec{v} \cdot \hat{n} dA = \oint \Gamma_{\eta} \nabla\eta \cdot \hat{n} dA + \int_{c.v.} S_{\eta} dV \quad (2-1)$$

Where  $\eta$  is the scalar quality,  $V$  is volume, c.v. is a control volume,  $\rho$  is density,  $\hat{n}$  is the outward point normal vector on the control surface,  $A$  is the surface area, and  $\nabla$  is the gradient operator.  $\rho\eta \vec{v} \cdot \hat{n}$  is the convective vector normal to the surface, and  $\Gamma_{\eta} \nabla\eta \cdot \hat{n}$  is the diffusive vector normal to the surface. The net flux passing though the boundary of control volume can be expressed in the following form:

$$\int_A f dA = \sum_{i=1}^n \int_{A_i} f_i dA \quad (2-2)$$

Where  $f_i$  is diffusive or convective vector normal to  $i$ th face, and  $A_i$  is the surface area of the  $i$ th face.

## 2.2 Discretization method

### 2.2.1 Discretization of diffusive term

For computational convenience, the transport equation is discretized. If the geometry is two dimensional, from equations (2-1) and (2-2), the discretization of the diffusive and source terms can be stated in the following:

$$\oint \Gamma_\eta \nabla \eta \cdot \hat{n} dA + \int_{c.v.} S_\eta dV = \left( \Gamma_\eta A \frac{\partial \eta}{\partial x} \right)_e - \left( \Gamma_\eta A \frac{\partial \eta}{\partial x} \right)_w + \left( \Gamma_\eta A \frac{\partial \eta}{\partial y} \right)_n - \left( \Gamma_\eta A \frac{\partial \eta}{\partial y} \right)_s + \bar{S}_\eta \Delta V \quad (2-3)$$

Where the gradient of  $\eta$  can be approximated using linear profile approximation.

$$\Gamma_{\eta,e} \left( \frac{\partial \eta}{\partial x} \right)_e \approx \Gamma_{\eta,e} \frac{\eta_E - \eta_P}{x_E - x_P}$$

$$\Gamma_{\eta,w} \left( \frac{\partial \eta}{\partial x} \right)_w \approx \Gamma_{\eta,w} \frac{\eta_P - \eta_W}{x_P - x_W}$$

$$\Gamma_{\eta,n} \left( \frac{\partial \eta}{\partial x} \right)_n \approx \Gamma_{\eta,n} \frac{\eta_N - \eta_P}{y_N - y_P}$$

$$\Gamma_{\eta,s} \left( \frac{\partial \eta}{\partial x} \right)_s \approx \Gamma_{\eta,s} \frac{\eta_P - \eta_S}{y_P - y_S}$$

Because the average value of  $S_\eta$  may be a function of the dependent variables, it can be approximated in the following form:

$$\bar{S}_\eta \approx S_{\eta,u} + S_{\eta,p} \eta_P$$

(2-4)

Hence, the discretization of the diffusive and source terms can be formulated in the following:

$$\Gamma_{\eta,e} A_e \frac{\eta_E - \eta_P}{x_E - x_P} - \Gamma_{\eta,w} A_w \frac{\eta_P - \eta_W}{x_P - x_W} + (S_{\eta,u} + S_{\eta,p} \eta_P) \Delta V$$

(2-5)



### 2.2.2 Discretization of the convective terms

From the discussion above, the values of scalar variables are located at the centers of each cell. However, the values on surface are required for the convection term. In this study, face values of scalar variable are function of values at the center of the cells. Here, Quadratic Upwind Interpolation for Convective Kinematics (QUICK) [14] and second-order Upwind [15] schemes are adopted for this study. There are three cell points involved in the scheme. If the control volume is as shown in Figure 2.1, the discretized form can be expressed as follows:

$$\eta_e = \begin{cases} \lambda \left[ \frac{d_E}{d_E + d_P} \eta_P + \frac{d_{Px}}{d_E + d_{Px}} \eta_E \right] + (1 - \lambda) \left[ \frac{d_W + 2d_{Px}}{d_W + d_P} \eta_P - \frac{d_{Px}}{d_E + d_{Px}} \eta_W \right] & \text{if } (\mathbf{v} \cdot \mathbf{n})_e > 0 \\ \lambda \left[ \frac{d_{EE}}{d_{EE} + d_E} \eta_E + \frac{d_E}{d_{EE} + d_E} \eta_{EE} \right] + (1 - \lambda) \left[ \frac{d_{Px} + 2d_E}{d_{Px} + d_E} \eta_E - \frac{d_E}{d_{EE} + d_E} \eta_P \right] & \text{if } (\mathbf{v} \cdot \mathbf{n})_e < 0 \end{cases} \quad (2-6)$$

$\eta_n$

$$= \begin{cases} \lambda \left[ \frac{d_N}{d_N + d_{Py}} \eta_P + \frac{d_{Py}}{d_N + d_{Py}} \eta_N \right] + (1 - \lambda) \left[ \frac{d_S + 2d_{Py}}{d_S + d_{Py}} \eta_P - \frac{d_{Py}}{d_S + d_{Py}} \eta_S \right] & \text{if } (\mathbf{v} \cdot \mathbf{n})_n > 0 \\ \lambda \left[ \frac{d_{NN}}{d_{NN} + d_N} \eta_N + \frac{d_N}{d_{NN} + d_N} \eta_{NN} \right] + (1 - \lambda) \left[ \frac{d_{Py} + 2d_N}{d_{Py} + d_N} \eta_N - \frac{d_N}{d_{Py} + d_N} \eta_P \right] & \text{if } (\mathbf{v} \cdot \mathbf{n})_n < 0 \end{cases} \quad (2-7)$$

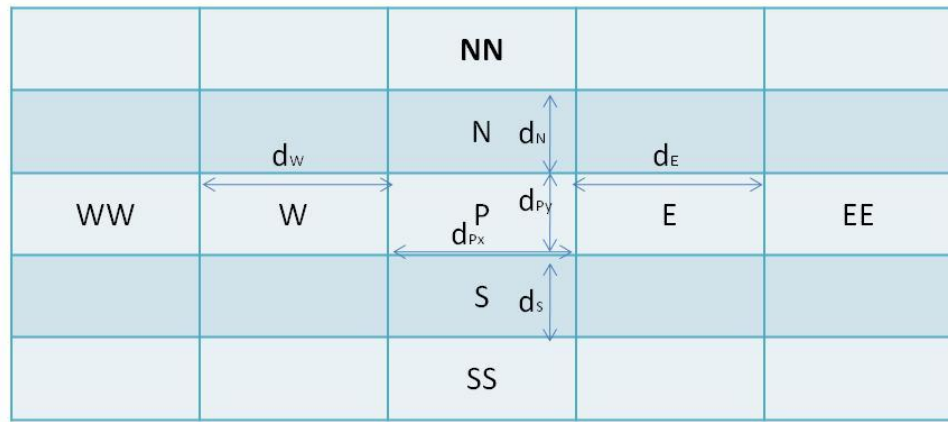


Fig. 2.1 Two dimension cell structure

The value of  $\lambda$  is setting to 6/8 for the QUICK scheme. However, switching between schemes is made possible by changing  $\lambda$ . For example, if  $\lambda$  is 1, equation 5 will be a second-order central interpolation. If  $\lambda$  is 0, a second-order upwind scheme will be developed.

With the approximation of scalar variables on the surface, the convective

terms can be obtained as follows:

$$(\rho v_x \eta A)_e - (\rho v_x \eta A)_w + (\rho v_y \eta A)_n - (\rho v_y \eta A)_s$$

(2-8)

Where  $\eta$  can be expressed by using equations (3-7) and (3-8).

### 2.2.3 Discretization of transient terms

In the transient problem, time is another “dimension” needs to be considered.

However, discretization in the temporal is different than in the spatial dimensions.

The main difference is that the time dependent variables only influence the system in the future. In other words, there is no backward affect in this domain.

From equation (2-1), the integration can be done as follows:

$$\begin{aligned} & \int_t^{t+\Delta t} (\rho v_x \eta A)_e dt - \int_t^{t+\Delta t} (\rho v_x \eta A)_w dt + \int_t^{t+\Delta t} (\rho v_y \eta A)_n dt - \int_t^{t+\Delta t} (\rho v_y \eta A)_s dt = \\ & - \int_t^{t+\Delta t} \frac{d}{dt} (\rho \eta) dt \Delta V + \int_t^{t+\Delta t} \left( \Gamma_\eta A \frac{\partial \eta}{\partial x} \right)_e dt - \int_t^{t+\Delta t} \left( \Gamma_\eta A \frac{\partial \eta}{\partial x} \right)_w dt + \int_t^{t+\Delta t} \left( \Gamma_\eta A \frac{\partial \eta}{\partial x} \right)_n dt - \\ & \int_t^{t+\Delta t} \left( \Gamma_\eta A \frac{\partial \eta}{\partial x} \right)_s dt + \int_t^{t+\Delta t} \bar{S}_\eta \Delta V dt \end{aligned}$$

(2-9)

From the previous discussion, the spatial, diffusive, convective and source terms, have an appropriate discretization, thus the equation above can be simplified into the following form:

$$\int_t^{t+\Delta t} \frac{d\eta}{dt} dt = \int_t^{t+\Delta t} F(\eta(t)) dt$$

Or:

$$\frac{d\eta}{dt} = F(\eta(t))$$

Here, the temporal discretization can be expressed as:

First order: 
$$\frac{\eta_{m+1} - \eta_m}{\Delta t} = F(\eta)$$

Second order: 
$$\frac{3\eta_{m+1} - 4\eta_m + \eta_{m-1}}{2\Delta t} = F(\eta)$$

Where  $\eta_{m-1}$  is the value of the scalar at the previous time step,  $\eta_m$  is the value at current time step, and  $\eta_{m+1}$  is the value at the next time step.

### 2.2.4 Discretized equation of the system

If the scheme is applied to the system of equations, scalar variables at the surface can be expressed in the following form:

$$\eta_{e,m} = \begin{cases} k_1\eta_{E,m} + k_2\eta_{P,m} + k_3\eta_{W,m} & \text{if } (\mathbf{v} \cdot \mathbf{n})_{e,m} > 0 \\ k_4\eta_{EE,m} + k_5\eta_{E,m} + k_6\eta_{P,m} & \text{if } (\mathbf{v} \cdot \mathbf{n})_{e,m} < 0 \end{cases} \quad (2-10)$$

Where

$$\begin{aligned} k_1 &= \frac{\lambda d_P}{d_E + d_P}, \quad k_2 = \frac{\lambda d_E}{d_E + d_P} + (1 - \lambda) \frac{d_W + 2d_P}{d_W + d_P}, \quad k_3 = (\lambda - 1) \frac{d_P}{d_E + d_P} \\ k_4 &= \frac{\lambda d_E}{d_{EE} + d_E}, \quad k_5 = \frac{\lambda d_{EE}}{d_E + d_{EE}} + (1 - \lambda) \frac{d_P + 2d_E}{d_P + d_E}, \quad k_6 = (\lambda - 1) \frac{d_E}{d_{EE} + d_E} \\ \eta_{n,m} &= \begin{cases} k_7\eta_{N,m} + k_8\eta_{P,m} + k_9\eta_{S,m} & \text{if } (\mathbf{v} \cdot \mathbf{n})_{n,m} > 0 \\ k_{10}\eta_{NN,m} + k_{11}\eta_{N,m} + k_{12}\eta_{P,m} & \text{if } (\mathbf{v} \cdot \mathbf{n})_{n,m} < 0 \end{cases} \end{aligned} \quad (2-11)$$

where

$$k_7 = \frac{\lambda d_P}{d_N + d_P}, \quad k_8 = \frac{\lambda d_N}{d_N + d_P} + (1 - \lambda) \frac{d_S + 2d_P}{d_S + d_P}, \quad k_9 = (\lambda - 1) \frac{d_P}{d_N + d_P}$$

$$k_{10} = \frac{\lambda d_N}{d_{NN} + d_N}, \quad k_{11} = \frac{\lambda d_{NN}}{d_N + d_{NN}} + (1 - \lambda) \frac{d_P + 2d_N}{d_P + d_N},$$

$$k_{12} = (\lambda - 1) \frac{d_N}{d_{NN} + d_N}$$

If we combine all discretization equations together into equation (2-1), the following form can be obtained:

$$\begin{aligned} B_{P,m} \eta_{P,m} = & B_{W,m} \eta_{W,m} + B_{E,m} \eta_{E,m} + B_{N,m} \eta_{N,m} + B_{S,m} \eta_{S,m} \\ & + S'_{\eta,u,m} \Delta V \end{aligned}$$

(2-12)

where

$$B_{W,m} = a_w + \max((\rho v_x A)_{w,m}, 0)$$

$$B_{E,m} = a_e + \max(0, -(\rho v_x A)_{e,m})$$

$$B_{S,m} = a_s + \max((\rho v_y A)_{s,m}, 0)$$

$$B_{N,m} = a_n + \max(0, -(\rho v_y A)_{n,m})$$

$$B_{P,m} = a_{w,m} + a_{e,m} + a_{n,m} + a_{s,m} + (\rho v_x A)_{e,m} + (\rho v_y A)_{n,m} - (\rho v_x A)_{w,m} \\ - (\rho v_y A)_{s,m} - S_{\eta,P,m} \Delta V$$

$$a_{e,m} = \frac{\Gamma_{\eta,e,m}}{x_E - x_P}$$

$$a_{w,m} = \frac{\Gamma_{\eta,w,m}}{x_P - x_W}$$

$$a_{n,m} = \frac{\Gamma_{\eta,n,m}}{y_N - y_P}$$

$$a_{s,m} = \frac{\Gamma_{\eta,s,m}}{y_P - y_S}$$

$$S'_{\eta,u,m} \Delta V = (S_{\eta,u,m} + S_{\eta,u,m}^c) \Delta V$$

$$S_{\eta,u,m}^c =$$

$$\left[ (k_1 \eta_{P,m} - (1 - k_2) \eta_{W,m} + k_3 \eta_{WW,m}) \max((\rho v_x \eta A)_{w,m}, 0) + \right. \\ (-k_1 \eta_{E,m} + (1 - k_2) \eta_{P,m} - k_3 \eta_{W,m}) \max((\rho v_x \eta A)_{e,m}, 0) + \\ (-k_4 \eta_{E,m} + (1 - k_5) \eta_{P,m} - k_6 \eta_{W,m}) \max(-(\rho v_x \eta A)_{w,m}, 0) + \\ (k_4 \eta_{EE,m} - (1 - k_5) \eta_{E,m} + k_6 \eta_{P,m}) \max(-(\rho v_x \eta A)_{e,m}, 0) + \\ \left. (k_7 \eta_{P,m} - (1 - k_8) \eta_{S,m} + k_9 \eta_{SS,m}) \max((\rho v_y \eta A)_{s,m}, 0) + \right]$$

$$\begin{aligned}
& (-k_7\eta_{N,m} + (1 - k_8)\eta_{P,m} - k_9\eta_{S,m}) \max\left((\rho v_y \eta A)_{n,m}, 0\right) + \\
& (-k_{10}\eta_{N,m} + (1 - k_{11})\eta_{P,m} - \\
& k_{12}\eta_{S,m}) \max\left(-(\rho v_y \eta A)_{s,m}, 0\right) + (k_{10}\eta_{NN,m} - (1 - \\
& k_{11})\eta_{N,m} + k_{12}\eta_{P,m}) \max\left(-(\rho v_y \eta A)_{n,m}, 0\right) + \eta_{P,m}/\Delta t \Big]
\end{aligned}
\tag{2-13}$$

In general, the discretized equation can be stated in the following:

$$B_{P,m}\eta_{P,m} = \sum_{i=1}^n B_{i,m}\eta_{i,m} + S'_{\eta,u,m}\Delta V$$

(2-14)

In Equation (3-14), n is the number of faces surrounding the calculating volume,  $\eta_i$  is the value of  $\eta$  passing through face i,  $S_\eta$  is the source term.

## 2.3 Multiphase model

Since there are two phases involved in the system, the multiphase modeling is required. In this part, two different modeling methods will be introduced.



### 2.3.1 Mixture Model Theory

**Continuity equation:**

$$\frac{\partial \rho_{ave}}{\partial t} + \nabla \cdot (\rho_{ave} \vec{v}_{ave}) = 0 \quad (2-15)$$

In Equation (3-15),  $\rho_{ave}$  is the average density of the mixture, and  $\vec{v}_{ave}$  is the average mass velocity. The average density and mass velocity of the mixture can be expressed as follows [16]:

$$\rho_{ave} = \sum_{i=1}^n \alpha_i \rho_i \quad (2-16)$$

$$\vec{v}_{ave} = \frac{\sum_{i=1}^n \alpha_i \rho_i \vec{v}_i}{\rho_{ave}} \quad (2-17)$$

Where  $\alpha_i$  is the volume fraction of phase i.

**Momentum equation:**

$$\begin{aligned} \frac{\partial}{\partial t} (\rho_{ave} \vec{v}_{ave}) + \nabla \cdot (\rho_{ave} \vec{v}_{ave} \vec{v}_{ave}) \\ = -\nabla p + \nabla \cdot [\mu_{ave} (\nabla \vec{v}_{ave} + \nabla \vec{v}_{ave}^T)] + \rho_{ave} \vec{g} + \vec{F} \\ - \frac{\mu}{\alpha} \vec{v}_{ave} + \nabla \cdot \left( \sum_{i=1}^n \alpha_i \rho_i \vec{v}_{r,i} \vec{v}_{r,i} \right) \end{aligned}$$

(2-18)

Where  $\vec{\mathbf{F}}$  is the body force,  $\mu_{ave}$  is the average viscosity of the mixture and  $\vec{v}_{r,i}$  is relative velocity between phase I and the average mass velocity.

We can define:

$$\vec{v}_{sp} = \vec{v}_s - \vec{v}_p$$

where  $\vec{v}_s$  is the velocity of the secondary phase, and  $\vec{v}_p$  is the velocity of the primary phase. There is another parameter, mass fraction of any phase i, that needs to be defined:

$$c_i = \frac{\alpha_i \rho_i}{\rho_{ave}}$$

Combined these terms results in the following equation:

$$\vec{v}_{r,i} = \vec{v}_{sp} - \sum_{i=1}^n c_i \vec{v}_{pi} \quad (2-19)$$

### 2.3.2 Volume of Fluid Model Theory

Basically, the Volume of Fluid Model Theory [16] solves the multiphase fluid dynamics by tracking the ration of each fluid in the control volume. If  $\alpha_k$  is the volume fraction of kth phase, following expression can be obtained:

$\alpha_k = 1$ : The cell is full of the kth phase

$\alpha_k = 0$ : The cell is empty of the kth phase

$0 < \alpha_k < 1$ : The cell contains an interface between the kth phase and other phases

The continuity equation of the kth phase can be stated in the following form:

$$\frac{\partial}{\partial t} (\alpha_k \rho_k + \nabla \cdot (\alpha_k \rho_k \vec{v}_k)) = S_{\alpha_k} + \sum_{i=1}^n \dot{m}_{ik} - \dot{m}_{ki} \quad (2-20)$$

where  $\dot{m}_{ik}$  is the mass transfer from phase I to phase k.

Since there is only one momentum equation required in this method, the properties in the transport equations are required to be defined. Generally, the

properties can be calculated in the following form:

$$\delta = \sum_{k=1}^n \alpha_k \delta_k \quad (2-21)$$

where  $\delta$  is the property.

The momentum equation in the Volume of Fluid Model theory is given in equation 2-22:

$$\begin{aligned} & \frac{\partial}{\partial t} (\alpha_a \rho_a \vec{v}_a + \alpha_w \rho_w \vec{v}_w) + \nabla \cdot (\alpha_a \rho_a \vec{v}_a \vec{v}_a + \alpha_w \rho_w \vec{v}_w \vec{v}_w) = \\ & -\nabla p + \nabla \cdot [\alpha_a \mu_a (\nabla \vec{v}_a + \nabla \vec{v}_a^T) + \alpha_w \mu_w (\nabla \vec{v}_w + \nabla \vec{v}_w^T)] + (\alpha_a \rho_a + \\ & \alpha_w \rho_w) \vec{g} + \vec{F} \end{aligned} \quad (2-22)$$

In this research, momentum equation for the algae [17] phase is added:

$$\rho_a V_a \frac{D\vec{v}_a}{Dt} = \rho_a V_a \vec{g} + V_a \nabla p + \vec{F} \quad (2-23)$$

Where [18][19][20]

$$\begin{aligned}\vec{\mathbf{F}} = & -\frac{3}{4}\frac{\alpha_a}{d}\frac{24}{Re_a}(1 + 0.1Re_a^{0.75})\rho_w|\vec{v}_a - \vec{v}_w|(\vec{v}_a - \vec{v}_w) + \frac{1}{2}\rho_a\alpha_a(\vec{v}_a - \vec{v}_w) \\ & \times (\nabla \times \vec{v}_a)\end{aligned}\tag{2-24}$$

Where

$$Re_a = \frac{|\vec{v}_a - \vec{v}_w|}{\mu_w}$$

## 2.4 Porous media conditions

It follows that, more resistance is added when flow through porous media is considered. In this study, a resistance term is added to the momentum equation for the fluid dynamics in porous media. The resistance term can be dealt with as a negative effect source term in the modeling, and it can be expressed in the following form [16]:

$$S_j = -\left(\sum_{i=1}^2 D_{j,i}\mu v_i + \frac{1}{2}\sum_{i=1}^2 C_{j,i}\rho |v|v_i\right)\tag{2-25}$$

where  $S_j$  is the source term for the  $j$ th momentum equation, and  $|v|$  is the magnitude of the velocity. The first term on the right hand side is the viscous loss term, and the second term on the right hand side is the initial loss term. If the porous media is homogenous, the following source term results:

$$S_j = - \left( \frac{\mu}{\alpha} v_j + \frac{1}{2} C' \rho |v| v_i \right)$$

where  $\alpha$  is permeability, and  $C'$  is the initial resistance factor. Hence, the matrices  $D$  and  $C$  can be stated in the following form:

$$D = \begin{bmatrix} \frac{1}{\alpha} & 0 \\ 0 & \frac{1}{\alpha} \end{bmatrix}, \quad C = \begin{bmatrix} C' & 0 \\ 0 & C' \end{bmatrix}$$

## 2.5 Modeling Surface Tension

Although the effect of surface tension effect has been shown empirically by AVS to have the same effect as a 4 cm pressure head in the capillary zone, mathematical modeling is still important to be discussed. Brackbill [21][22] and others have proposed that surface tension can be expressed as a volume force term that is, added it to the momentum equation as source term. The source term

can be stated in the following form:

$$\mathbf{F}_{\text{vol}} = \sum \sigma_{i,j} \frac{\alpha_i \rho_i \kappa_j \nabla \alpha_j + \alpha_j \rho_j \kappa_i \nabla \alpha_i}{0.5(\rho_i + \rho_j)} \quad (2-26)$$

Where  $\sigma_{i,j}$  is the surface tension coefficient, and  $\kappa_i$  is the curvature of the  $i$ th phase, which can be defined in the following:

$$\kappa = \nabla \cdot \frac{\nabla \alpha_i}{|\nabla \alpha_i|} \quad (2-27)$$

## 2.6 Pressure Correction

Generally, the momentum equation can be discretized in the following form (x direction):

$$B_{P,m+1} v_{P,x,m+1} = \sum_{i=1}^n B_{i,m+1} v_{i,x,m+1} + S_{m+1} - \left( \frac{\delta p_{m+1}}{\delta x} \right)$$

Since the non-linear equations of the system are linearized in each time step, the entire iterative process occurs in two different steps. In the outer iterations, the coefficient and source terms are updated, while the linear systems are solved with fixed coefficients in the inner iterations. For each outer iteration, the

equations can be solved in the following form:

$$\mathbf{v}_x^* = \frac{1}{B_p} \left( \sum_{i=1}^n B_i \mathbf{v}_{x,i}^* + S_m - \left( \frac{\delta p_m}{\delta x} \right) \right) \quad (2-28)$$

Where  $\mathbf{v}_x^*$  is a temporary value of  $\mathbf{v}_{x,m+1}$ . Due to the reason that the pressure term applied in equation (2-28) is from the previous iteration, the velocities calculated do not satisfy the continuity equation. Therefore, the velocity is required to be corrected to enforce the continuity equation. A velocity and pressure correction can be defined as:

$$\mathbf{v}_x^{m+1} = \mathbf{v}_x^* + \mathbf{v}'_x$$

$$p^{m+1} = p^m + p'$$

Define

$$\mathbf{v}' = \frac{1}{B_p} \left( \sum_{i=1}^n B_i \mathbf{v}'_i - \frac{\delta p'}{\delta x} \right) \quad (2-29)$$



Since the continuity equation must be satisfied, the following equation

(discrete Poisson equation for the pressure) can be obtained:

$$\left[ \frac{\partial \rho}{\partial t} + \frac{\delta}{\delta x_i} (\rho \mathbf{v}_x^{m+1}) \right]_p = \left[ \frac{\partial \rho}{\partial t} \right]_p + \frac{\delta}{\delta x_i} \left[ \rho \left( \mathbf{v}_x^* + \frac{1}{\mathbf{B}_p} \left( \sum_{i=1}^n \mathbf{B}_i \mathbf{v}'_i - \frac{\delta \mathbf{p}'}{\delta \mathbf{x}} \right) \right) \right]_p = 0$$

The term  $\sum_{i=1}^n \mathbf{B}_i \mathbf{v}'_i$  can be approximated to  $\sum_{i=1}^n \mathbf{B}_i \mathbf{v}'$ , the discrete

Poisson equation for the pressure correction can be stated as follows:

$$\frac{\delta}{\delta x_i} \left[ \frac{\rho}{\mathbf{B}_p + \sum_{i=1}^n \mathbf{B}_i} \left( \frac{\delta \mathbf{p}'}{\delta \mathbf{x}} \right) \right]_p = \left[ \frac{\partial \rho}{\partial t} \right]_p + \frac{\delta}{\delta x_i} [\rho \mathbf{v}_x^*]_p$$

(2-30)

The velocity field is updated when equation 2-30 is solved. This procedure is

known as SIMPLEC [23] algorithm, and the procedure can be states as follows:

1. Velocity field is available at time step m
2. Calculate a temporary value of velocity at time step m+1
3. Solve the Possion equation for the pressure correction

4. Solve the velocity correction equation, and calculate momentum equation
5. If converge, go to next time step. If not, repeat the procedure until both continuity and momentum equations converge

## 2.7 Solver for Discretization equations

### 2.7.1 Gauss-Siedel method

In this study, the solver adopted here is based on the Gauss-Siedel method

[24]. An introduction to this method is provided next:

Assume a square system of linear equations given by:

$$Ax = b$$

Where:

$$A = \begin{bmatrix} a_{11} & a_{12} & \cdots & a_{1n} \\ a_{21} & a_{22} & \cdots & a_{2n} \\ \vdots & \vdots & \ddots & \vdots \\ a_{n1} & a_{n2} & \cdots & a_{nn} \end{bmatrix}, \quad x = \begin{bmatrix} x_1 \\ x_2 \\ \vdots \\ x_n \end{bmatrix}, \quad b = \begin{bmatrix} b_1 \\ b_2 \\ \vdots \\ b_n \end{bmatrix}$$

The matrix  $A$  can be decomposed into the sum of an upper triangular, and lower triangular matrix.

$$A = L + U$$

The system equation can be rewritten as:

$$Lx = b - Ux$$

$x$  can be solved by using Gauss-Siedel method and the value of  $x$  from the previous step. The iterative formulation can be stated as follows:

$$x^{k+1} = L^{-1}(b - Ux^k) \quad (2-29)$$

Once the calculating matrix is formed, the solver can have the solution for every iteration.

## **Chapter 3 Web Tension Control System Design**

Web tension is a key factor to controlling fluid dynamics in the capillary zone. In this chapter, we develop a web tension control system for the HDD system. There are several issues that need to be considered in the design of the HDD system. To begin with, the material chosen for the capillary belt should be able to draw as much water from the algae belt as possible. Second, the tension range for the belt needs to be sufficient to achieve the operating goals of the system; insufficient tension can cause the web sag, wrinkle and rail, and if the tension is too high it can cause deformation or breakage. The tension and the transport velocity combine to define the operating characteristics of the capillary belt and need to be controlled simultaneously in order to achieve good performance.

### **3.1 Web Transport System**

#### ***3.1.1 Wind/Unwind Transport System***

There are two dynamic behaviors in the transport process: lateral and longitudinal. The longitudinal behavior is due to the variation of tension and

transport velocity, while the lateral behavior is due to the variation of lateral displacements in the transport process. From Hook's law, the web deformation is directly related to tension and velocity. In a conventional wind/unwind process, the rotational inertia on the wind and unwind rolls changes with radius [40], and the radius can be calculated by knowledge of the angular velocity. Before setting up the model, there are some assumptions: (1) the web material is an ideal elastic body, (2) there is no slip age between the roller and the web, (3) web tension caused by the unwind roller is negligible, and (4) the torque due to coulomb friction on the unwind roll is negligible.

Figure 3.1 shows the roller-to-roller control system in a conventional wind/unwind process where the web material is transferred from the unwind roller to the rewind roller. According to the mass conservation law:

$$\frac{d}{dt} \int_{CV} \rho dV = - \oint_{AC} \rho v dA \quad (3-1)$$

Temporal change of mass in the control volume given on the left hand side of the equation are equated to the difference between the input and output

mass of the control volume given on the right hand side of the equation.

Therefore, the following nonlinear equation can be obtained:

$$\frac{d}{dt} \left( \frac{L_{jk}(t)}{1+\varepsilon_{jk}(t)} \right) = \frac{v_j(t)}{1+\varepsilon_{jk}(t)} - \frac{v_k(t)}{1+\varepsilon_{jk}(t)} \quad (3-2)$$

where

$$\frac{d}{dt} \left( \frac{L_{jk}(t)}{1+\varepsilon_{jk}(t)} \right) = \frac{1}{1+\varepsilon_{jk}(t)} \frac{dL_{jk}(t)}{dt} - \frac{L_{jk}(t)}{(1+\varepsilon_{jk}(t))^2} \frac{d\varepsilon_{jk}(t)}{dt}$$

And  $\rho$  Density of the web

$v$  Reference velocity of the web

$L_{jk}$  The length of the web between the rollers, where j represents the unwind roller and k represents the rewind roller.

$\varepsilon_{jk}$  The strain of the web between rollers

Substitute equation (3-2) into equation (3-1), we have the following equation:

$$\left( 1 + \varepsilon_{jk}(t) \right) \frac{dL_{jk}(t)}{dt} - L_{jk}(t) \frac{d\varepsilon_{jk}(t)}{dt} = \left( 1 + \varepsilon_{jk}(t) \right) \left( v_j(t) - v_k(t) \right)$$

(3-3)

According to Hook's Law, the relationship between strain of the web and the tension can be described as follows:

$$T = AE\varepsilon$$

Therefore, following equation can be obtained:

$$\left(1 + \frac{T_{jk}(t)}{AE}\right) \frac{dL_{jk}(t)}{dt} - \frac{L_{jk}(t)}{AE} \frac{dT_{jk}(t)}{dt} = \left(1 + \frac{T_{jk}(t)}{AE}\right) (v_j(t) - v_k(t)) \quad (3-4)$$

$$\frac{dT_{jk}(t)}{dt} = \frac{EA}{L_{jk}} (v_k(t) - v_j(t)) + \frac{T_{jk}(t)}{L_{jk}} (v_k(t) - v_j(t)) \quad (3-5)$$

Here, the spring constant  $= \frac{EA}{L_{jk}}$ , and the above equation can be rewritten as follows:

$$\frac{dT_{jk}(t)}{dt} = K(v_k(t) - v_j(t)) + \frac{T_{jk}(t)}{L_{jk}} (v_k(t) - v_j(t)) \quad (3-6)$$

In the wind process, the radius of the rewind roll changes continuously, and the rotational inertia varies with the radius. The dynamics of the unwind radius is:

$$\dot{R}_j(t) = -\frac{hv_j(t)}{2\pi R_j(t)} \quad (3-7)$$

And the dynamics of the rewind radius is:

$$\dot{R}_k(t) = \frac{hv_k(t)}{2\pi R_k(t)} \quad (3-8)$$

Where

$R$  Radius of roller

$h$  The thickness of the web

$v$  The velocity

The rotational inertia of the rolls can be controlled by the motor torque [40][42],

and the state equation can be described as follows:

$$\begin{aligned} \frac{d}{dt} \frac{J_j(t)V_j(t)}{R_j(t)} &= \frac{dH_1(t)}{dt} \\ &= \frac{1}{R_j^2(t)} [-\dot{R}_j(t)J_j(t)v_j(t) + R_j(t)\dot{J}_j(t)v_j(t) + R_j(t)J_j(t)\dot{v}_j(t)] \\ &= -\tau_j - D_j \frac{V_j(t)}{R_j(t)} + T_{jk}(t)R_j(t) = K_j U_j - D_j \frac{V_j(t)}{R_j(t)} + T_{jk}(t)R_j(t) \end{aligned}$$

(3-9)

Where



$\tau_j(N \cdot m)$  Output torque of unwind roll

$K_j(N \cdot \frac{m}{volt})$  Unwind motor torque constant

$D_j(N \cdot m \cdot \frac{sec}{rad})$  Friction coefficient of unwind roll

Since the cylinder is composed of the web and metal, the rotational inertia of the cylinder can be described as follow:

$$J_j = J_{jm} + \frac{\rho h_w \pi (R_j^4(t) - R_m^4)}{2} \quad (3-10)$$

Where  $J_m$  is the inertia of the metal roll,  $R_m$  is the radius of the metal roll, and  $h_w$  is the width of the web. Therefore, the differential equation of the rotational inertia will be:

$$\frac{dJ_j(t)}{dt} = - \frac{4hK_w R_j^2(t)}{2\pi} \quad (3-11)$$

Where  $K_w = \frac{\rho h_w \pi}{2}$ , and the following equation can be obtained:

$$\dot{v}_j(t) = \frac{1}{J_{jm} + K_w [R_j^4(t) - R_{jm}^4]} \left\{ R_j(t) K_j U_j - D_j v_j(t) + T_{jk}(t) R_j^2(t) + \frac{4hK_w R_j^2(t) v_j^2(t)}{2\pi} \right\} - \frac{h v_j^2(t)}{2\pi R_j^2(t)} \quad (3-12)$$

Similarly, the differential equation for the rotational inertia of the rewind roll

can be described as follow:

$$v_k(t) = \frac{1}{J_{km} + K_w[R_k^4(t) - R_{km}^4]} \left\{ R_k(t)K_k U_k - D_k v_k(t) + T_{jk}(t)R_k^2(t) - \frac{4hK_w R_k^2(t)v_k^2(t)}{2\pi} \right\} + \frac{h v_k^2(t)}{2\pi R_k^2(t)} \quad (3-13)$$

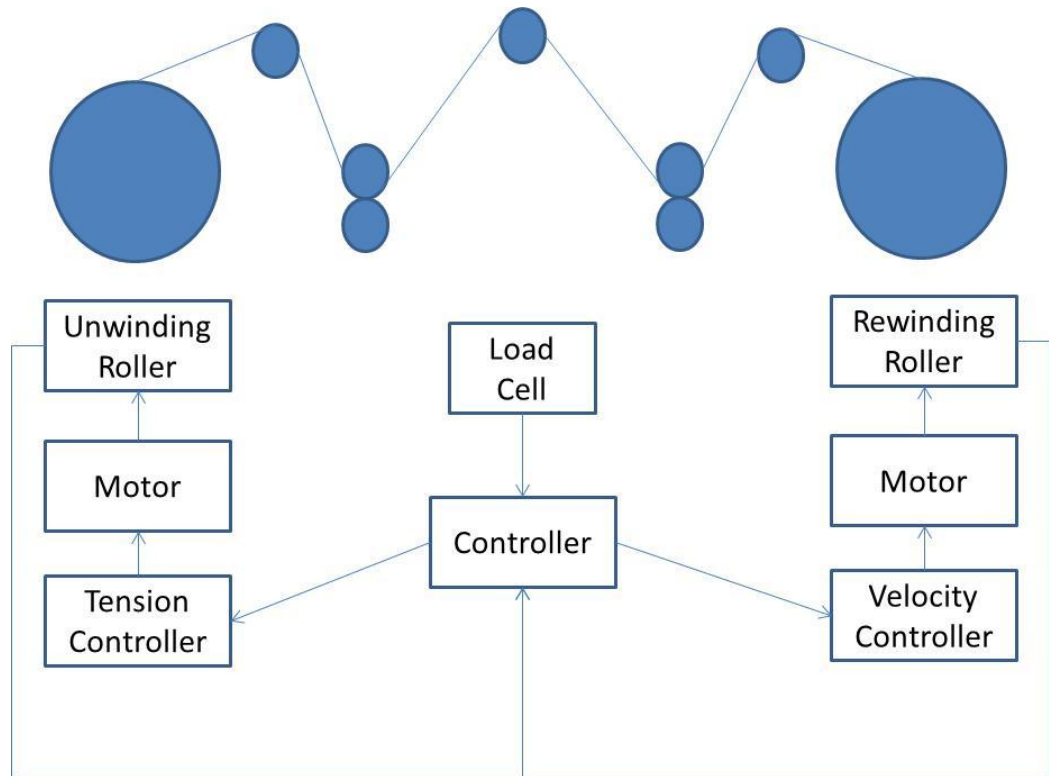


Fig. 3.1 Web tension control system

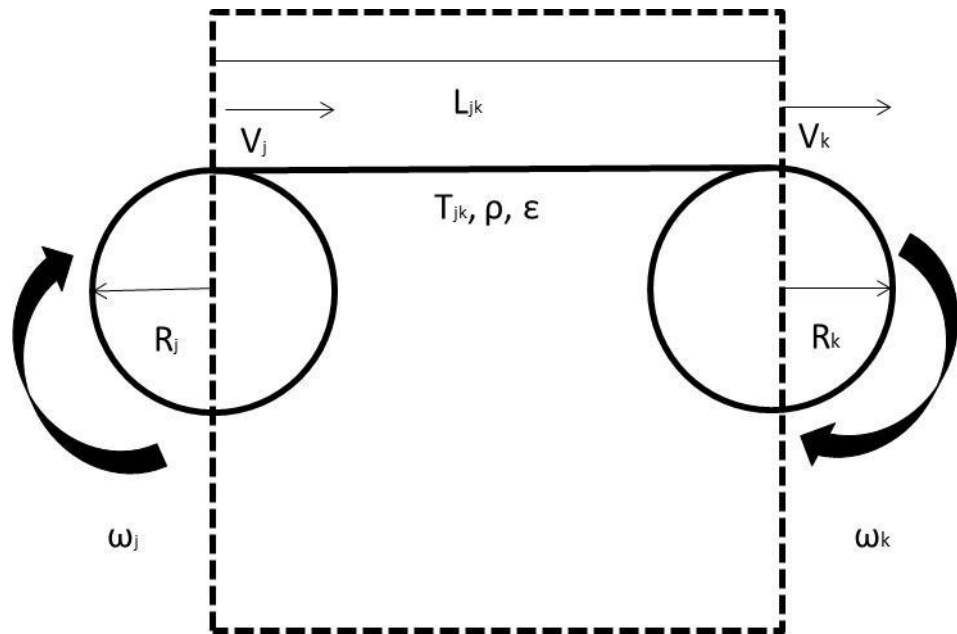


Fig.3.2 Simplified web tension system

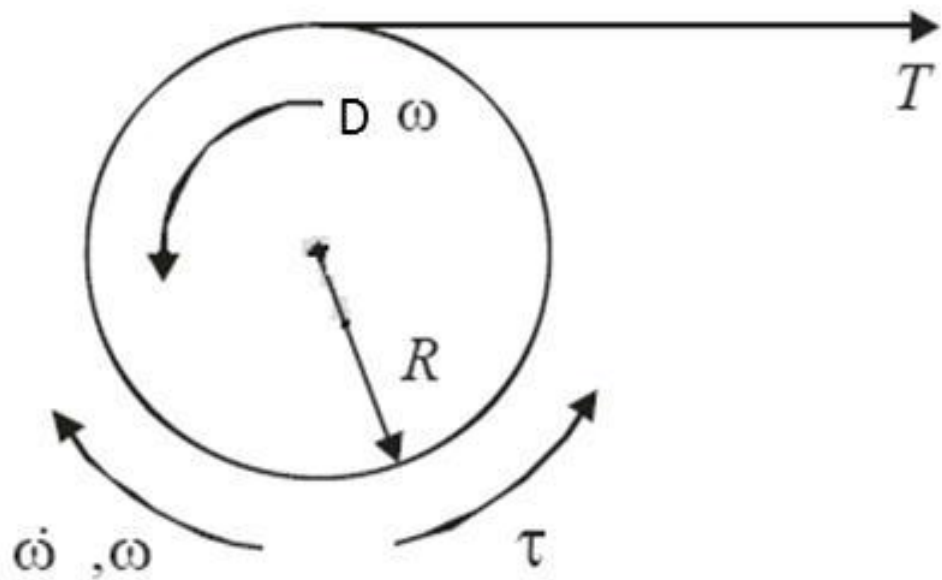


Fig. 3.3 Unwind roll

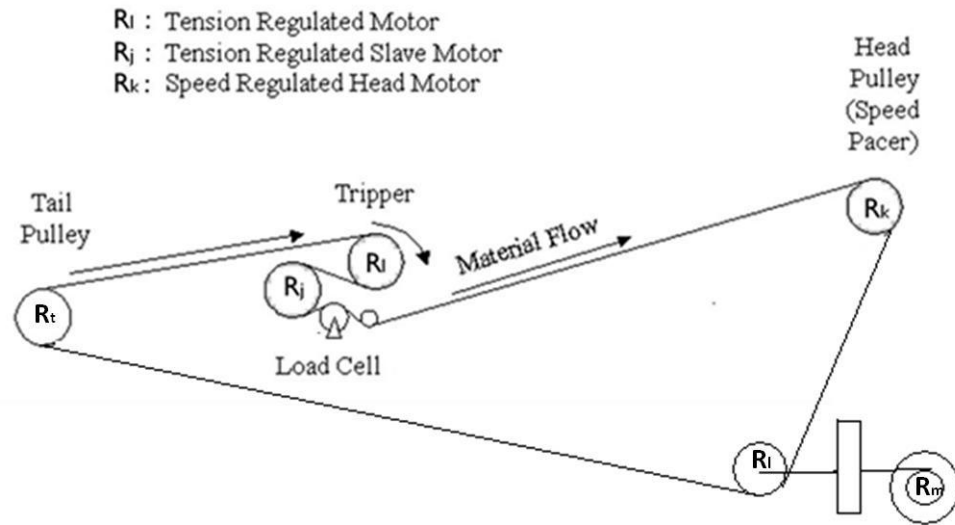


Fig. 3.4 HDD web transport system

### 3.1.2 HDD web transport system

Figure 3.4 shows the HDD web transport system, including four rollers and tension regulators  $R_i$  and  $R_j$  that are used to control web tension;  $R_k$  is a velocity regulator, which is used to control transport velocity;  $R_m$  is the displacement regulator, which is used to maintain the tension between tail and head pulleys. In this system, the radius of rollers can be considered as constant since there is no wind/unwind process involved. The governing equations can be adjusted as follows:

$$\left(1 + \frac{T_{jk}(t)}{AE}\right) \frac{dL_{jk}(t)}{dt} - \frac{L_{jk}(t)}{AE} \frac{dT_{jk}(t)}{dt} = \left(1 + \frac{T_{jk}(t)}{AE}\right) (R_j \omega_j(t) - R_k \omega_k(t))$$

(3-14)

$$\frac{dT_{jk}(t)}{dt} = \frac{EA}{L_{jk}} (R_k \omega_k(t) - R_j \omega_j(t)) + \frac{T_{jk}(t)}{L_{jk}} (R_k \omega_k(t) - R_j \omega_j(t))$$

(3-15)

Here, the spring constant  $= \frac{EA}{L_{jk}}$ , and the above equation can be rewritten as follows:

$$\frac{dT_{jk}(t)}{dt} = K_{jk} (R_k \omega_k(t) - R_j \omega_j(t)) + \frac{T_{jk}(t)}{L_{jk}} (R_k \omega_k(t) - R_j \omega_j(t))$$

(3-16)

Using the same method,

$$\frac{dT_{ij}(t)}{dt} = K_{ij} (R_j \omega_j(t) - R_i \omega_i(t)) + \frac{T_{ij}(t)}{L_{ij}} (R_j \omega_j(t) - R_i \omega_i(t))$$

(3-17)

$$\begin{aligned} \frac{dT_{ki}(t)}{dt} &= K_{ki} (R_i \omega_i(t) - R_k \omega_k(t)) + \frac{T_{ki}(t)}{L_{ki}(t)} (R_i \omega_i(t) - R_k \omega_k(t)) + \\ &\left(K + \frac{T_{ki}(t)}{L_{ki}(t)}\right) \frac{dL_{ki}(t)}{dt} \end{aligned}$$

(3-18)

Since

$$L_{ki}$$

$$= L_{it} + \sqrt{(x_l - x_k)^2 + (y_l(t) - y_k)^2 - (R_l - R_k)^2} + \sqrt{(x_l - x_t)^2 + (y_l(t) - y_t)^2 - (R_l - R_t)^2} \\ + R_l \cos^{-1} \left\{ \frac{(x_l - x_k)^2 + (y_l(t) - y_k)^2 - (R_l - R_k)^2 + (x_l - x_t)^2 + (y_l(t) - y_t)^2 - (R_l - R_t)^2 - c}{2\sqrt{(x_l - x_k)^2 + (y_l(t) - y_k)^2 - (R_l - R_k)^2} \sqrt{(x_l - x_t)^2 + (y_l(t) - y_t)^2 - (R_l - R_t)^2}} \right\}$$

=>

$$\frac{dL_{ki}(t)}{dt} = \frac{y_l(t) - y_k}{\sqrt{a + (y_l(t) - y_k)^2}} \dot{y}_l(t) + \frac{y_l(t) - y_t}{\sqrt{b + (y_l(t) - y_t)^2}} \dot{y}_l(t) \\ - R_l \left\{ 1 - \left( \frac{a + (y_l(t) - y_k)^2 + b + (y_l(t) - y_t)^2 - c}{2\sqrt{a + (y_l(t) - y_k)^2} \sqrt{b + (y_l(t) - y_t)^2}} \right)^2 \right\}^{\frac{1}{2}} \\ \frac{1}{2(a + (y_l(t) - y_k)^2)(b + (y_l(t) - y_t)^2)} \\ \left\{ (4y_l(t) - 2y_k - 2y_t) \sqrt{a + (y_l(t) - y_k)^2} \sqrt{b + (y_l(t) - y_t)^2} \dot{y}_l(t) \right. \\ - (a + (y_l(t) - y_k)^2 + b + (y_l(t) - y_t)^2 \\ - c) \left\{ \frac{(y_l(t) - y_k) \sqrt{b + (y_l(t) - y_t)^2}}{\sqrt{a + (y_l(t) - y_k)^2}} \right. \\ \left. + \frac{(y_l(t) - y_t) \sqrt{a + (y_l(t) - y_k)^2}}{\sqrt{b + (y_l(t) - y_t)^2}} \right\} \dot{y}_l(t) \left. \right\}$$

(3-19)

Where

$$a = (x_l - x_k)^2 - (R_l - R_k)^2$$

$$b = (x_l - x_t)^2 - (R_l - R_t)^2$$

$$c = (x_t - x_k)^2 + (y_t - y_k)^2$$

$$\dot{y}_l(t) = R_m \omega_m(t)$$

The rotational inertia of the rolls can be controlled by the motor torque, and the state equation can be described as follows:

$$\begin{aligned} \frac{d}{dt} J_j \omega_j(t) &= -\tau_j - D_j \omega_j(t) + (T_{jk}(t) - T_{ij}(t)) R_j \\ &= K_j U_j - D_j \omega_j(t) + (T_{jk}(t) - T_{ij}(t)) R_j \end{aligned}$$

(3-20)

$$\begin{aligned} \frac{d}{dt} J_k \omega_k(t) &= -\tau_k - D_k \omega_k(t) + (T_{ki}(t) - T_{jk}(t)) R_k \\ &= K_k U_k - D_k \omega_k(t) + (T_{ki}(t) - T_{jk}(t)) R_k \end{aligned}$$

(3-21)

$$\begin{aligned}
\frac{d}{dt}J_i\omega_i(t) &= -\tau_i - D_i\omega_i(t) + (T_{ij}(t) - T_{ki}(t))R_i \\
&= K_iU_i - D_i\omega_i(t) + (T_{ij}(t) - T_{ki}(t))R_i
\end{aligned}
\tag{3-22}$$

$$\frac{d}{dt}J_m\omega_m(t) = -\tau_m - D_m\omega_m(t) = K_mU_m - D_m\omega_m(t)
\tag{3-23}$$

Where

$\tau(N \cdot m)$	Output torque of roll
$K(N \cdot \frac{m}{volt})$	Motor torque constant
$D(N \cdot m \cdot \frac{sec}{rad})$	Friction coefficient of roll

## 3.2 Control Theory and Controller Design

From the mathematical model obtained in the previous section, we can see that the system is highly nonlinear. In this study, we develop a controller based on



sliding mode control (SMC), which is a well known control method providing a robust controller for nonlinear dynamic systems [43]. However, chattering phenomena caused by discontinuous control will take place while the system is operated near the sliding surface. One of the most common solutions to this problem is to introduce a boundary layer on the sliding surface [44]. The details of the design of the controller are introduced in the following paragraphs.

### ***3.2.1 Sliding Mode Control***

Sliding mode control is a form of variable structure control (VSC). It is a nonlinear control method that changes the dynamics of a nonlinear system by applying a high-frequency switching control function. There are two modes; the approaching mode and the sliding mode. In the approaching mode, the trajectory is directed toward the sliding surface in limited time, while in the sliding mode the trajectory is confined to the sliding surface where it moves and toward the equilibrium point. The surface function ( $S$ ) can be described as follows:

$$S = \dot{e}(t) + \alpha e(t) + \beta \int e \, dt$$

(3-24)

where  $e(t) \in R^1$  is the tracking error.  $\alpha$  and  $\beta$  are constants. Let's assume an n-th order nonlinear system that is linear in the control input (u)

$$\dot{x}(t) = f(x, t) + B(x, t)u$$

where  $x = [x, x', \dots, x^{n-1}]$ , and  $x_d = [x_d, x'_d, \dots, x_d^{n-1}]$  is the desired value.

Hence, the tracking error is:

$$e = x - x_d$$

The sliding surface can be described as:

$$S(e, t) = C_0 \int e(t)dt + e^r(t) + \sum_{n=1}^{r-1} C_n e^n(t) \quad (3-25)$$

where  $C_0, C_1, \dots, C_n$  are positive, p and q are positive odd integers, and n is the relative degree, r is positive integer.

Since the sliding surface is the index of tracking error, it can be the index of tracking performance. Therefore, the control logic can be described as follow:

$$\begin{cases} \dot{S}(e, t) < 0, \text{ when } S(e, t) > 0 \\ \dot{S}(e, t) > 0, \text{ when } S(e, t) < 0 \end{cases}$$

$$\Rightarrow S\dot{S} < 0$$

Since there exists chattering in SMC, the sign function is replaced by saturation function in this study in order to ease the chattering phenomena. Therefore,  $\dot{S}$  can be described as  $\dot{S} = -\mu \text{sat}(S)$ , where  $\mu$  is a control gain, and  $\text{sat}(S)$  is the saturation function.

$$\text{sat}(S, d) = \begin{cases} 1 & S > d \\ f(S, d) & -d \leq S \leq d \\ -1 & S < -d \end{cases}$$

Then using the control logic as define, we can define a candidate Lyapunov function as:

$$Ly(S) = \frac{1}{2}S^2 > 0, \text{ and } \dot{Ly}(S) = S\dot{S} \leq 0$$

Therefore,  $Ly$  is uniformly stable,  $S$  is bounded, and  $S \in L_2$ . Since, each term of  $S$  is bounded, and  $S \in L_2$ ,  $\dot{S}$  is bounded. From Barbalat's lemma, the following conclusion can be reached:

$$\lim_{t \rightarrow \infty} |S| = \lim_{t \rightarrow \infty} |x - x_d| = 0$$

### 3.2.2 Sliding Mode Controller

In this study, the tracking error is defined as follow:

$$e_{T_{jk}}(t) = T_{jk}(t) - T_d$$

The differential of the tracking error of the web tension is:

$$\begin{aligned} \dot{e}_{T_{jk}}(t) = \dot{T}_{jk}(t) = K \left( R_k \omega_k(t) - R_j \omega_j(t) \right) + \frac{T_{jk}(t)}{L_{jk}} \left( R_k \omega_k(t) - \right. \\ \left. R_j \omega_j(t) \right) \end{aligned} \quad (3-26)$$

$$\begin{aligned} \ddot{e}_{T_{jk}}(t) = \ddot{T}_{jk}(t) = \\ \frac{R_k \dot{\omega}_k(t) T_{jk}(t) + R_k \omega_k(t) \dot{T}_{jk}(t) - R_j \dot{\omega}_j(t) T_{jk}(t) - R_j \omega_j(t) \dot{T}_{jk}(t)}{L_{jk}} + K(R_k \dot{\omega}_k(t) - \\ R_j \dot{\omega}_j(t)) \end{aligned} \quad (3-27)$$

Now, we can define the sliding function.

$$S_{T_{jk}}(t) = \dot{e}_{T_{jk}}(t) + \alpha_{T_{jk}} e_{T_{jk}}(t) + \beta_{T_{jk}} \int e_{T_{jk}} dt$$

$$\dot{S}_{T_{jk}}(t) = \ddot{e}_{T_{jk}}(t) + \alpha_{T_{jk}} \dot{e}_{T_{jk}}(t) + \beta_{T_{jk}} e_{T_{jk}}(t) = -\mu_{T_{jk}} \text{sat}(S_{T_{jk}})$$

$$\Rightarrow \dot{S}_{T_{jk}}(t) =$$

$$\frac{R_k \dot{\omega}_k(t) T_{jk}(t) + R_k \omega_k(t) \dot{T}_{jk}(t) - R_j \dot{\omega}_j(t) T_{jk}(t) - R_j \omega_j(t) \dot{T}_{jk}(t)}{L_{jk}}$$

$$+ K(R_k \dot{\omega}_k(t) - R_j \dot{\omega}_j(t)) + \alpha_{T_{jk}} \dot{T}_{jk}(t)$$

$$+ \beta_{T_{jk}} [T_{jk}(t) - T_d]$$

$$= \left( K R_k + \frac{R_k T_{jk}(t)}{L_{jk}} \right) \dot{\omega}_k(t)$$

$$+ \left( \alpha_{T_{jk}} + \frac{R_k \omega_k(t)}{L_{jk}} - \frac{R_j T_{jk}(t)}{L_{jk}} \right) \dot{T}_{jk}(t)$$

$$- \left( K R_j + \frac{R_j T_{jk}(t)}{L_{jk}} \right) \dot{\omega}_j(t) + \beta_{T_{jk}} [T_{jk}(t) - T_d]$$

$$\Rightarrow \dot{S}_{T_{jk}}(t) =$$

$$\frac{\left( K R_k + \frac{R_k T_{jk}(t)}{L_{jk}} \right)}{J_k} \{ K u_k - D_k \omega_k(t) + (T_{ki}(t) - T_{jk}(t)) R_k \} -$$

$$\frac{\left( K R_j + \frac{R_j T_{jk}(t)}{L_{jk}} \right)}{J_j} \{ K u_j - D_j \omega_j(t) + (T_{jk}(t) - T_{ij}(t)) R_j \} + \left( \alpha_{T_{jk}} + \frac{R_k \omega_k(t)}{L_{jk}} - \right.$$

$$\left. \frac{R_j T_{jk}(t)}{L_{jk}} \right) \left[ K (R_k \omega_k(t) - R_j \omega_j(t)) + \frac{T_{jk}(t)}{L_{jk}} (R_k \omega_k(t) - R_j \omega_j(t)) \right] +$$

$$\beta_{T_{jk}} [T_{jk}(t) - T_d] = -\mu_{T_{jk}} \text{sat}(S_{T_{jk}})$$

Hence,  $u_j$  can be chosen as follows:

$$u_j =$$

$$\begin{aligned} & \frac{1}{K_j} \left\{ D_j \omega_j(t) - (T_{jk}(t) - T_{ij}(t)) R_j + \frac{J_j}{\left( K R_j + \frac{R_j T_{jk}(t)}{L_{jk}} \right)} \left\{ \frac{\left( K R_k + \frac{R_k T_{jk}(t)}{L_{jk}} \right)}{J_k} [K_k u_k - \right. \\ & D_k \omega_k(t) + (T_{ki}(t) - T_{jk}(t)) R_k] + \left( \alpha_{T_{jk}} + \frac{R_k \omega_k(t)}{L_{jk}} - \frac{R_j T_{jk}(t)}{L_{jk}} \right) \left[ K (R_k \omega_k(t) - \right. \\ & R_j \omega_j(t)) + \frac{T_{jk}(t)}{L_{jk}} (R_k \omega_k(t) - R_j \omega_j(t)) \Big] + \beta_{T_{jk}} [T_{jk}(t) - T_d] + \\ & \left. \left. \mu_{T_{jk}} \text{sat}(S_{T_{jk}}) \right\} \right\} \end{aligned} \quad (3-28)$$

Similarly,  $u_i$  can be chosen as follows:

$$u_i =$$

$$\begin{aligned}
& \frac{1}{K_i} \left\{ D_i \omega_i(t) - (T_{ij}(t) - T_{ki}(t)) R_i \right. \\
& \quad + \frac{J_i}{KR_i + \frac{R_i T_{ij}(t)}{L_{ij}}} \left\{ \left( KR_k - \frac{R_j T_{ij}(t)}{L_{ij}} \right) \frac{1}{J_k} [K_j u_j - D_j \omega_j(t) \right. \\
& \quad + (T_{jk}(t) - T_{ij}(t)) R_j] \\
& \quad + \left( \alpha_{T_{ij}} + \frac{R_j \omega_j(t)}{L_{ij}} - \frac{R_i T_{ij}(t)}{L_{ij}} \right) \left[ K (R_j \omega_j(t) - R_i \omega_i(t)) \right. \\
& \quad + \frac{T_{ij}(t)}{L_{ij}} (R_j \omega_j(t) - R_i \omega_i(t)) \left. \right] + \beta_{T_{ij}} [T_{ij}(t) - T_d] \\
& \quad \left. \left. + \mu_{T_{ij}} \text{sat}(S_{T_{ij}}) \right\} \right\} \\
& \hspace{25em} (3-29)
\end{aligned}$$

Define the velocity error function

$$e_v(t) = R_k \omega_k(t) - R_k \omega_{kd} \Rightarrow \dot{e}_v(t) = R_k \dot{\omega}_k(t)$$

The sliding function can be defined as follows:

$$S_v(t) = e_v(t) + \beta_v \int e_v(t) dt$$

$$\Rightarrow \dot{S}_v(t) = \dot{e}_v(t) + \beta_v e_v(t) = -\mu_v \text{sat}(S_v)$$

$$\Rightarrow \dot{S}_v(t) = \frac{R_k}{J_k} \{K_k u_k - D_k \omega_k(t) + (T_{ki}(t) - T_{jk}(t)) R_k\} + \beta_v (R_k \omega_k(t) - R_k \omega_{kd}) = -\mu_v \text{sat}(S_v)$$

(3-30)

Hence,  $u_k$  can be chosen as:

$$u_k =$$

$$\frac{1}{K_k} \left\{ D_k \omega_k(t) - (T_{ki}(t) - T_{jk}(t)) R_k - \frac{J_k}{R_k} \left( \beta_v (R_k \omega_k(t) - R_k \omega_{kd}) + \mu_v \text{sat}(S_v) \right) \right\}$$

(3-31)

Since  $u_m$  is adopted to control the displacement of displacement regulator,

and the only concern is that the tension between  $i$ th and  $k$ th roller has to be

bigger than zero, the controller can be chosen as follows:

$$u_m = \frac{D_m \omega_m}{K_m}, \quad \omega_m = \begin{cases} 0.01 & T_{ki} < 0.5N \\ 0 & 0.5N \leq T_{ki} \leq 1N \\ -0.01 & T_{ki} > 1N \end{cases}$$

(3-32)



## **Chapter 4 Experimental Methods**

One of the main objectives of the study is to establish analytical model for the hydraulic system of the HDD process in both the gravity well and capillary zone. This requires some characteristics studied. First of all, it is important to know if the fluid is laminar or turbulent. If the fluid dynamics is laminar, then the general form of Darcy's Law can be adopted in the modeling. If it is not, a turbulent flow model is required. Second, the permeability in the gravity well will change with the volume of fluid, so it is necessary to quantify this characteristic in the model. Third, temperature on the fluid dynamics is a concern. Since the algae are alive during the dewatering process, the temperature may change the fluid dynamics properties of the system. Hence, the temperature effect needs further study. In this study, there are a series of experiments that are done for testing these characteristics. The experimental method and results will be provided in this chapter.

### **4.1 Permeability test**

From previous chapter, the governing equations can be formulated in any

arbitrary geometry. However, some key factors are still unknown in the model. The main purpose of this chapter is to define and quantify them to complete the CFD modeling. Figure 4.1 provides the basic idea of the experiments, with the objective of determining the correct fluid dynamic model to use. In particular, the experiments are designed based on Darcy's Law. As we know, Darcy's Law was formulated based on the result of experiments and derived from the Navier-Stokes equations via homogenization, and it has been used to describe the fluid dynamic of flow through porous media in a wide array of applications. In this experiment, Darcy's Law can be simplified in the following equation if the driving force and the temperature are constants.

$$A \frac{dh}{dt} = \frac{-kA}{\mu} \frac{\Delta P}{L} \quad (4-1)$$

Based on this idea, the permeability of the filters and algae can be estimated by simply measuring the flow rate. In figure 4.1, there are several control modules that regulate the input operating conditions. The basic idea of the experiment is to feed algae solution into a testing tube, and deposit the algae on the filter to reach the desired amount of wet algae. Then, water is fed into the filter/algae at a

desired pressure head, where the pressure head control module controls the solution temperature to be constant. In these series of experiments, temperature, pressure head, and thickness of algae are our main concerns.

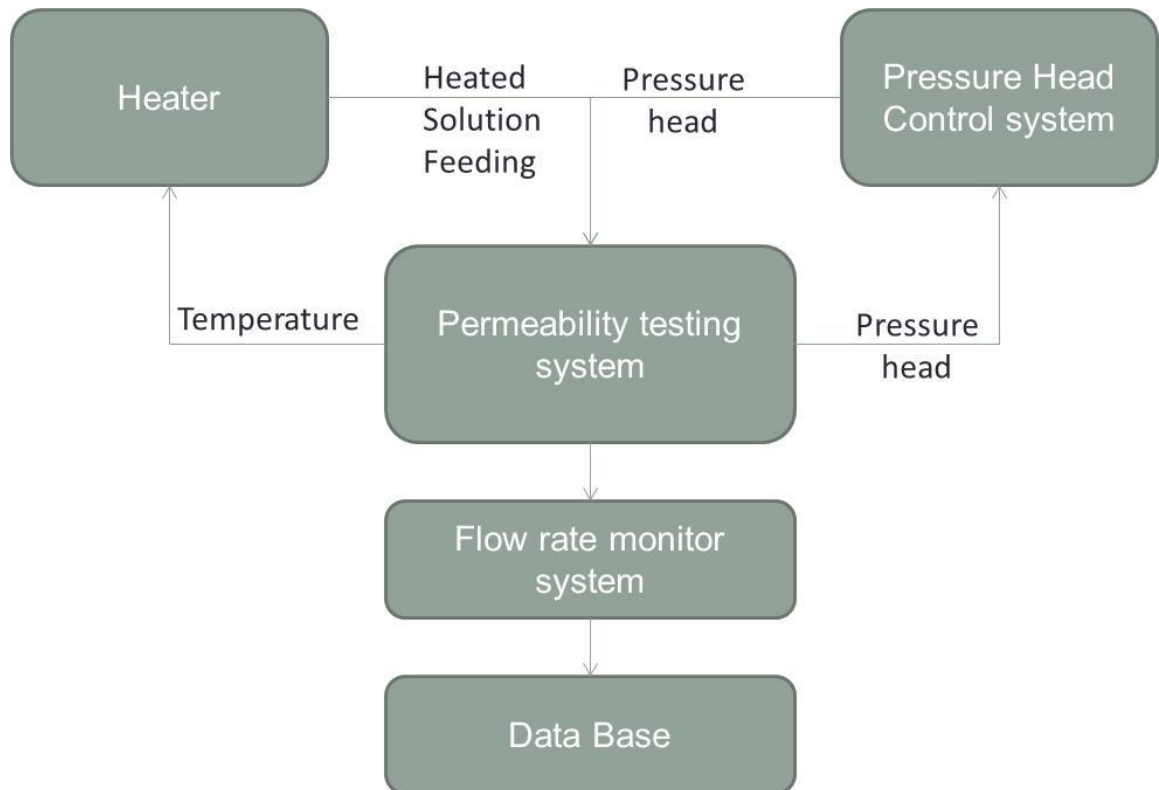


Fig. 4.1 Experiment method

A filter with 15 um pore size and 9% porosity was chosen for the testing. First of all, experiments to determine the permeability of 15-9 filter were conducted. Figure 4.2 shows the measurement of flow rate during the testing process. As you can see, the flow rate is very constant, and the Reynolds number in this case is around

2252. Therefore, the flow is laminar, and Darcy's Law can be applied in the tests.

Figure 4.3 demonstrates the measurement of flow rate for different pressure heads. Figure 4.4 shows the correlation between resistance (pressure head divided by flow rate) and pressure head, and it shows that resistance is not changing. The temperature was controlled at 75°F, and the total amount of algae deposited on the filter is around 0.105 g. Again, the flow rate remains constant for each pressure head, and it is highly linear to the pressure head. Hence, the experiments are consistent with Darcy's Law, pressure drop positively linearly correlated to flow rate.

Since flow rate is related to thickness of the porous media, the measurement of algae thickness is required. Because the thickness of wet algae changes with moisture content, the effect of changes in moisture content on algae thickness must be estimated. In this series of experiments, both the flow in the gravity well and the capillary belt are investigated. To begin with, the gravity well environment was simulated. The idea is to feed the algae solution into the simulated environment, and deposit algae on the filter. Then, water is fed into simulated gravity well, and the thickness of the wet algae is observed. As we know, the algae

solution keeps feeding into the gravity well in AVS system, and given the condition that resistance grows rapidly, the moisture content of the algae deposited on the belt will not change significantly. From experimental observations, the thickness of the algae didn't change with time passing or with changes in pressure head (fig. 4.5). Hence there is no need to explore the thickness module in gravity estimation model any further. In the second part, the phenomenon in the capillary zone is explored. Since the algae belt in capillary zone is oriented with an upward slope, the algae needs to reach a certain moisture content to stay on the belt. According to the experimental data, the moisture content has to be less than 99%, and it has to be in the form of sludge. The procedure is to use a vacuum filtration system to make samples, and use laser profilometer to measure the thickness of the samples. Usually, vacuum filtration is faster than a simple gravity filtration because the vacuum system creates a large driving force between the media. The vacuum filtration system setup is shown in figure 4.6. A laser profilometer (Fig. 4.7) is a non-contact measurement device that can measure surface roughness and film thickness if a ground reference is given. The calculation of roughness is given in the following equation:

$$R_{rms} = \sqrt{\frac{1}{n} \sum_{i=1}^n y_i^2} \quad (4-2)$$

Where  $R_{rms}$  is the surface roughness on the basis of the root mean square deviations, where  $y_i$  is the difference in height between i-th point and mean value. The surface roughness of the algae sample is around 2.79  $\mu\text{m}$  while the thickness of wet algae is around 327  $\mu\text{m}$ . Hence, the assumption that the thickness of the algae sludge is very uniform is valid. Figure 4.8 is the measurement of wet algae thickness for different moisture contents. As the figure shows, the thickness of wet algae in our range of interesting doesn't change too much although it shrinks very fast thereafter. From these experiments we conclude that it is reasonable to assume that thickness of the wet algae is approximately constant in both the gravity and capillary zone. In order to properly include thickness into the model, the resistance part of the model needs to be replaced by another parameter, which should be a function of the depositing area, viscosity, concentration of the algae solution and permeability. Before developing this model, there are some parameters that require further investigation. First of all, temperature is known as a key factor that can influence flow rate through changes in the viscosity of water and perhaps characteristics of the algae. The experimental setup is just like Fig. 4.1.

Figures 4.9 and 4.10 show the results of the temperature tests. The flow rate was monitored at 75, 88, 96, and 106°F, the pressure head is controlled at 13.25 inches of water, and the total amount of algae was controlled at the same level for each test. The results show that the flow rate doesn't change too much across the temperature range. However, we know that the dynamic viscosity of water changes with temperature. The dynamic viscosity at 75°F is around 8.9091E-4 kg/m•s, while it is 6.2232E-4 kg/m•s, which is more than a 20% difference, which means the permeability of algae should be changing with temperature. Either the change in resistance is too small to be determined by our experiments or the algae are somehow be able to adjust to maintain a constant resistance. Permeability tests for different algae amounts were done next. There were 19 samples made for these series of experiments. The weights of the algae were from 0.007 to 0.075 g, and were uniformly deposited on a filter, 11.39 cm<sup>2</sup> pass through area. Figure 4.11 shows the relationship between the total amount of algae and resistance. It looks as if they are linearly correlated across the testing range. As we know, resistance should be a function of viscosity, permeability, and thickness of the porous media. In this series of experiments, since the temperature was maintained at 75°F, and,

theoretically, permeability of porous media is constant, the resistance is only the function of thickness of porous media. From the results shown in fig. 4.11, the resistance is linearly related to the total amount of algae deposited on pass through area. This is consistent with Darcy's Law, and we conclude that the permeability of the wet algae is constant throughout the testing range.

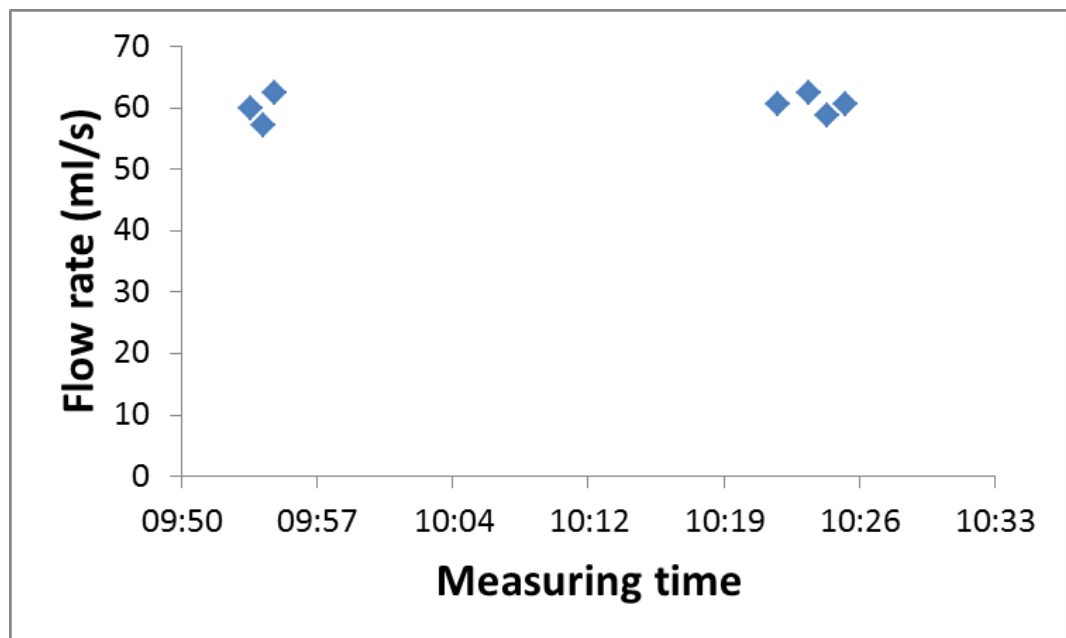


Fig. 4.2 Permeability test for 15-9 filter



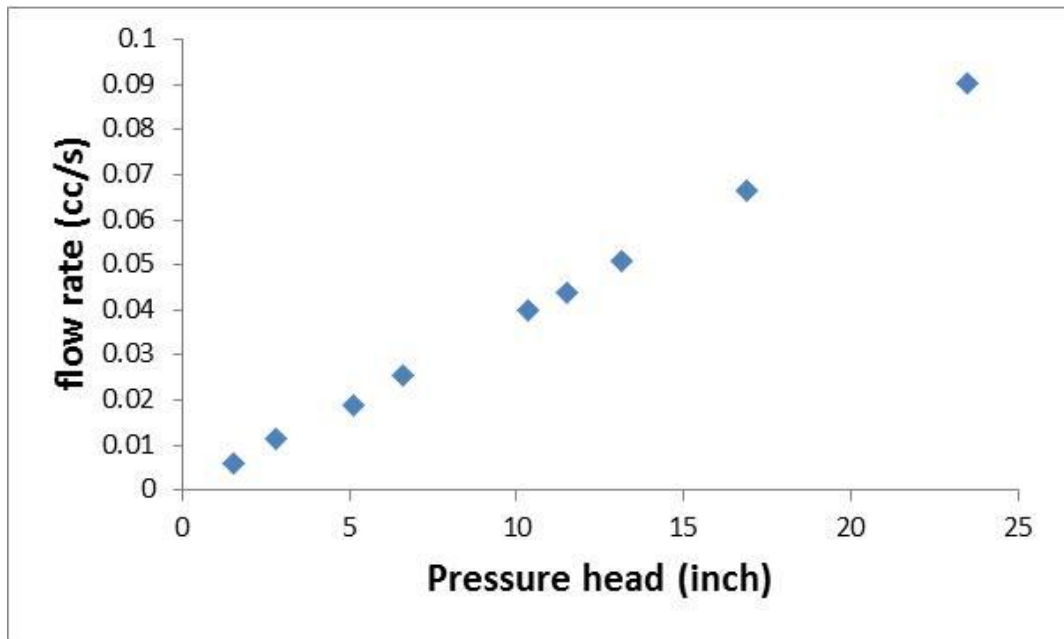


Fig. 4.3 Flow rate v.s Pressure head for 15-9 filter

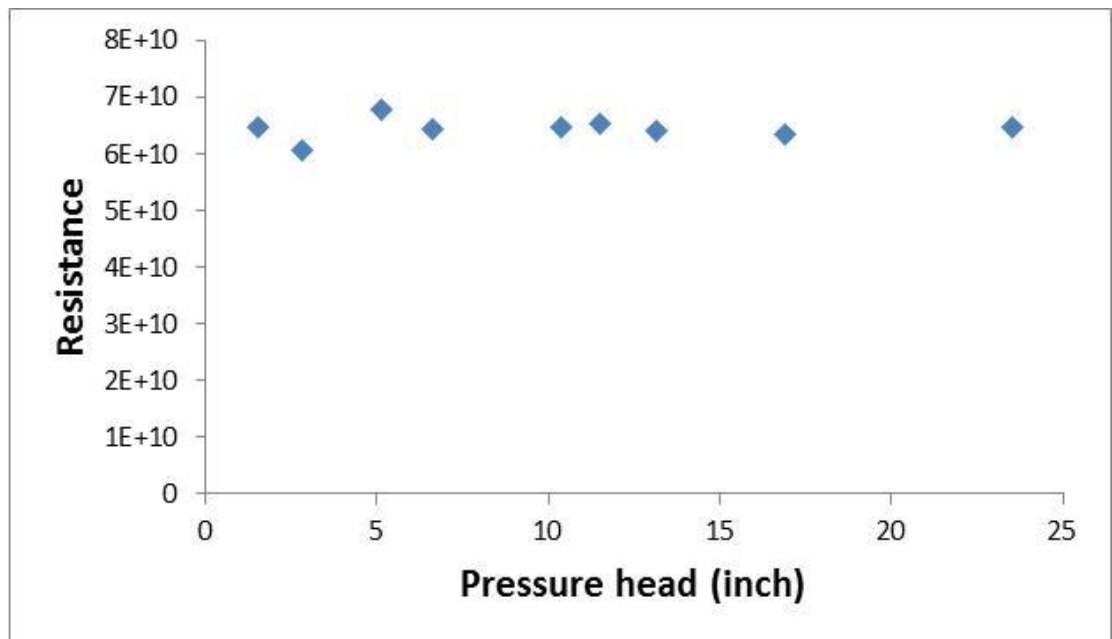


Fig. 4.4 Resistance v.s. Pressure head for 15-9 filter

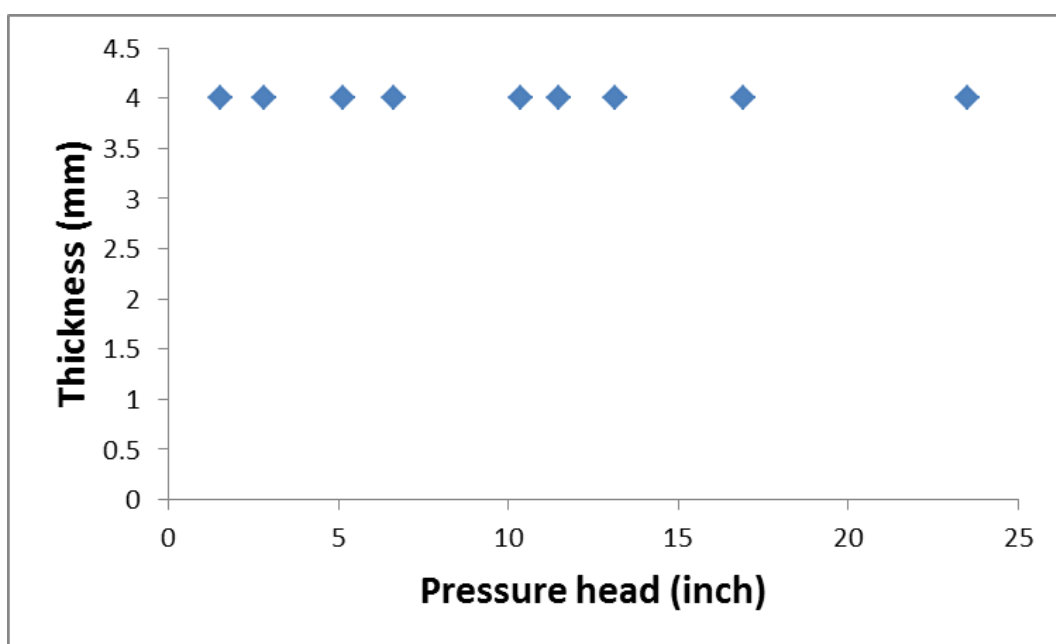


Fig. 4.5 Observation of thickness changing over pressure head



Fig. 4.6 Vacuum filtration system setup



Fig. 4.7 Laser Profilometer

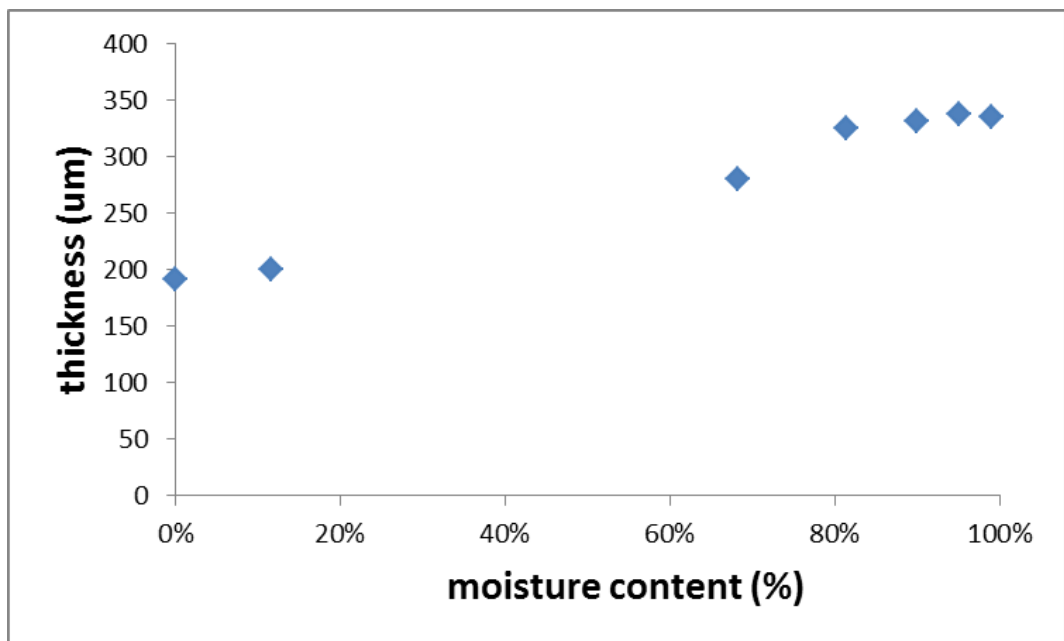


Fig. 4.8 Thickness of wet algae v.s. moisture content

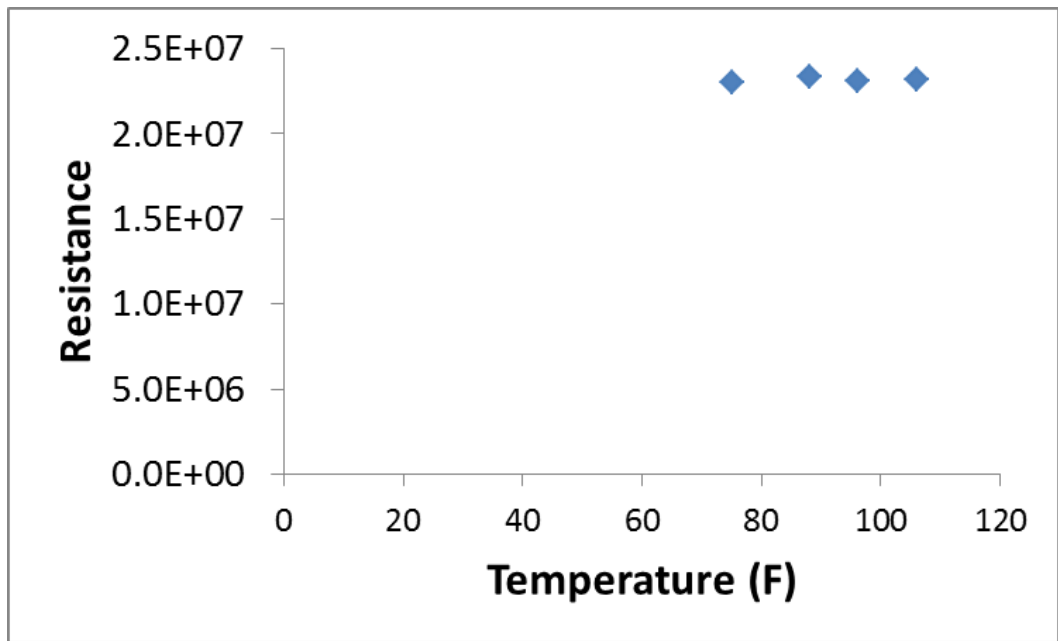


Fig. 4.9 Temperature test for 15-9 filter

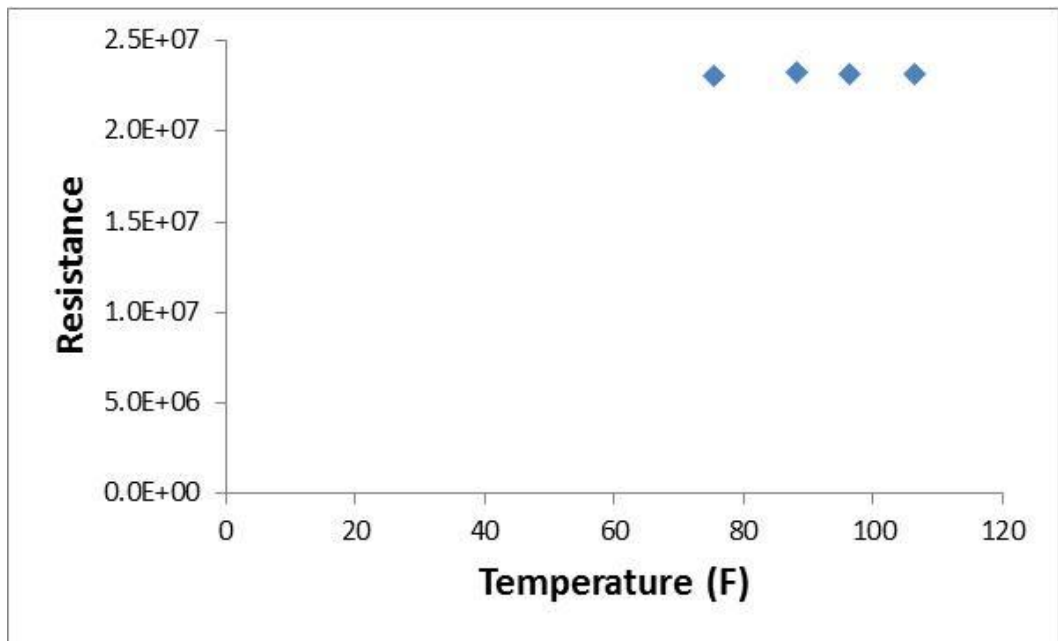


Fig. 4.10 Resistance v.s. Temperature for 15-9 filter

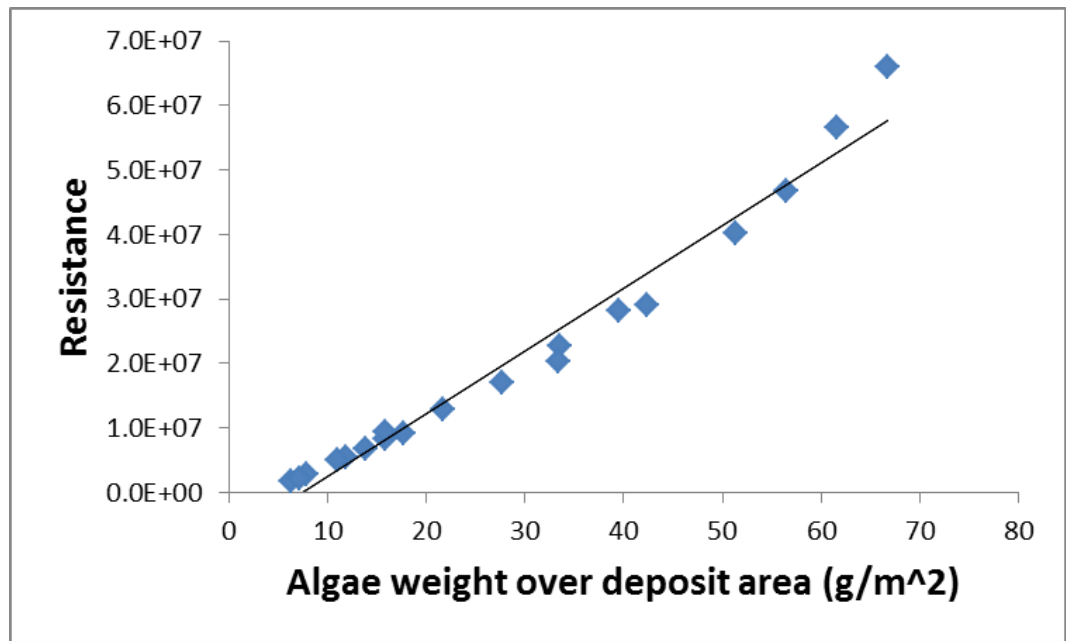


Fig. 4.11 Resistance v.s. Algae weight over deposit area

## 4.2 Free Flow Tests and CFD Mdeling

In order to test the CFD model, free flow tests were run. The idea of the experiments is to feed solution into the testing device, and monitor the flow rate and free surface during the entire processes. The experimental data will be used to compare the simulation results based on the CFD model discussed in the previous chapter. The testing device in this experiment will be simple and easy to establish the calculation grids for the CFD model. Therefore, the simulation will be less complex than the real HDD system. Before testing the real fluid behavior in the

simple HDD system model, water will be used for several different filters. Table 4.1 is the permeability table obtaining by the permeability testing. If the fluid used in the tests is water, the following analytical equation can be obtained according to Darcy's Law.

$$A \frac{dh}{dt} = \frac{-kA \Delta P}{\mu L} \implies h = h_0 \exp\left(\frac{-kA \rho g}{\mu L}\right)$$

(4-3)

**Table 4.1 Permeability divided by L of each filter**

Filter	Permeability/L
1_2	1.50912E-08
6_5	5.85138E-08
7_2	1.34753E-08
18_13	1.04091E-07
25_20	2.84981E-07
6_3	6.98285E-09

In this case, the control volume is not constant because the flow surface

keeps changing during the test. Hence, a dynamic control volume has to be adopted. The CFD modeling method is demonstrated:

Since the boundary is changing in this case, and the only changing boundary is the free water surface, the spring-based smoothing method can be used. The edges between any two calculating nodes can be modeled as a spring using the following:

$$\vec{F}_i = \sum_j^n k_{ij}(\Delta\vec{x}_j - \Delta\vec{x}_i) \quad (4-4)$$

Where  $\Delta\vec{x}_j$  and  $\Delta\vec{x}_i$  are the displacements of node i and neighboring nodes j,  $k_{ij}$  is the spring constant between nodes i and j. The spring constant can be approximated using the following form:

$$k_{ij} = \frac{1}{\sqrt{|\vec{x}_i - \vec{x}_j|}} \quad (4-5)$$

According to Hooke's law, the force generated between any two nodes is proportional to the spring constant, and the net force will be zero when it reaches equilibrium. Hence, the iterative equation can be represented in the following

form:

$$\Delta \vec{x}_i^{n+1} = \frac{\sum_j^n k_{ij} \Delta \vec{x}_i^n}{\sum_j^n k_{ij}} \quad (4-6)$$

After updating the boundary nodes, displacements can be calculated, and all the interior nodes can be obtained by solving Equation 4-6. Hence, the position at the next time step can be determined from the following equation:

$$\vec{x}_i^{m+1} = \vec{x}_i^m + \Delta \vec{x}_i^m \quad (4-7)$$

The dynamic meshes are shown in the figure 4.12, and the calculation and the modeling method are described in chapter 2. The simulation results are shown in figs. 4.13 to 4.18.

Comparing the free water flow experiments and the simulation results from figs. 4.13 to fig. 4.18, we observe that the three curves almost match perfectly in each case. The results show that the CFD model can predict the fluid dynamics in free water flow tests very well. Now, we need to consider the algae flow. As we know, as more fluid passes through filter, resistance will increase. Therefore, the permeability in free algae fluid test is dynamics and as a result, the governing



equations are nonlinear, and obtaining an analytical solution is not possible.

However, the algae flow in HDD system can be considered homogeneous since it is well mixed. Hence, the assumption that algae are deposited uniformly on the belt, and the amount of algae deposited on the belt is only related to the total flow passing through the filter. In order to substantiate this assumption, several experiments are conducted. The idea is to deposit algae on the filter, and use the laser profilometer to measure the roughness and thickness of the deposited algae.

A laser profilometer is a non-contact measurement device that can measure the roughness of a surface, and the thickness of a film if a ground reference is given.

As previously discussed, the assumption that the thickness of the algae sludge is uniform is valid since experimental data yields a roughness of around 2.79  $\mu\text{m}$  with a thickness of wet algae of around 327  $\mu\text{m}$ .

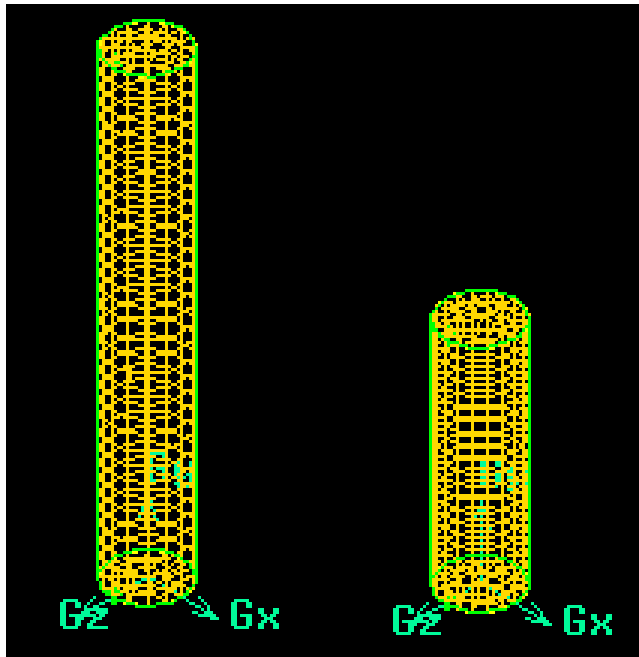


Fig. 4.12 Dynamic meshes

Moreover, from measurements, we know that the average size of algae is around 15~18 micrometer. Therefore, the pore size of filter should not be greater than 15  $\mu\text{m}$  to prevent the algae from flowing through the filter. In this test, there are only four filters that meet this requirement. Therefore only the 1-2 filter and the 7-2 filter were tested to validate the CFD modeling. Figs. 4.19~4.26 demonstrate the relationship between the experimental data and CFD modeling results. As can be seen, CFD model is good at predicting the fluid dynamic for both filters. According to the data, the free water surface height can be predicted very well for the different filters. Therefore, we may conclude that CFD method used in

this study can be a good predictor for HDD system.

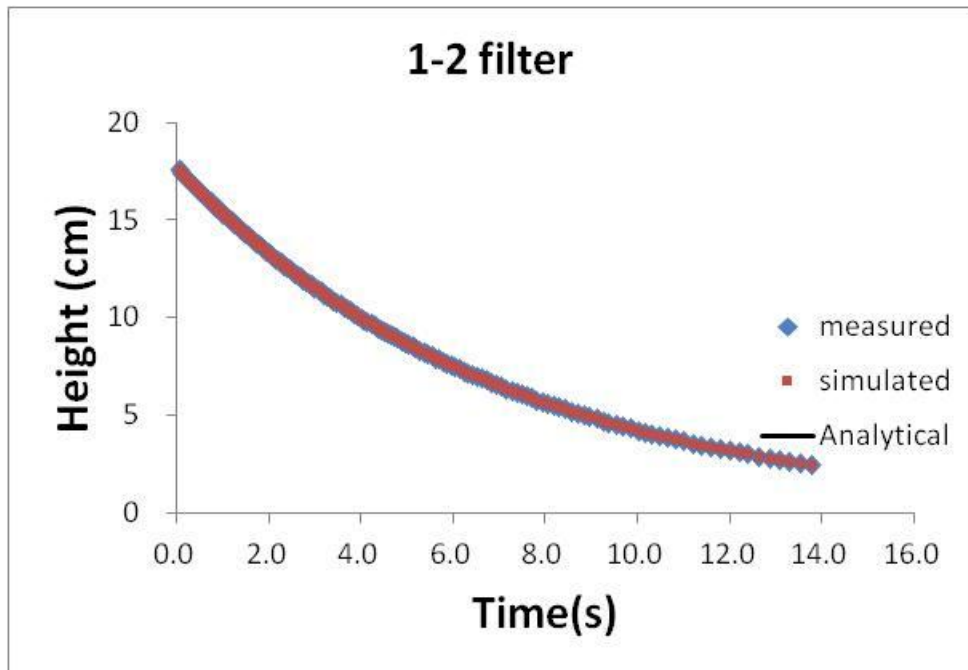


Fig.4.13 Simulated v.s. measured changing heights of free water test (1-2 filter)

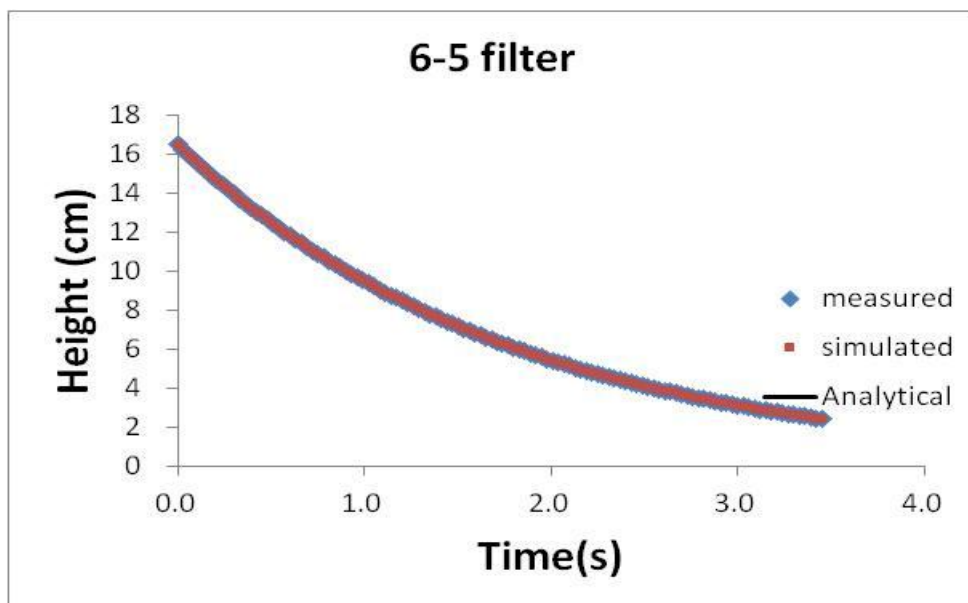


Fig. 4.14 Simulated v.s. measured changing heights of free water test (6-5 filter)

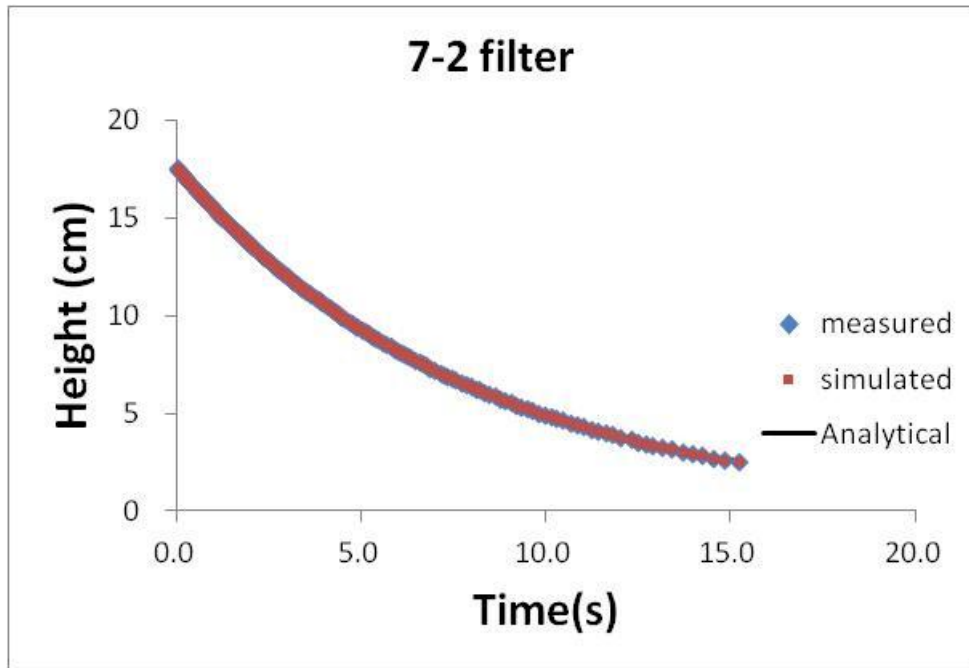


Fig. 4.15 Simulated v.s. measured changing heights of free water test (7-2 filter)

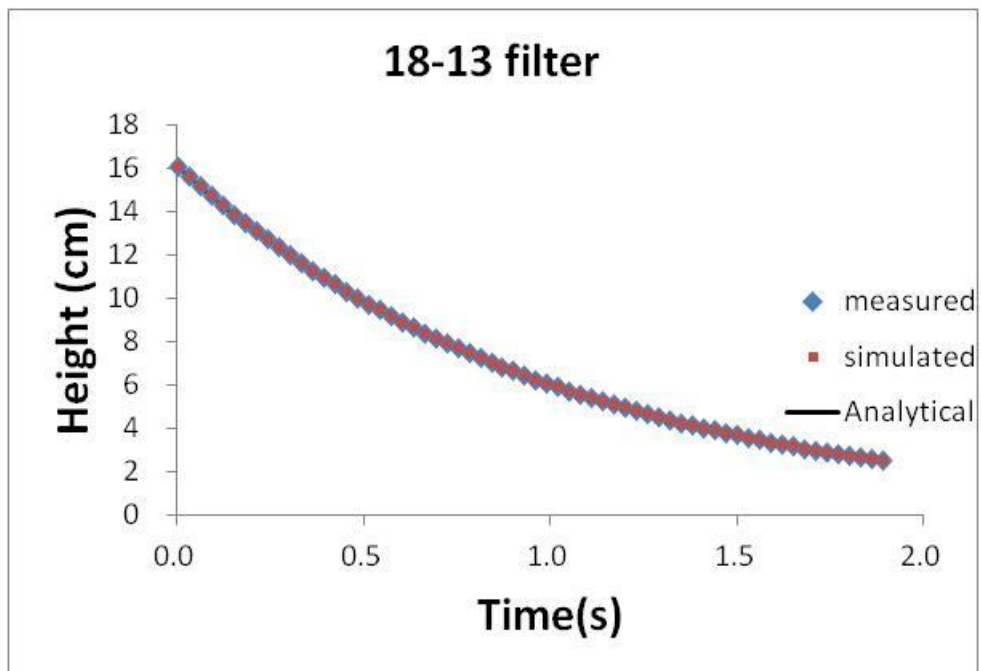


Fig. 4.16 Simulated v.s. measured changing heights of free water test 18-13 filter)

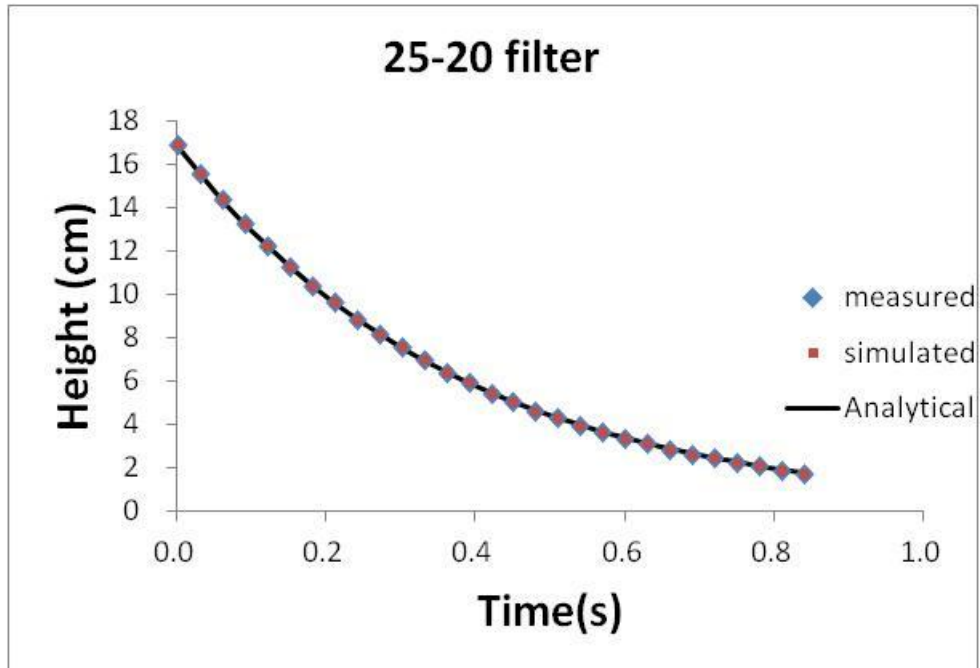


Fig. 4.17 Simulated v.s. measured changing heights of free water test (25-20 filter)

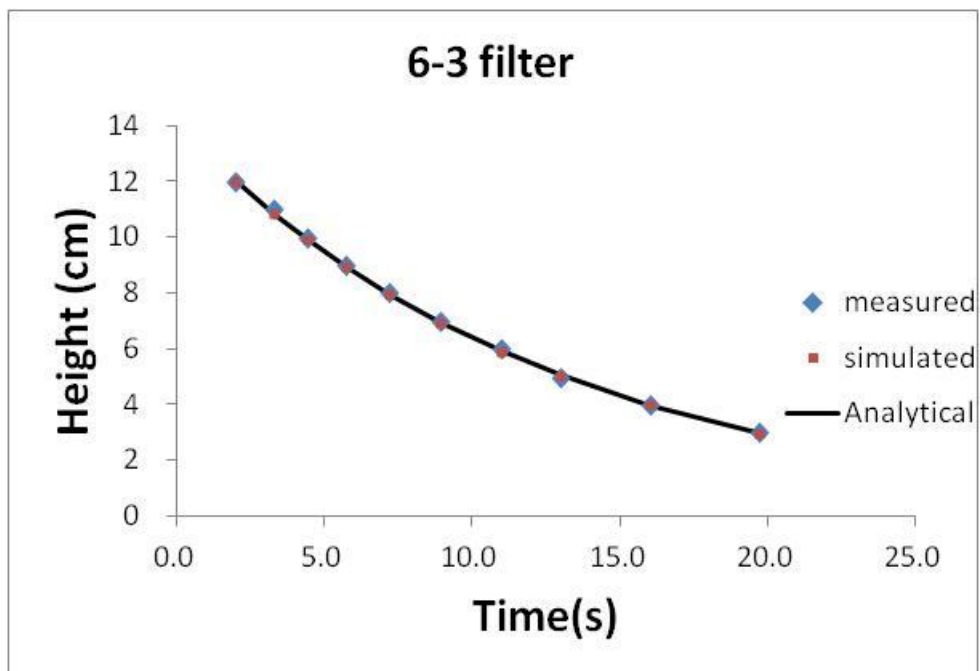


Fig. 4.18 Simulated v.s. measured changing heights of free water test (6-3 filter)

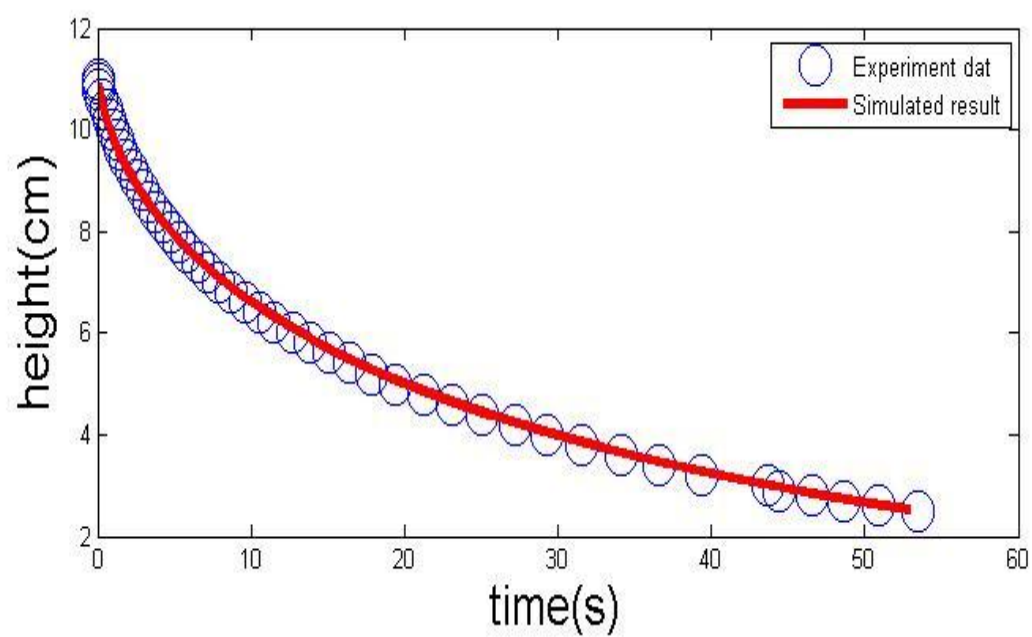


Fig. 4.19 Simulated results and measured data (0.01g/L, 1-2 filter)

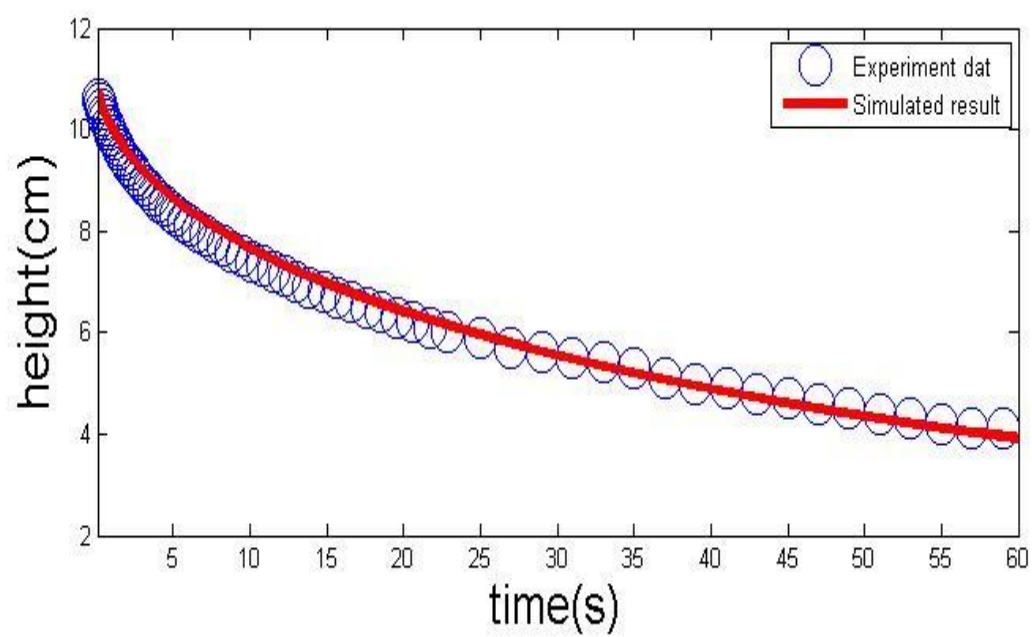


Fig. 4.20 Simulated results and measured data (0.02g/L, 1-2 filter)

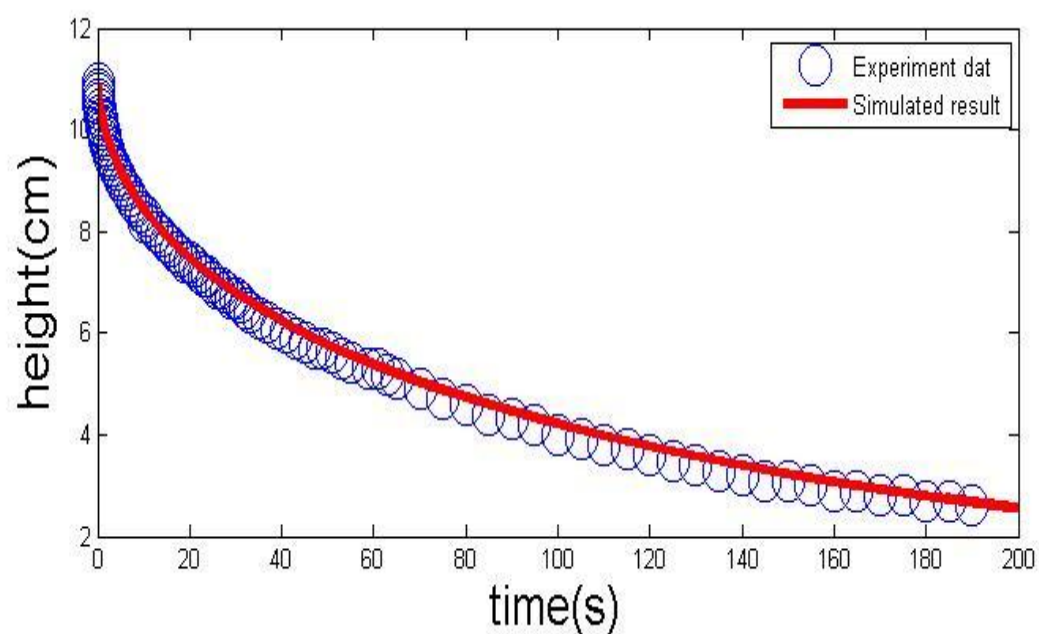


Fig. 4.21 Simulated results and measured data (0.04g/L, 1-2 filter)

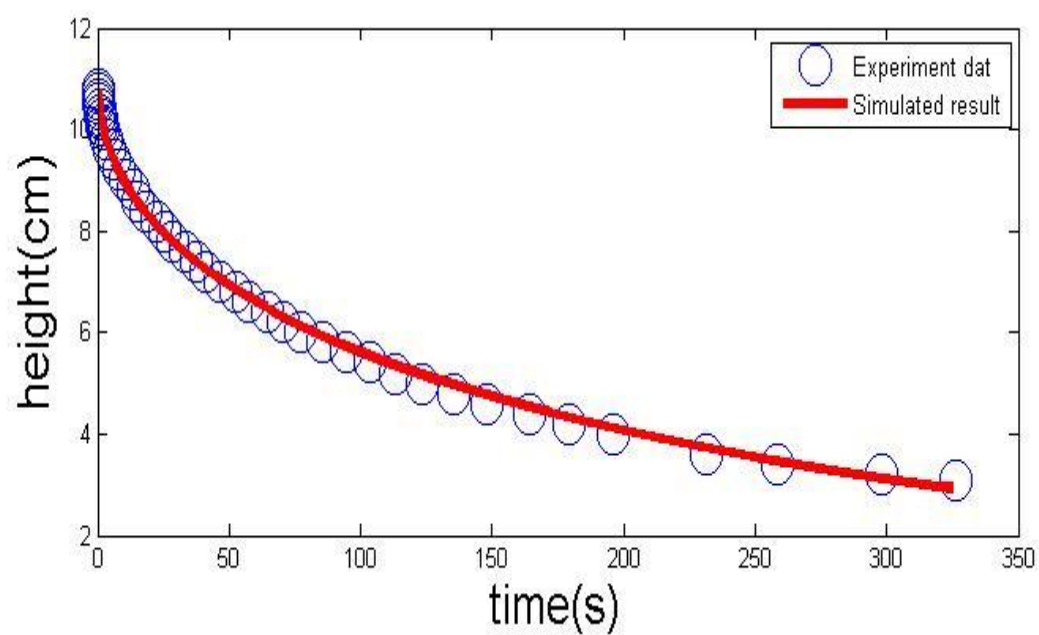


Fig. 4.22 Simulated results and measured data (0.08g/L, 1-2 filter)

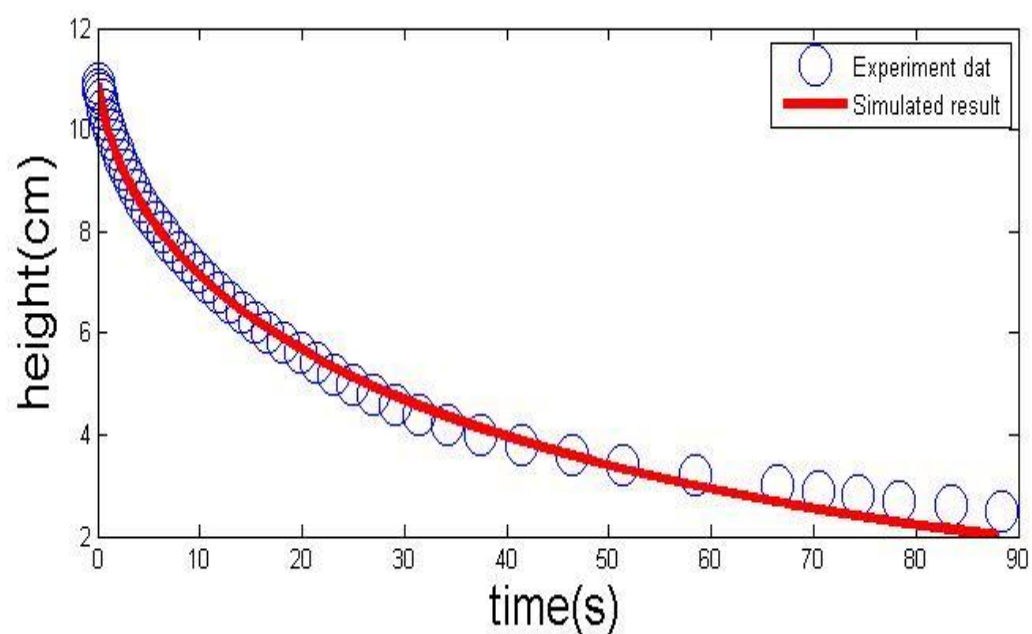


Fig. 4.23 Simulated results and measured data (0.01g/L, 7-2 filter)

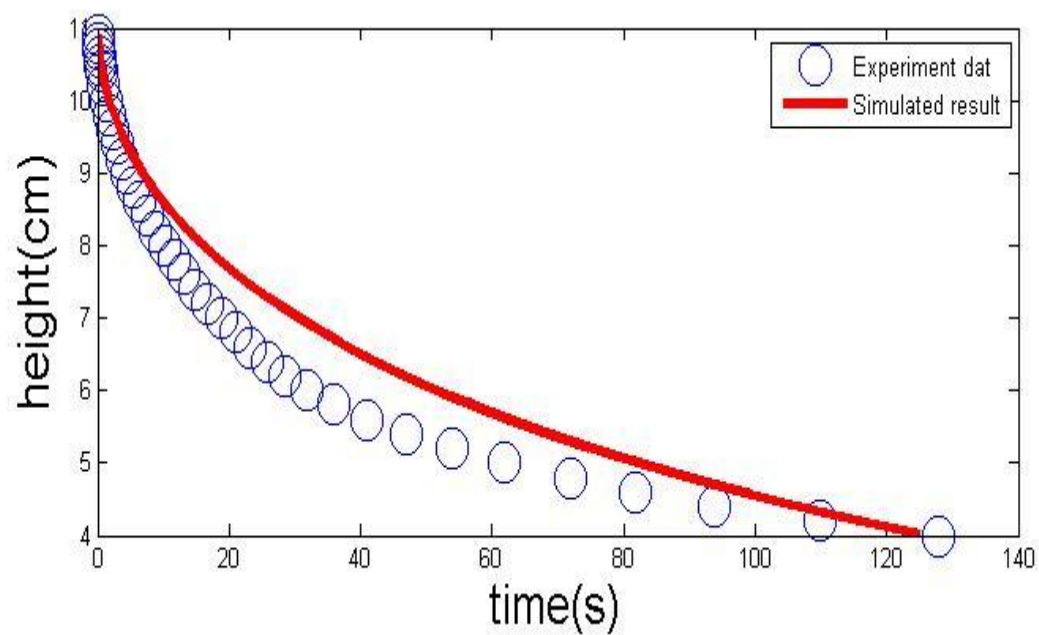


Fig. 4.24 Simulated results and measured data (0.02g/L, 7-2 filter)



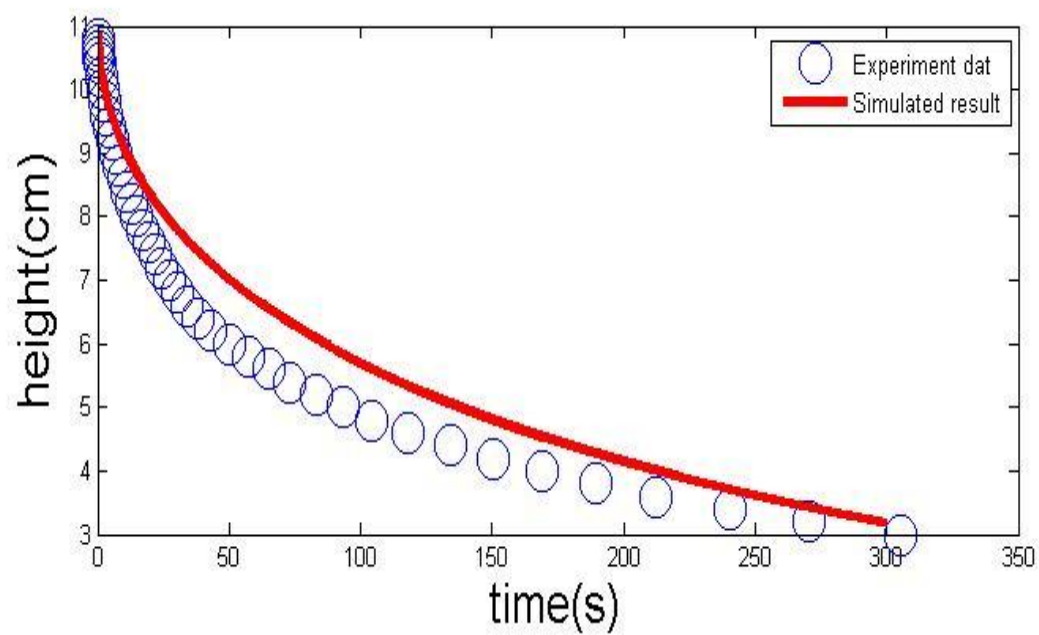


Fig. 4.25 Simulated results and measured data (0.04g/L, 7-2 filter)

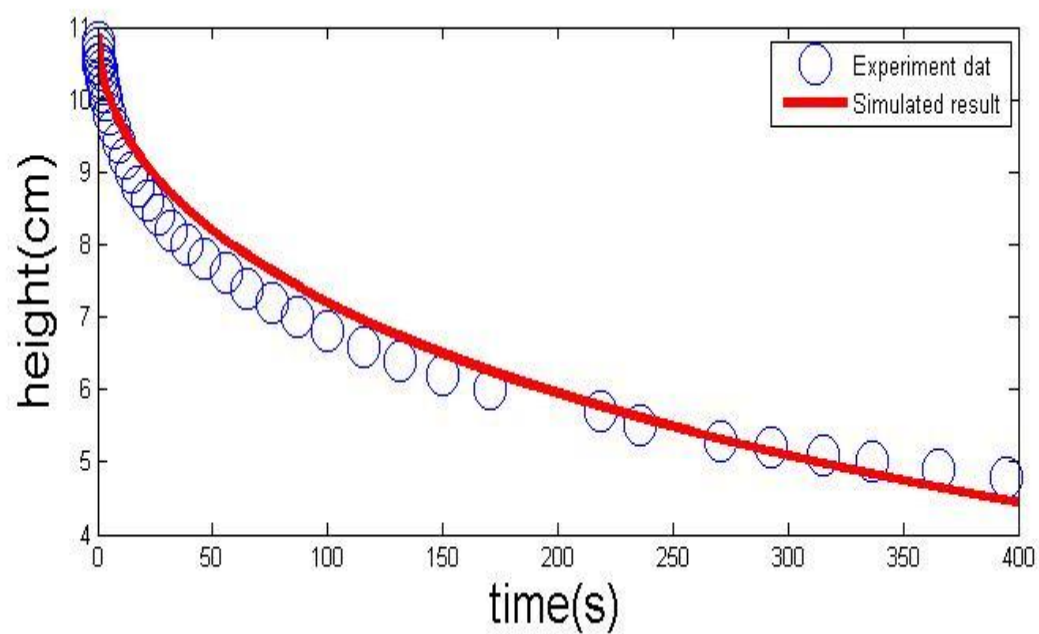


Fig. 4.26 Simulated results and measured data (0.08g/L, 7-2 filter)

## **Chapter 5 Results and Discussion**

As discussed earlier in this thesis, the main purpose of the study is to develop a predictive model of the HDD process that can be used in an optimal control system for producing high quality dried algae for fuel manufacturing facilities. The strategy is to take advantage of CFD modeling to predict the fluid dynamics in different operating conditions and to develop a lookup table that can be used for monitoring and control of the HDD system. There are several control modules including web tension control, input (algae feedstock) control, and transport control in the design. The web tension control module and CFD simulation method have been demonstrated in the earlier chapters, and the simulation results will be discussed in this part. Once the lookup table is complete, the optimal control system for the HDD system can be deployed. The simulation process and the results of simulation study will also be discussed in this chapter.

### **5.1 CFD Simulation and Results**

Like the discussions in Chapters 2 and 4, CFD modeling is an important part of

this study. CFD modeling and simulation can save time and effort by eliminating unnecessary trial-and-error investigations. In our research, we use CFD to model the system in different operating conditions, and build up a lookup table that can be used for the control of the HDD process. The details of the method and theory are given elsewhere in this thesis, the simulation results are to be given in this chapter.

### ***5.1.1 Grid testing***

The objective is to develop spatial and temporal grids that can avoid excess calculations and reduce the computational time and resources required. This objective must be balanced by the need to manage the errors caused from an inadequate computational grid. Therefore, choosing an appropriate number of calculating grids is an important aspect of the computational development. In this regard, the time step and spatial dimensions both need to be considered. The time grid is set up from  $\Delta t = 1/2$  to  $\Delta t = 1/64$ , and the spatial grids are from  $20 \times 20 \sim 320 \times 320$ . Because the flow is laminar and the geometry is not complicated, the CFD simulations are all chosen to be two-dimensional. Figs.

5.1~5.3 are the performance between different calculating grids for different concentrations of algae in the fluid testing. As can be observed, if the spatial grid is 160x160 and  $\Delta t = 1/32$ , this is sufficient for our work since there is less than a 2% difference with the 320x320 grid and  $\Delta t = 1/64$ . However, the calculation time is reduced by 1/8 when compared to the finer grid. Hence, we conclude that 1/32x160x160 grid is sufficient for this study.

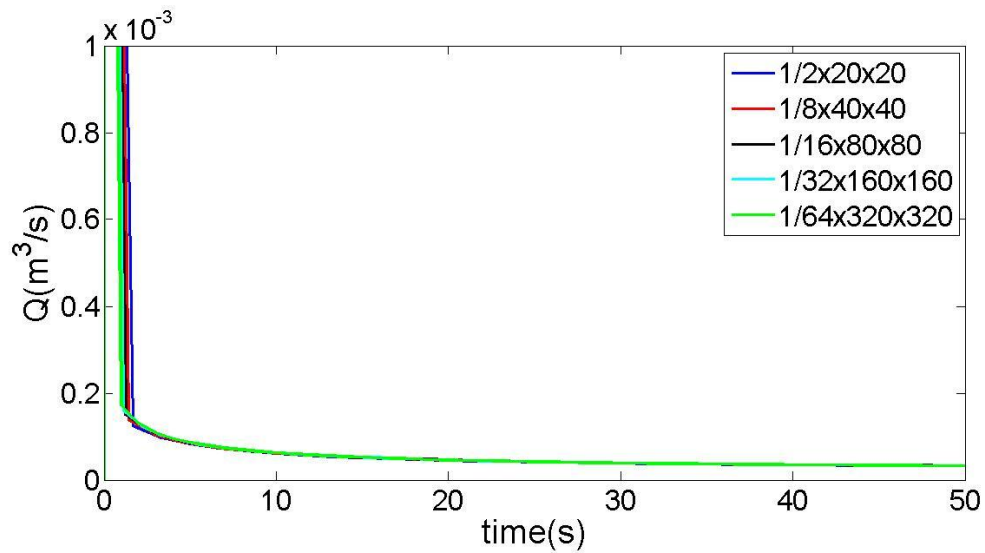


Fig 5.1 Grid test for 1g/L concentration fluid (flow rate)

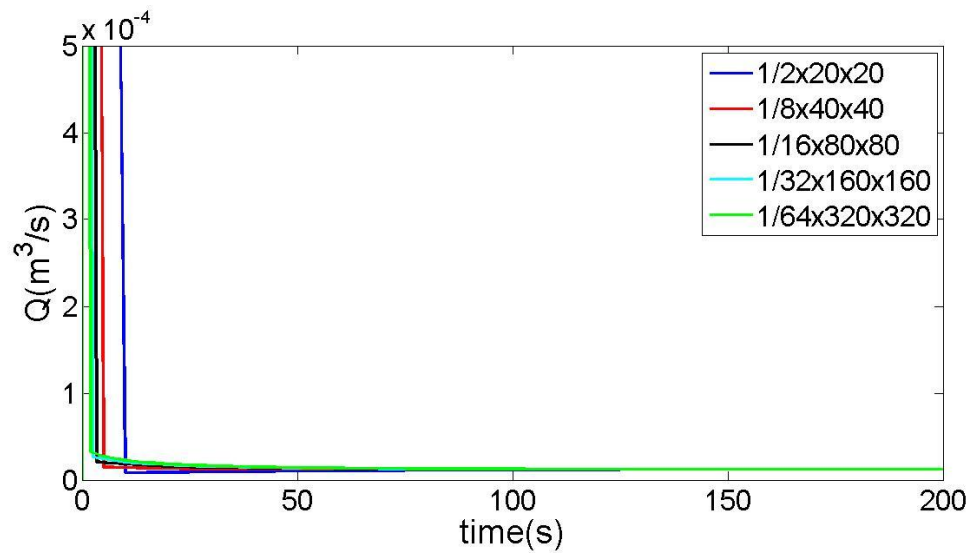


Fig 5.2 Grid test for 5g/L concentration fluid (flow rate)

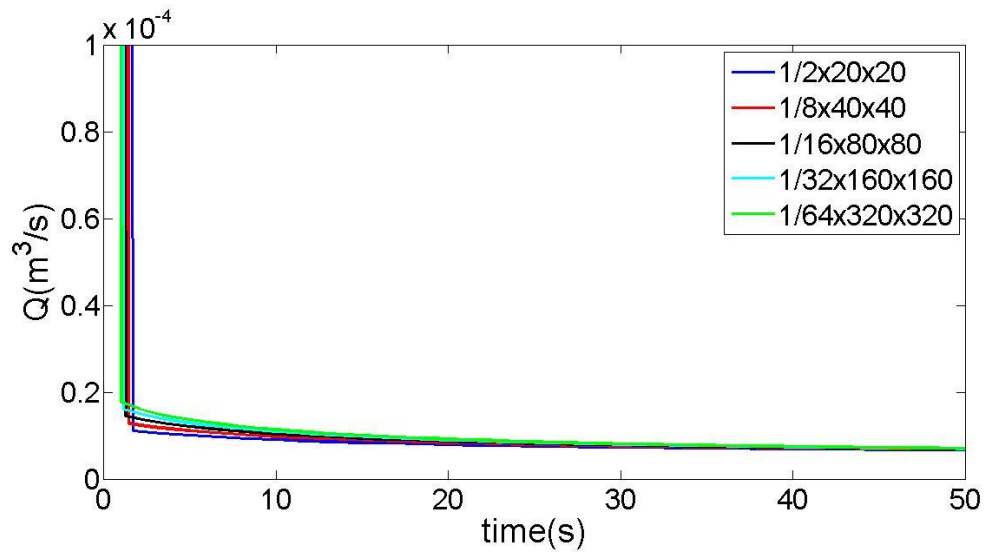


Fig 5.3 Grid test for 20g/L concentration fluid (flow rate)

### 5.1.2 Lookup table

The simulation grid is chosen as  $1/32 \times 160 \times 160$ . Tables 5.1~5.4 are the

lookup tables for gravity draining flow rate (GFR), capillary draining flow rate (CFR), mass flow rate of the dried algae output, and the remaining water at the exit of the capillary zone for different concentrations of the input solution and different web velocities. If an ideal heater is designed as in fig. 5.4, a heating condition table can be developed. Tables 5.5~5.7 are the tables for the heating temperature, required inlet air flow, and required energy for producing 1 lb of appropriately dried algae. As these tables show, it seems that the concentration of the input solution and the web velocity are two key parameters for the yield of dried algae cake. This is reasonable because the more dense the input solution, the faster the algae deposits, and the faster the web velocity, the greater the production rate of dewatered algae. If we look more closely, an increase in heating energy is also expected as the web velocity increases or the concentration of input solution decreases, given the desired to have dried algae cake at the completion of the HDD process. Table 5.7 demonstrates the efficiency of the overall HDD process. As can be observed, an increase in the concentration of the input solution can improve the efficiency dramatically.

According to Hooke's Law, and Darcy's Law, changes in resistance can be

expected when there exists tension in the web. Moreover, the porosity, pore sizes, and thickness of web will change. The fluid dynamics and dryer requirements are therefore going to be different. Hence, an alternative approach to HDD control is necessary. The data on different web tensions, input solution concentrations, and web velocities is needed from either CFD simulations or experiments with the process. In this study, CFD modeling and simulations are used because of the difficulty in getting access to the AVS HDD process and the appropriate experimental resources. Tables 5.8~5.25 are the relative tables estimated by CFD simulations for different web tensions and input solution concentrations. As the tables show, the energy efficiency can be improved especially when concentration is low and velocity is high. The possible reason is that algae do not dominate the resistance in those conditions. Fig. 5.5, shows the trend of energy efficiency with different input solution concentrations and web tension. As is demonstrated, the higher the input solution concentration, the higher the efficiency. The black line is the net energy content of 1 lb of dried algae, and the intersection, at about 12 g/L, between the concentration curve and net energy content curve defines the operating

point where it doesn't make sense to use more energy to make products with lower energy content. Again, if we compare the energy efficiency for different web tensions at 10 g/L concentration, we can find the energy efficiency tradeoff point at 15 N web tension. If we compare the price of producing dried algae, it follows that using 4.81 kBtu/hr per lb of dried algae is the best energy efficiency option among all cases. If we assume that the algae contains 60% oil, and the density of oil is  $0.8 \text{ kg/m}^3$ , the total drying energy to produce 1 gallon of bio-diesel will be about 19.59 kW. If the energy cost is 8 cent per kW, the price to produce 1 gallon of bio-diesel will be 1.56 US dollar. If the yield of algae is 5,000 gallons per year, and the operating cost of producing algae is 5,000 dollars per acre per year, the selling price of biodiesel will be \$2.89 plus the cost to transport the algae, extract oil from the algae, and profit. The cost will be very competitive if the concentration of algae can be increased, and the cost of extracting oil from the algae can be decreased. Hence, the AVS HDD system should be an efficient way to generate oil. From the data available in the tables, appropriate real-time control of the HDD system can be used to accommodate for different operating situations such as limitations on the input solution, web



velocity, heater performance, maximum heat supply, and so on. It can also be used to adjust the operation to meet specific machine or operator requirements, or performance restrictions such as heater, web tension limits, pore size limits, or material limits. Also, the tables can provide important data to estimate the economic cost of production for different algae yields, including the cost of preprocessing the input solution to increase concentration or the modifying the drying method.

**Table 5.1 Expected draining Gravity flow rate (m<sup>3</sup>/s)**

web velocity (in/min) concentration (g/L)	1	2	3	4	5	6	7	8	9	10
1	5.8509E-06	8.7766E-06	1.1125E-05	1.3164E-05	1.4998E-05	1.6685E-05	1.8258E-05	1.9739E-05	2.1146E-05	2.2488E-05
2	3.9002E-06	5.8510E-06	7.4174E-06	8.7769E-06	1.0001E-05	1.1126E-05	1.2175E-05	1.3164E-05	1.4102E-05	1.4998E-05
3	3.0763E-06	4.6153E-06	5.8511E-06	6.9236E-06	7.8892E-06	8.7770E-06	9.6051E-06	1.0385E-05	1.1126E-05	1.1833E-05
4	2.5997E-06	3.9002E-06	4.9446E-06	5.8512E-06	6.6672E-06	7.4176E-06	8.1176E-06	8.7770E-06	9.4030E-06	1.0001E-05
5	2.2814E-06	3.4228E-06	4.3394E-06	5.1350E-06	5.8512E-06	6.5099E-06	7.1242E-06	7.7030E-06	8.2525E-06	8.7770E-06
6	2.0505E-06	3.0764E-06	3.9003E-06	4.6154E-06	5.2592E-06	5.8512E-06	6.4035E-06	6.9238E-06	7.4176E-06	7.8892E-06
7	1.8736E-06	2.8110E-06	3.5638E-06	4.2173E-06	4.8056E-06	5.3466E-06	5.8512E-06	6.3267E-06	6.7780E-06	7.2089E-06
8	1.7327E-06	2.5997E-06	3.2960E-06	3.9003E-06	4.4444E-06	4.9448E-06	5.4115E-06	5.8512E-06	6.2687E-06	6.6672E-06
9	1.6174E-06	2.4265E-06	3.0764E-06	3.6406E-06	4.1484E-06	4.6155E-06	5.0511E-06	5.4616E-06	5.8512E-06	6.2233E-06
10	1.5278E-06	2.2814E-06	2.8925E-06	3.4229E-06	3.9004E-06	4.3395E-06	4.7492E-06	5.1351E-06	5.5014E-06	5.8512E-06
11	1.4382E-06	2.1576E-06	2.7355E-06	3.2372E-06	3.6888E-06	4.1041E-06	4.4915E-06	4.8566E-06	5.2031E-06	5.5339E-06
12	1.3667E-06	2.0505E-06	2.5997E-06	3.0765E-06	3.5057E-06	3.9004E-06	4.2686E-06	4.6155E-06	4.9448E-06	5.2592E-06
13	1.3042E-06	1.9567E-06	2.4808E-06	2.9357E-06	3.3453E-06	3.7219E-06	4.0733E-06	4.4043E-06	4.7185E-06	5.0186E-06
14	1.2488E-06	1.8736E-06	2.3755E-06	2.8111E-06	3.2033E-06	3.5640E-06	3.9004E-06	4.2174E-06	4.5183E-06	4.8056E-06
15	1.1994E-06	1.7995E-06	2.2815E-06	2.6999E-06	3.0765E-06	3.4229E-06	3.7461E-06	4.0505E-06	4.3395E-06	4.6155E-06
16	1.1549E-06	1.7328E-06	2.1969E-06	2.5998E-06	2.9625E-06	3.2961E-06	3.6072E-06	3.9004E-06	4.1787E-06	4.4444E-06
17	1.1146E-06	1.6724E-06	2.1203E-06	2.5092E-06	2.8592E-06	3.1812E-06	3.4815E-06	3.7645E-06	4.0331E-06	4.2895E-06
18	1.0780E-06	1.6173E-06	2.0505E-06	2.4266E-06	2.7652E-06	3.0765E-06	3.3670E-06	3.6406E-06	3.9004E-06	4.1484E-06
19	1.0444E-06	1.5670E-06	1.9867E-06	2.3510E-06	2.6790E-06	2.9807E-06	3.2621E-06	3.5272E-06	3.7789E-06	4.0192E-06
20	1.0135E-06	1.5206E-06	1.9279E-06	2.2815E-06	2.5998E-06	2.8926E-06	3.1656E-06	3.4229E-06	3.6672E-06	3.9004E-06

**Table 5.2 Expected draining Capillary flow rate (m<sup>3</sup>/s)**

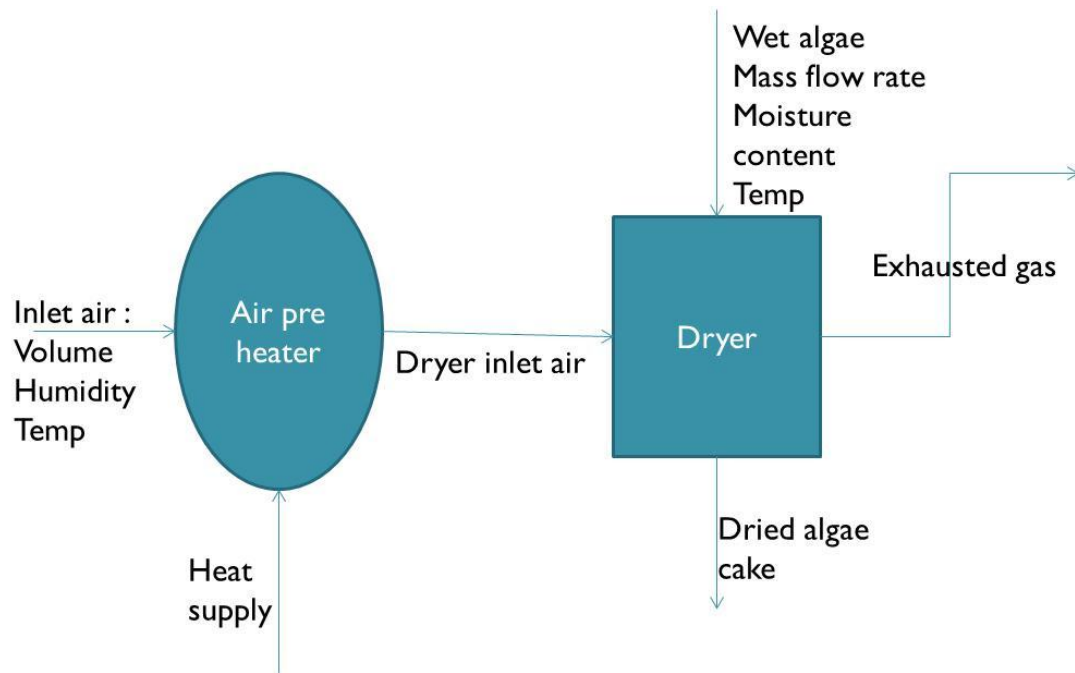
web velocity (in/min) concentration (g/L)	1	2	3	4	5	6	7	8	9	10
1	1.3217E-06	1.9833E-06	2.5148E-06	2.9762E-06	3.3917E-06	3.7739E-06	4.1305E-06	4.4664E-06	4.7854E-06	5.0900E-06
2	8.8081E-07	1.3217E-06	1.6758E-06	1.9832E-06	2.2600E-06	2.5146E-06	2.7522E-06	2.9760E-06	3.1885E-06	3.3913E-06
3	6.9468E-07	1.0424E-06	1.3216E-06	1.5641E-06	1.7824E-06	1.9832E-06	2.1705E-06	2.3469E-06	2.5145E-06	2.6745E-06
4	5.8700E-07	8.8079E-07	1.1168E-06	1.3216E-06	1.5060E-06	1.6757E-06	1.8340E-06	1.9832E-06	2.1248E-06	2.2600E-06
5	5.1512E-07	7.7292E-07	9.7999E-07	1.1597E-06	1.3216E-06	1.4705E-06	1.6094E-06	1.7403E-06	1.8645E-06	1.9832E-06
6	4.6297E-07	6.9467E-07	8.8077E-07	1.0423E-06	1.1878E-06	1.3216E-06	1.4464E-06	1.5641E-06	1.6757E-06	1.7824E-06
7	4.2302E-07	6.3472E-07	8.0476E-07	9.5237E-07	1.0853E-06	1.2075E-06	1.3216E-06	1.4291E-06	1.5311E-06	1.6285E-06
8	3.9121E-07	5.8699E-07	7.4424E-07	8.8075E-07	1.0037E-06	1.1167E-06	1.2222E-06	1.3216E-06	1.4159E-06	1.5060E-06
9	3.6515E-07	5.4788E-07	6.9465E-07	8.2206E-07	9.3677E-07	1.0423E-06	1.1408E-06	1.2335E-06	1.3216E-06	1.4057E-06
10	3.4331E-07	5.1510E-07	6.5310E-07	7.7289E-07	8.8073E-07	9.7995E-07	1.0725E-06	1.1597E-06	1.2425E-06	1.3216E-06
11	3.2594E-07	4.8715E-07	6.1765E-07	7.3094E-07	8.3293E-07	9.2676E-07	1.0143E-06	1.0968E-06	1.1751E-06	1.2499E-06
12	3.0856E-07	4.6296E-07	5.8698E-07	6.9464E-07	7.9156E-07	8.8073E-07	9.6392E-07	1.0423E-06	1.1167E-06	1.1878E-06
13	2.9443E-07	4.4176E-07	5.6011E-07	6.6284E-07	7.5532E-07	8.4041E-07	9.1979E-07	9.9458E-07	1.0656E-06	1.1334E-06
14	2.8193E-07	4.2301E-07	5.3632E-07	6.3469E-07	7.2325E-07	8.0473E-07	8.8073E-07	9.5235E-07	1.0203E-06	1.0853E-06
15	2.7077E-07	4.0626E-07	5.1509E-07	6.0957E-07	6.9462E-07	7.7287E-07	8.4586E-07	9.1465E-07	9.7995E-07	1.0423E-06
16	2.6073E-07	3.9120E-07	4.9599E-07	5.8696E-07	6.6886E-07	7.4421E-07	8.1450E-07	8.8073E-07	9.4361E-07	1.0037E-06
17	2.5164E-07	3.7756E-07	4.7870E-07	5.6650E-07	6.4554E-07	7.1826E-07	7.8610E-07	8.5002E-07	9.1070E-07	9.6865E-07
18	2.4336E-07	3.6513E-07	4.6295E-07	5.4785E-07	6.2430E-07	6.9462E-07	7.6022E-07	8.2204E-07	8.8073E-07	9.3677E-07
19	2.3578E-07	3.5376E-07	4.4852E-07	5.3078E-07	6.0484E-07	6.7298E-07	7.3654E-07	7.9643E-07	8.5329E-07	9.0758E-07
20	2.2880E-07	3.4329E-07	4.3525E-07	5.1508E-07	5.8695E-07	6.5307E-07	7.1475E-07	7.7287E-07	8.2804E-07	8.8073E-07

**Table 5.3 Expected output algae mass flow rate (kg/s)**

web velocity (in/min) concentration (g/L)	1	2	3	4	5	6	7	8	9	10
1	5.85673E-06	8.78539E-06	1.11366E-05	1.31769E-05	1.50133E-05	1.67018E-05	1.83E-05	1.98E-05	2.12E-05	2.25E-05
2	7.81593E-06	1.17254E-05	1.48645E-05	1.7589E-05	2.00413E-05	2.22966E-05	2.44E-05	2.64E-05	2.83E-05	3.01E-05
3	9.25677E-06	1.38875E-05	1.7606E-05	2.08334E-05	2.37388E-05	2.64107E-05	2.89E-05	3.13E-05	3.35E-05	3.56E-05
4	1.04404E-05	1.56635E-05	1.9858E-05	2.34986E-05	2.6776E-05	2.97902E-05	3.26E-05	3.53E-05	3.78E-05	4.02E-05
5	1.14642E-05	1.71999E-05	2.1806E-05	2.58041E-05	2.94033E-05	3.27135E-05	3.58E-05	3.87E-05	4.15E-05	4.41E-05
6	1.23772E-05	1.85697E-05	2.35429E-05	2.78596E-05	3.17458E-05	3.532E-05	3.87E-05	4.18E-05	4.48E-05	4.76E-05
7	1.32075E-05	1.98157E-05	2.51228E-05	2.97294E-05	3.38765E-05	3.76908E-05	4.12E-05	4.46E-05	4.78E-05	5.08E-05
8	1.39736E-05	2.09653E-05	2.65804E-05	3.14543E-05	3.58422E-05	3.9878E-05	4.36E-05	4.72E-05	5.06E-05	5.38E-05
9	1.46888E-05	2.20371E-05	2.79393E-05	3.30627E-05	3.7675E-05	4.19173E-05	4.59E-05	4.96E-05	5.31E-05	5.65E-05
10	1.16371E-05	2.30446E-05	2.92169E-05	3.45746E-05	3.9398E-05	4.38344E-05	4.8E-05	5.19E-05	5.56E-05	5.91E-05
11	1.59962E-05	2.39981E-05	3.04257E-05	3.60052E-05	4.10283E-05	4.56459E-05	5E-05	5.4E-05	5.79E-05	6.16E-05
12	1.65996E-05	2.4905E-05	3.15757E-05	3.73662E-05	4.25792E-05	4.7374E-05	5.18E-05	5.61E-05	6.01E-05	6.39E-05
13	1.71779E-05	2.57717E-05	3.26747E-05	3.86667E-05	4.40613E-05	4.90231E-05	5.37E-05	5.8E-05	6.22E-05	6.61E-05
14	1.77314E-05	2.66031E-05	3.37287E-05	3.99141E-05	4.54828E-05	5.06047E-05	5.54E-05	5.99E-05	6.42E-05	6.82E-05
15	1.8265E-05	2.7403E-05	3.4743E-05	4.11145E-05	4.68507E-05	5.21268E-05	5.7E-05	6.17E-05	6.61E-05	7.03E-05
16	1.87789E-05	2.8175E-05	3.57218E-05	4.22728E-05	4.81707E-05	5.35955E-05	5.87E-05	6.34E-05	6.8E-05	7.23E-05
17	1.92759E-05	2.89217E-05	3.66686E-05	4.33933E-05	4.94476E-05	5.50162E-05	6.02E-05	6.51E-05	6.98E-05	7.42E-05
18	1.97597E-05	2.96456E-05	3.75864E-05	4.44795E-05	5.06854E-05	5.63935E-05	6.17E-05	6.67E-05	7.15E-05	7.6E-05
19	2.02279E-05	3.03487E-05	3.84779E-05	4.55346E-05	5.18877E-05	5.77313E-05	6.32E-05	6.83E-05	7.32E-05	7.79E-05
20	2.06837E-05	3.10328E-05	3.93453E-05	4.65611E-05	5.30575E-05	5.90329E-05	6.46E-05	6.99E-05	7.48E-05	7.96E-05

**Table 5.4 Expected water flow rate (kg/s) in the output of capillary zone**

web velocity (in/min) concentration (g/L)	1	2	3	4	5	6	7	8	9	10
1	0.000502665	0.000753322	0.000954237	0.00112836	0.001284908	0.001428635	0.001562531	0.001688543	0.001808033	0.001921997
2	0.000332614	0.00049869	0.000631913	0.000747446	0.000851379	0.000946844	0.001035834	0.001119618	0.001199099	0.001274937
3	0.000260308	0.000390351	0.000494706	0.000585226	0.000666681	0.000741514	0.00081128	0.000876988	0.000939328	0.000998821
4	0.000218211	0.000327258	0.00041478	0.000490711	0.000559048	0.000621803	0.000680305	0.000735395	0.000787664	0.000837545
5	0.000189935	0.000284872	0.000361079	0.0004272	0.000486712	0.00054137	0.000592328	0.000640316	0.000685849	0.000729306
6	0.0001693	0.000253936	0.000321879	0.000380838	0.000433905	0.000482644	0.000528091	0.000570889	0.000611501	0.000650262
7	0.0001534	0.000230095	0.000291669	0.000345103	0.0003932	0.000437378	0.000478569	0.000517367	0.000554181	0.000589319
8	0.000140665	0.000211001	0.000267471	0.000316479	0.000360595	0.000401115	0.000438899	0.000474485	0.000508255	0.000540492
9	0.000130189	0.000195262	0.000247525	0.000292884	0.000333715	0.000371221	0.000406193	0.000439134	0.000470393	0.000500231
10	0.000123518	0.000181996	0.000230713	0.000272995	0.000311058	0.000346021	0.000378624	0.000409333	0.000438475	0.000466293
11	0.000112505	0.000170615	0.000216289	0.00025593	0.000291618	0.000324399	0.000354968	0.000383761	0.000411086	0.00043717
12	0.000107122	0.000160708	0.000203732	0.000241075	0.000274694	0.000305575	0.000334373	0.000361498	0.000387241	0.000411814
13	0.000101323	0.000151979	0.000192668	0.000227985	0.000259781	0.000289888	0.000316225	0.000341881	0.000366229	0.000389471
14	9.61296E-05	0.000144209	0.00018282	0.000216333	0.000246505	0.000274223	0.00030007	0.000324417	0.000347523	0.00036958
15	9.14853E-05	0.000137232	0.000173976	0.00020587	0.000234585	0.000260964	0.000285562	0.000308733	0.000330724	0.000351716
16	8.72658E-05	0.000130919	0.000165974	0.000196403	0.000223799	0.000248966	0.000272435	0.000294542	0.000315524	0.000335552
17	8.34203E-05	0.00012517	0.000158687	0.00018778	0.000213975	0.000238037	0.000260478	0.000281616	0.000301678	0.000320829
18	7.99302E-05	0.000119902	0.00015201	0.000179881	0.000204974	0.000228025	0.000249523	0.000269773	0.000288992	0.000307339
19	7.66883E-05	0.000115051	0.000145861	0.000172604	0.000196685	0.000218804	0.000239434	0.000258866	0.000277309	0.000294915
20	7.36987E-05	0.000110563	0.000140172	0.000165873	0.000189014	0.000210273	0.000230098	0.000248774	0.000266499	0.000283419



**Fig. 5.4 Schematic for algae drying process**

**Table 5.5 Required airflow for heater to dry algae (klb/hr)**

web velocity (in/min) concentration (g/L)	1	2	3	4	5	6	7	8	9	10
1	3.5580E-02	5.3322E-02	6.7543E-02	7.9868E-02	9.0949E-02	1.0112E-01	1.1060E-01	1.1952E-01	1.2798E-01	1.3604E-01
2	2.3538E-02	3.5290E-02	4.4717E-02	5.2893E-02	6.0248E-02	6.7004E-02	7.3301E-02	7.9230E-02	8.4854E-02	9.0221E-02
3	1.8416E-02	2.7617E-02	3.4999E-02	4.1403E-02	4.7166E-02	5.2460E-02	5.7396E-02	6.2045E-02	6.6455E-02	7.0664E-02
4	1.5434E-02	2.3147E-02	2.9337E-02	3.4708E-02	3.9542E-02	4.3980E-02	4.8118E-02	5.2014E-02	5.5711E-02	5.9240E-02
5	1.3431E-02	2.0144E-02	2.5533E-02	3.0208E-02	3.4416E-02	3.8281E-02	4.1885E-02	4.5278E-02	4.8498E-02	5.1571E-02
6	1.1968E-02	1.7952E-02	2.2755E-02	2.6923E-02	3.0674E-02	3.4120E-02	3.7333E-02	4.0358E-02	4.3229E-02	4.5969E-02
7	1.0841E-02	1.6262E-02	2.0614E-02	2.4390E-02	2.7789E-02	3.0912E-02	3.3823E-02	3.6565E-02	3.9167E-02	4.1650E-02
8	9.9388E-03	1.4908E-02	1.8898E-02	2.2361E-02	2.5478E-02	2.8341E-02	3.1011E-02	3.3525E-02	3.5911E-02	3.8189E-02
9	9.1961E-03	1.3793E-02	1.7484E-02	2.0688E-02	2.3572E-02	2.6222E-02	2.8692E-02	3.1019E-02	3.3227E-02	3.5334E-02
10	8.7227E-03	1.2852E-02	1.6292E-02	1.9278E-02	2.1966E-02	2.4435E-02	2.6737E-02	2.8906E-02	3.0963E-02	3.2928E-02
11	7.9422E-03	1.2045E-02	1.5269E-02	1.8068E-02	2.0587E-02	2.2901E-02	2.5059E-02	2.7092E-02	2.9021E-02	3.0862E-02
12	7.5601E-03	1.1342E-02	1.4378E-02	1.7014E-02	1.9387E-02	2.1566E-02	2.3598E-02	2.5513E-02	2.7330E-02	2.9064E-02
13	7.1487E-03	1.0723E-02	1.3594E-02	1.6085E-02	1.8329E-02	2.0389E-02	2.2311E-02	2.4121E-02	2.5839E-02	2.7479E-02
14	6.7803E-03	1.0171E-02	1.2895E-02	1.5259E-02	1.7387E-02	1.9342E-02	2.1165E-02	2.2882E-02	2.4512E-02	2.6067E-02
15	6.4507E-03	9.6763E-03	1.2267E-02	1.4516E-02	1.6541E-02	1.8401E-02	2.0135E-02	2.1769E-02	2.3320E-02	2.4800E-02
16	6.1512E-03	9.2283E-03	1.1699E-02	1.3844E-02	1.5775E-02	1.7549E-02	1.9203E-02	2.0762E-02	2.2241E-02	2.3652E-02
17	5.8782E-03	8.8201E-03	1.1182E-02	1.3232E-02	1.5078E-02	1.6773E-02	1.8355E-02	1.9844E-02	2.1258E-02	2.2607E-02
18	5.6304E-03	8.4461E-03	1.0708E-02	1.2671E-02	1.4439E-02	1.6063E-02	1.7577E-02	1.9003E-02	2.0357E-02	2.1649E-02
19	5.4002E-03	8.1017E-03	1.0271E-02	1.2154E-02	1.3850E-02	1.5408E-02	1.6860E-02	1.8229E-02	1.9528E-02	2.0767E-02
20	5.1879E-03	7.7829E-03	9.8672E-03	1.1676E-02	1.3305E-02	1.4802E-02	1.6197E-02	1.7512E-02	1.8760E-02	1.9951E-02

**Table 5.6 Heating energy requirements for heating air (kBtu/hr)**

web velocity (in/min) concentration (g/L)	1	2	3	4	5	6	7	8	9	10
1	5.7659E+00	8.6410E+00	1.0946E+01	1.2943E+01	1.4739E+01	1.6387E+01	1.7923E+01	1.9369E+01	2.0739E+01	2.2046E+01
2	3.8150E+00	5.7199E+00	7.2479E+00	8.5731E+00	9.7652E+00	1.0860E+01	1.1881E+01	1.2842E+01	1.3753E+01	1.4623E+01
3	2.9855E+00	4.4770E+00	5.6738E+00	6.7120E+00	7.6462E+00	8.5045E+00	9.3046E+00	1.0058E+01	1.0773E+01	1.1456E+01
4	2.5025E+00	3.7531E+00	4.7568E+00	5.6276E+00	6.4113E+00	7.1310E+00	7.8020E+00	8.4337E+00	9.0332E+00	9.6052E+00
5	2.1781E+00	3.2668E+00	4.1407E+00	4.8989E+00	5.5814E+00	6.2082E+00	6.7925E+00	7.3428E+00	7.8650E+00	8.3633E+00
6	1.9413E+00	2.9118E+00	3.6909E+00	4.3670E+00	4.9755E+00	5.5344E+00	6.0555E+00	6.5462E+00	7.0119E+00	7.4564E+00
7	1.7589E+00	2.6383E+00	3.3443E+00	3.9569E+00	4.5084E+00	5.0149E+00	5.4872E+00	5.9321E+00	6.3542E+00	6.7571E+00
8	1.6127E+00	2.4191E+00	3.0666E+00	3.6285E+00	4.1343E+00	4.5988E+00	5.0320E+00	5.4400E+00	5.8272E+00	6.1968E+00
9	1.4925E+00	2.2385E+00	2.8377E+00	3.3577E+00	3.8258E+00	4.2558E+00	4.6567E+00	5.0343E+00	5.3927E+00	5.7348E+00
10	1.4159E+00	2.0863E+00	2.6448E+00	3.1294E+00	3.5658E+00	3.9666E+00	4.3403E+00	4.6923E+00	5.0264E+00	5.3453E+00
11	1.2896E+00	1.9557E+00	2.4792E+00	2.9336E+00	3.3427E+00	3.7184E+00	4.0688E+00	4.3989E+00	4.7121E+00	5.0111E+00
12	1.2278E+00	1.8420E+00	2.3351E+00	2.7631E+00	3.1484E+00	3.5024E+00	3.8325E+00	4.1434E+00	4.4384E+00	4.7201E+00
13	1.1612E+00	1.7418E+00	2.2081E+00	2.6129E+00	2.9773E+00	3.3120E+00	3.6242E+00	3.9182E+00	4.1972E+00	4.4636E+00
14	1.1016E+00	1.6526E+00	2.0951E+00	2.4791E+00	2.8249E+00	3.1425E+00	3.4387E+00	3.7177E+00	3.9825E+00	4.2353E+00
15	1.0483E+00	1.5725E+00	1.9936E+00	2.3590E+00	2.6881E+00	2.9903E+00	3.2722E+00	3.5377E+00	3.7897E+00	4.0303E+00
16	9.9988E-01	1.5001E+00	1.9017E+00	2.2504E+00	2.5643E+00	2.8526E+00	3.1215E+00	3.3748E+00	3.6152E+00	3.8447E+00
17	9.5573E-01	1.4341E+00	1.8180E+00	2.1514E+00	2.4515E+00	2.7272E+00	2.9843E+00	3.2264E+00	3.4563E+00	3.6757E+00
18	9.1567E-01	1.3736E+00	1.7414E+00	2.0607E+00	2.3482E+00	2.6122E+00	2.8585E+00	3.0905E+00	3.3106E+00	3.5208E+00
19	8.7845E-01	1.3179E+00	1.6708E+00	1.9772E+00	2.2530E+00	2.5064E+00	2.7427E+00	2.9653E+00	3.1765E+00	3.3782E+00
20	8.4413E-01	1.2664E+00	1.6055E+00	1.8999E+00	2.1649E+00	2.4084E+00	2.6355E+00	2.8494E+00	3.0524E+00	3.2462E+00

**Table 5.7 Energy efficiency (kBtu/lb of dried algae)**

web velocity (in/min) concentration (g/L)	1	2	3	4	5	6	7	8	9	10
1	1.2415E+05	1.2404E+05	1.2395E+05	1.2387E+05	1.2380E+05	1.2374E+05	1.2368E+05	1.2362E+05	1.2356E+05	1.2351E+05
2	6.1556E+04	6.1520E+04	6.1492E+04	6.1468E+04	6.1448E+04	6.1427E+04	6.1408E+04	6.1390E+04	6.1373E+04	6.1356E+04
3	4.0673E+04	4.0655E+04	4.0641E+04	4.0630E+04	4.0620E+04	4.0610E+04	4.0600E+04	4.0591E+04	4.0583E+04	4.0575E+04
4	3.0228E+04	3.0217E+04	3.0209E+04	3.0202E+04	3.0197E+04	3.0188E+04	3.0181E+04	3.0174E+04	3.0167E+04	3.0160E+04
5	2.3960E+04	2.3952E+04	2.3947E+04	2.3942E+04	2.3939E+04	2.3933E+04	2.3928E+04	2.3923E+04	2.3918E+04	2.3913E+04
6	1.9780E+04	1.9775E+04	1.9771E+04	1.9768E+04	1.9765E+04	1.9761E+04	1.9757E+04	1.9753E+04	1.9750E+04	1.9746E+04
7	1.6794E+04	1.6790E+04	1.6787E+04	1.6785E+04	1.6783E+04	1.6780E+04	1.6777E+04	1.6774E+04	1.6771E+04	1.6768E+04
8	1.4555E+04	1.4552E+04	1.4549E+04	1.4548E+04	1.4546E+04	1.4544E+04	1.4541E+04	1.4539E+04	1.4536E+04	1.4534E+04
9	1.2814E+04	1.2810E+04	1.2809E+04	1.2807E+04	1.2806E+04	1.2804E+04	1.2802E+04	1.2800E+04	1.2798E+04	1.2796E+04
10	1.1571E+04	1.1417E+04	1.1416E+04	1.1415E+04	1.1414E+04	1.1412E+04	1.1410E+04	1.1409E+04	1.1407E+04	1.1405E+04
11	1.0167E+04	1.0277E+04	1.0276E+04	1.0275E+04	1.0275E+04	1.0273E+04	1.0271E+04	1.0270E+04	1.0269E+04	1.0267E+04
12	9.3278E+03	9.3272E+03	9.3262E+03	9.3255E+03	9.3250E+03	9.3236E+03	9.3223E+03	9.3210E+03	9.3198E+03	9.3187E+03
13	8.5251E+03	8.5232E+03	8.5224E+03	8.5218E+03	8.5215E+03	8.5202E+03	8.5191E+03	8.5180E+03	8.5169E+03	8.5159E+03
14	7.8351E+03	7.8341E+03	7.8335E+03	7.8330E+03	7.8326E+03	7.8316E+03	7.8305E+03	7.8296E+03	7.8286E+03	7.8277E+03
15	7.2381E+03	7.2369E+03	7.2363E+03	7.2359E+03	7.2356E+03	7.2347E+03	7.2338E+03	7.2329E+03	7.2320E+03	7.2312E+03
16	6.7148E+03	6.7142E+03	6.7137E+03	6.7134E+03	6.7132E+03	6.7124E+03	6.7115E+03	6.7107E+03	6.7100E+03	6.7093E+03
17	6.2528E+03	6.2531E+03	6.2527E+03	6.2524E+03	6.2522E+03	6.2514E+03	6.2507E+03	6.2500E+03	6.2493E+03	6.2486E+03
18	5.8440E+03	5.8432E+03	5.8428E+03	5.8426E+03	5.8425E+03	5.8417E+03	5.8411E+03	5.8404E+03	5.8398E+03	5.8392E+03
19	5.4767E+03	5.4764E+03	5.4761E+03	5.4759E+03	5.4758E+03	5.4751E+03	5.4745E+03	5.4739E+03	5.4733E+03	5.4728E+03
20	5.1468E+03	5.1462E+03	5.1460E+03	5.1458E+03	5.1458E+03	5.1451E+03	5.1446E+03	5.1440E+03	5.1435E+03	5.1430E+03

**Table 5.8 Expected draining Gravity flow rate (m<sup>3</sup>/s) for different web tension (1 g/L input solution)**

web velocity (in/min) simulated height	1	2	3	4	5	6	7	8	9	10
0	5.8509E-06	8.7766E-06	1.1125E-05	1.3164E-05	1.4998E-05	1.6685E-05	1.8258E-05	1.9739E-05	2.1146E-05	2.2488E-05
5	5.9094E-06	8.8644E-06	1.1237E-05	1.3295E-05	1.5148E-05	1.6852E-05	1.8440E-05	1.9937E-05	2.1357E-05	2.2713E-05
10	5.9386E-06	8.9083E-06	1.1292E-05	1.3361E-05	1.5223E-05	1.6935E-05	1.8532E-05	2.0035E-05	2.1463E-05	2.2825E-05
15	5.9562E-06	8.9346E-06	1.1326E-05	1.3401E-05	1.5268E-05	1.6985E-05	1.8586E-05	2.0095E-05	2.1526E-05	2.2893E-05
20	5.9679E-06	8.9521E-06	1.1348E-05	1.3427E-05	1.5298E-05	1.7019E-05	1.8623E-05	2.0134E-05	2.1569E-05	2.2938E-05

**Table 5.9 Expected draining Capillary flow rate (m<sup>3</sup>/s) for different web tension (1 g/L input solution)**

web velocity (in/min) simulated height	1	2	3	4	5	6	7	8	9	10
0	1.3217E-06	1.9833E-06	2.5148E-06	2.9762E-06	3.3917E-06	3.7739E-06	4.1305E-06	4.4664E-06	4.7854E-06	5.0900E-06
5	1.3307E-06	2.0009E-06	2.5399E-06	3.0081E-06	3.4300E-06	3.8181E-06	4.1803E-06	4.5217E-06	4.8459E-06	5.1555E-06
10	1.3425E-06	2.0219E-06	2.5689E-06	3.0445E-06	3.4730E-06	3.8674E-06	4.2355E-06	4.5826E-06	4.9122E-06	5.2270E-06
15	1.3554E-06	2.0444E-06	2.5997E-06	3.0827E-06	3.5181E-06	3.9190E-06	4.2932E-06	4.6461E-06	4.9813E-06	5.3014E-06
20	1.3688E-06	2.0677E-06	2.6315E-06	3.1221E-06	3.5646E-06	3.9720E-06	4.3525E-06	4.7113E-06	5.0521E-06	5.3777E-06

**Table 5.10 Expected output algae mass flow rate (kg/s) for different web tension (1 g/L input solution)**

web velocity (in/min) simulated height	1	2	3	4	5	6	7	8	9	10
0	5.8567E-06	8.7854E-06	1.1137E-05	1.3177E-05	1.5013E-05	1.6702E-05	1.8276E-05	1.9759E-05	2.1167E-05	2.2510E-05
5	5.9153E-06	8.8732E-06	1.1248E-05	1.3309E-05	1.5163E-05	1.6869E-05	1.8459E-05	1.9957E-05	2.1378E-05	2.2736E-05
10	5.9446E-06	8.9172E-06	1.1304E-05	1.3375E-05	1.5238E-05	1.6952E-05	1.8550E-05	2.0056E-05	2.1484E-05	2.2848E-05
15	5.9622E-06	8.9435E-06	1.1337E-05	1.3414E-05	1.5283E-05	1.7002E-05	1.8605E-05	2.0115E-05	2.1548E-05	2.2916E-05
20	5.9739E-06	8.9611E-06	1.1359E-05	1.3440E-05	1.5314E-05	1.7036E-05	1.8642E-05	2.0154E-05	2.1590E-05	2.2961E-05

**Table 5.11 Airflow (klb/hr) requirements for heater to dry algae for different web tension (1 g/L input solution)**

web velocity (in/min) concentration (g/L)	1	2	3	4	5	6	7	8	9	10
0	0.0356	0.0533	0.0675	0.0799	0.0909	0.1011	0.1106	0.1195	0.1280	0.1360
5	0.0362	0.0540	0.0682	0.0805	0.0916	0.1017	0.1111	0.1200	0.1284	0.1364
10	0.0360	0.0535	0.0674	0.0794	0.0902	0.1000	0.1092	0.1178	0.1260	0.1338
15	0.0355	0.0525	0.0660	0.0776	0.0880	0.0975	0.1063	0.1146	0.1225	0.1300
20	0.0348	0.0512	0.0642	0.0754	0.0853	0.0945	0.1029	0.1109	0.1184	0.1256

**Table 5.12 Heating energy requirements for heating air (kBtu/hr) for different web tension (1 g/L input solution)**

web velocity (in/min) concentration (g/L)	1	2	3	4	5	6	7	8	9	10
0	5.7659	8.6410	10.9457	12.9430	14.7386	16.3873	17.9231	19.3686	20.7392	22.0464
5	5.8714	8.7535	11.0561	13.0480	14.8365	16.4771	18.0043	19.4407	20.8021	22.1000
10	5.8412	8.6692	10.9217	12.8668	14.6114	16.2101	17.6973	19.0953	20.4196	21.6817
15	5.7566	8.5053	10.6878	12.5691	14.2543	15.7971	17.2312	18.5784	19.8540	21.0690
20	5.6445	8.3009	10.4031	12.2114	13.8290	15.3083	16.6822	17.9721	19.1926	20.3545

**Table 5.13 Energy efficiency (kBtu/lb of dried algae) for different web tension (1 g/L input solution)**

web velocity (in/min) concentration (g/L)	1	2	3	4	5	6	7	8	9	10
0	1.2415E+05	1.2404E+05	1.2395E+05	1.2387E+05	1.2380E+05	1.2374E+05	1.2368E+05	1.2362E+05	1.2356E+05	1.2351E+05
5	1.2518E+05	1.2441E+05	1.2396E+05	1.2364E+05	1.2339E+05	1.2318E+05	1.2301E+05	1.2285E+05	1.2271E+05	1.2259E+05
10	1.2392E+05	1.2260E+05	1.2185E+05	1.2132E+05	1.2092E+05	1.2059E+05	1.2031E+05	1.2007E+05	1.1986E+05	1.1967E+05
15	1.2176E+05	1.1993E+05	1.1889E+05	1.1817E+05	1.1762E+05	1.1717E+05	1.1680E+05	1.1648E+05	1.1620E+05	1.1595E+05
20	1.1916E+05	1.1682E+05	1.1549E+05	1.1458E+05	1.1389E+05	1.1332E+05	1.1286E+05	1.1246E+05	1.1211E+05	1.1180E+05

**Table 5.14 Expected draining Gravity flow rate (m<sup>3</sup>/s) for different web tension (10 g/L input solution)**

web velocity (in/min) simulated height	1	2	3	4	5	6	7	8	9	10
0	1.5278E-06	2.2814E-06	2.8925E-06	3.4229E-06	3.9004E-06	4.3395E-06	4.7492E-06	5.1351E-06	5.5014E-06	5.8512E-06
5	1.5385E-06	2.2974E-06	2.9127E-06	3.4468E-06	3.9277E-06	4.3699E-06	4.7824E-06	5.1710E-06	5.5400E-06	5.8922E-06
10	1.5477E-06	2.3111E-06	2.9301E-06	3.4674E-06	3.9511E-06	4.3959E-06	4.8109E-06	5.2018E-06	5.5730E-06	5.9273E-06
15	1.5553E-06	2.3225E-06	2.9445E-06	3.4845E-06	3.9706E-06	4.4176E-06	4.8346E-06	5.2275E-06	5.6005E-06	5.9566E-06
20	1.5614E-06	2.3316E-06	2.9561E-06	3.4982E-06	3.9862E-06	4.4350E-06	4.8536E-06	5.2481E-06	5.6225E-06	5.9800E-06

**Table 5.15 Expected draining Capillary flow rate (m<sup>3</sup>/s) for different web tension (10 g/L input solution)**

web velocity (in/min) simulated height	1	2	3	4	5	6	7	8	9	10
0	3.4331E-07	5.1510E-07	6.5310E-07	7.7289E-07	8.8073E-07	9.7995E-07	1.0725E-06	1.1597E-06	1.2425E-06	1.3216E-06
5	3.4398E-07	5.1704E-07	6.5626E-07	7.7724E-07	8.8623E-07	9.8655E-07	1.0802E-06	1.1684E-06	1.2523E-06	1.3323E-06
10	3.4485E-07	5.1923E-07	6.5972E-07	7.8191E-07	8.9207E-07	9.9353E-07	1.0883E-06	1.1776E-06	1.2625E-06	1.3435E-06
15	3.4590E-07	5.2166E-07	6.6346E-07	7.8691E-07	8.9829E-07	1.0009E-06	1.0968E-06	1.1872E-06	1.2731E-06	1.3552E-06
20	3.4715E-07	5.2435E-07	6.6752E-07	7.9227E-07	9.0488E-07	1.0087E-06	1.1057E-06	1.1973E-06	1.2843E-06	1.3675E-06

**Table 5.16 Expected output algae mass flow rate (kg/s) for different web tension (10 g/L input solution)**

web velocity (in/min) simulated height	1	2	3	4	5	6	7	8	9	10
0	1.5432E-05	2.3045E-05	2.9217E-05	3.4575E-05	3.9398E-05	4.3834E-05	4.7971E-05	5.1870E-05	5.5570E-05	5.9104E-05
5	1.5540E-05	2.3206E-05	2.9421E-05	3.4817E-05	3.9674E-05	4.4140E-05	4.8307E-05	5.2233E-05	5.5959E-05	5.9517E-05
10	1.5633E-05	2.3344E-05	2.9597E-05	3.5024E-05	3.9910E-05	4.4404E-05	4.8595E-05	5.2544E-05	5.6293E-05	5.9872E-05
15	1.5710E-05	2.3459E-05	2.9743E-05	3.5197E-05	4.0107E-05	4.4623E-05	4.8835E-05	5.2803E-05	5.6570E-05	6.0167E-05
20	1.5772E-05	2.3552E-05	2.9860E-05	3.5335E-05	4.0265E-05	4.4798E-05	4.9027E-05	5.3011E-05	5.6793E-05	6.0404E-05

**Table 5.17 Airflow (klb/hr) requirements for heater to dry algae for different web tension (10 g/L input solution)**

web velocity (in/min) concentration (g/L)	1	2	3	4	5	6	7	8	9	10
0	8.7227E-03	1.2852E-02	1.6292E-02	1.9278E-02	2.1966E-02	2.4435E-02	2.6737E-02	2.8906E-02	3.0963E-02	3.2928E-02
5	8.9061E-03	1.3060E-02	1.6506E-02	1.9488E-02	2.2167E-02	2.4624E-02	2.6912E-02	2.9065E-02	3.1106E-02	3.3053E-02
10	9.0433E-03	1.3201E-02	1.6636E-02	1.9601E-02	2.2259E-02	2.4692E-02	2.6956E-02	2.9083E-02	3.1098E-02	3.3019E-02
15	9.1339E-03	1.3276E-02	1.6684E-02	1.9617E-02	2.2241E-02	2.4639E-02	2.6867E-02	2.8959E-02	3.0938E-02	3.2823E-02
20	9.1777E-03	1.3282E-02	1.6647E-02	1.9534E-02	2.2111E-02	2.4463E-02	2.6644E-02	2.8690E-02	3.0624E-02	3.2463E-02

**Table 5.18 Heating energy (kBtu/hr) requirements for heating air for different web tension (10 g/L input solution)**

web velocity (in/min) concentration (g/L)	1	2	3	4	5	6	7	8	9	10
0	1.4159	2.0863	2.6448	3.1294	3.5658	3.9666	4.3403	4.6923	5.0264	5.3453
5	1.4457	2.1200	2.6794	3.1635	3.5984	3.9973	4.3687	4.7182	5.0496	5.3656
10	1.4679	2.1430	2.7006	3.1819	3.6134	4.0084	4.3759	4.7212	5.0484	5.3601
15	1.4826	2.1550	2.7083	3.1844	3.6105	3.9999	4.3616	4.7011	5.0225	5.3284
20	1.4897	2.1561	2.7023	3.1710	3.5895	3.9713	4.3255	4.6576	4.9716	5.2703

**Table 5.19 Energy efficiency (kBtu/lb of dried algae) for different web tension (10 g/L input solution)**

web velocity (in/min) concentration (g/L)	1	2	3	4	5	6	7	8	9	10
0	1.1571E+04	1.1417E+04	1.1416E+04	1.1415E+04	1.1414E+04	1.1412E+04	1.1410E+04	1.1409E+04	1.1407E+04	1.1405E+04
5	1.1732E+04	1.1521E+04	1.1485E+04	1.1459E+04	1.1438E+04	1.1420E+04	1.1405E+04	1.1392E+04	1.1380E+04	1.1369E+04
10	1.1842E+04	1.1577E+04	1.1507E+04	1.1457E+04	1.1418E+04	1.1384E+04	1.1356E+04	1.1331E+04	1.1310E+04	1.1290E+04
15	1.1902E+04	1.1585E+04	1.1483E+04	1.1410E+04	1.1353E+04	1.1304E+04	1.1263E+04	1.1228E+04	1.1196E+04	1.1168E+04
20	1.1912E+04	1.1545E+04	1.1413E+04	1.1317E+04	1.1242E+04	1.1180E+04	1.1126E+04	1.1080E+04	1.1040E+04	1.1003E+04

**Table 5.20 Expected draining Gravity flow rate (m<sup>3</sup>/s) for different web tension (20 g/L input solution)**

web velocity (in/min) simulated height	1	2	3	4	5	6	7	8	9	10
0	1.0135E-06	1.5206E-06	1.9279E-06	2.2815E-06	2.5998E-06	2.8926E-06	3.1656E-06	3.4229E-06	3.6672E-06	3.9004E-06
5	1.0135E-06	1.5206E-06	1.9279E-06	2.2815E-06	2.5998E-06	2.8926E-06	3.1656E-06	3.4229E-06	3.6672E-06	3.9004E-06
10	1.0186E-06	1.5282E-06	1.9376E-06	2.2929E-06	2.6128E-06	2.9070E-06	3.1815E-06	3.4401E-06	3.6855E-06	3.9199E-06
15	1.0226E-06	1.5343E-06	1.9453E-06	2.3020E-06	2.6232E-06	2.9186E-06	3.1941E-06	3.4537E-06	3.7002E-06	3.9355E-06
20	1.0257E-06	1.5389E-06	1.9511E-06	2.3089E-06	2.6310E-06	2.9273E-06	3.2036E-06	3.4640E-06	3.7112E-06	3.9472E-06

**Table 5.21 Expected draining Capillary flow rate (m<sup>3</sup>/s) for different web tension (20 g/L input solution)**

web velocity (in/min) simulated height	1	2	3	4	5	6	7	8	9	10
0	2.2880E-07	3.4329E-07	4.3525E-07	5.1508E-07	5.8695E-07	6.5307E-07	7.1475E-07	7.7287E-07	8.2804E-07	8.8073E-07
5	2.3004E-07	3.4556E-07	4.3846E-07	5.1917E-07	5.9186E-07	6.5877E-07	7.2121E-07	7.8006E-07	8.3594E-07	8.8932E-07
10	2.3044E-07	3.4667E-07	4.4028E-07	5.2168E-07	5.9505E-07	6.6261E-07	7.2569E-07	7.8517E-07	8.4168E-07	8.9566E-07
15	2.3098E-07	3.4798E-07	4.4233E-07	5.2445E-07	5.9852E-07	6.6677E-07	7.3051E-07	7.9064E-07	8.4777E-07	9.0237E-07
20	2.3167E-07	3.4948E-07	4.4462E-07	5.2749E-07	6.0229E-07	6.7124E-07	7.3567E-07	7.9647E-07	8.5426E-07	9.0949E-07



**Table 5.22 Expected output algae mass flow rate (kg/s) for different web tension (20 g/L input solution)**

web velocity (in/min) simulated height	1	2	3	4	5	6	7	8	9	10
0	2.0684E-05	3.1033E-05	3.9345E-05	4.6561E-05	5.3058E-05	5.9032E-05	6.4605E-05	6.9856E-05	7.4841E-05	7.9600E-05
4	2.0684E-05	3.1033E-05	3.9345E-05	4.6561E-05	5.3058E-05	5.9032E-05	6.4605E-05	6.9856E-05	7.4841E-05	7.9600E-05
8	2.0787E-05	3.1188E-05	3.9542E-05	4.6794E-05	5.3323E-05	5.9327E-05	6.4928E-05	7.0205E-05	7.5215E-05	7.9998E-05
12	2.0870E-05	3.1312E-05	3.9699E-05	4.6980E-05	5.3535E-05	5.9563E-05	6.5186E-05	7.0485E-05	7.5514E-05	8.0316E-05
16	2.0932E-05	3.1405E-05	3.9817E-05	4.7120E-05	5.3694E-05	5.9740E-05	6.5380E-05	7.0694E-05	7.5739E-05	8.0555E-05

**Table 5.23 Airflow (klb/hr) requirements for heater to dry algae for different web tension (20 g/L input solution)**

web velocity (in/min) concentration (g/L)	1	2	3	4	5	6	7	8	9	10
0	5.1879E-03	7.7829E-03	9.8672E-03	1.1676E-02	1.3305E-02	1.4802E-02	1.6197E-02	1.7512E-02	1.8760E-02	1.9951E-02
5	5.1000E-03	7.6221E-03	9.6400E-03	1.1387E-02	1.2958E-02	1.4398E-02	1.5740E-02	1.7003E-02	1.8201E-02	1.9343E-02
10	5.1789E-03	7.7041E-03	9.7148E-03	1.1450E-02	1.3007E-02	1.4431E-02	1.5756E-02	1.7002E-02	1.8182E-02	1.9306E-02
15	5.2261E-03	7.7401E-03	9.7325E-03	1.1447E-02	1.2980E-02	1.4381E-02	1.5683E-02	1.6904E-02	1.8059E-02	1.9159E-02
20	5.2415E-03	7.7299E-03	9.6926E-03	1.1376E-02	1.2878E-02	1.4248E-02	1.5518E-02	1.6708E-02	1.7833E-02	1.8902E-02

**Table 5.24 Heating energy (kBtu/hr) requirements for heating air for different web tension (20 g/L input solution)**

web velocity (in/min) concentration (g/L)	1	2	3	4	5	6	7	8	9	10
0	0.8441	1.2664	1.6055	1.8999	2.1649	2.4084	2.6355	2.8494	3.0524	3.2462
5	0.8299	1.2403	1.5687	1.8530	2.1086	2.3430	2.5614	2.7669	2.9618	3.1477
10	0.8427	1.2536	1.5808	1.8633	2.1165	2.3484	2.5641	2.7668	2.9588	3.1417
15	0.8503	1.2595	1.5837	1.8627	2.1123	2.3404	2.5522	2.7510	2.9390	3.1181
20	0.8528	1.2578	1.5773	1.8513	2.0958	2.3188	2.5255	2.7192	2.9023	3.0764

**Table 5.25 Energy efficiency (kBtu/lb of dried algae) for different web tension (20 g/L input solution)**

web velocity (in/min) concentration (g/L)	1	2	3	4	5	6	7	8	9	10
0	5.1468E+03	5.1462E+03	5.1460E+03	5.1458E+03	5.1458E+03	5.1451E+03	5.1446E+03	5.1440E+03	5.1435E+03	5.1430E+03
5	5.0599E+03	5.0403E+03	5.0280E+03	5.0190E+03	5.0119E+03	5.0055E+03	5.0000E+03	4.9951E+03	4.9908E+03	4.9869E+03
10	5.1124E+03	5.0691E+03	5.0417E+03	5.0216E+03	5.0057E+03	4.9921E+03	4.9803E+03	4.9701E+03	4.9609E+03	4.9527E+03
15	5.1384E+03	5.0726E+03	5.0309E+03	5.0002E+03	4.9759E+03	4.9552E+03	4.9375E+03	4.9220E+03	4.9083E+03	4.8959E+03
20	5.1382E+03	5.0510E+03	4.9956E+03	4.9547E+03	4.9223E+03	4.8949E+03	4.8714E+03	4.8509E+03	4.8326E+03	4.8163E+03

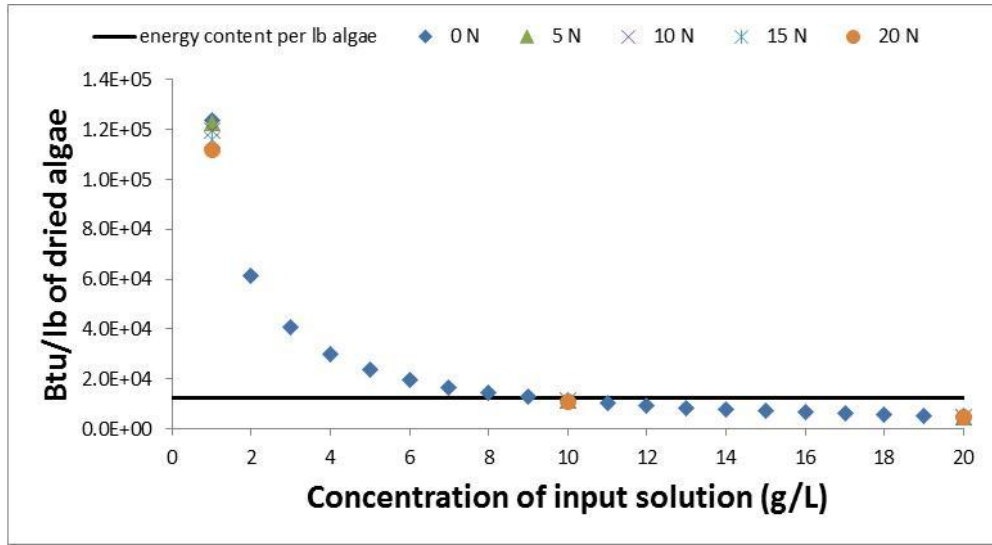


Fig. 5.5 Energy efficiency in different concentrations of input solution

## 5.2 Web tension control system simulation results

In this section, simulations of the web tension controller will be provided.

There are three different control algorithms to be compared in this study. A general SMC, and two SMCs with different saturation functions. SMC\_S represents the sliding mode controller with a linear saturation function, and SMC\_AS represents it with an automatically adjusted saturation function. Table 5.26 lists the parameters used for the simulation, and table 5.27 is the control gain and the control goal of each case. Figs. 5.6, 5.9, 5.12, 5.15, 5.18, 5.21, 5.24 and 5.27 show

the performance of the sliding mode controller in different cases. As indicated, there are some issues with control approach. The amplitude of chattering of controlled velocity is very high, and the tension overshoot is about 15% of the desired tension setpoint. From figs.5.7, 5.10, 5.13, 5.16, 5.19, 5.22, 5.25 and 5.28 show the performance of the sliding mode controller with a linear saturation function that has better performance than the general SMC especially in improving the chattering effect in controlled velocity. However, the tension overshoot still exists (7%). On the other hand, the performance of SMC\_AS as shown in Figs.5.8, 5.11, 5.14, 5.17, 5.20, 5.23, 5.26 and 5.29 can solve the chattering and overshoot problems. In addition, the transient response is improved and the settling time is about 250 times less than the other two methods. For the SMC\_S controller, changes in the web tension gain can improve the overshoot problem, but the settling time will still be significantly greater than for SMC\_AS. However with SMC\_S, if reduced settling time is necessary, the overshoot problem will be worse. Hence, SMC\_AS is a better solution.

In the real situation, there will be unexpected disturbances that may change the real tension. Fig.5.30 and Fig. 5.31 are the simulation results of performance of

the SMC\_S and SMC\_AS controllers with the inclusion of 30 dB white SNR noise. As illustrated, both of these methods can handle this situation very well. Although there is some chattering caused by noise, the controllers are able to control to the required set-point. Comparing the performance of the three methods, SMC\_AS is more appropriate for this study for the following reasons: (1) unexpected high web tension can cause the web to break, and (2) even if the material does not fail, characteristics of web material may change from this deformation and this can adversely affect the fluid dynamics. Therefore, for our study, the third method will be better choice.

**Table 5.26 Pre-set parameters of the web tension control system**

E	Plastic of elastic modules	396825(N/m <sup>2</sup> )
A	Cross section Area of the web	0.0001(m <sup>2</sup> )
$\rho$	Density of the web	1203.466(kg/m <sup>3</sup> )
$L_{jk}$	Length between jth and kth rollers	3 (m)
$L_{ij}$	Length between ith and jth rollers	1 (m)
$L_{ti}$	Length between ith roller and tail pulley	1.5 (m)
w	Width of the web	0.2 (m)
$R_i$	Radius of i-th roller	0.15 (m)
$R_j$	Radius of j-th roller	0.15 (m)
$R_k$	Radius of k-th roller	0.15 (m)
$R_m$	Radius of m-th roller	0.15 (m)
$R_l$	Radius of l-th roller	0.15 (m)
$R_t$	Radius of tail pulley	0.15 (m)
h	Thickness of the web	500 ( $\mu$ m)
$K_i$	velocity constant of i-th motor	27.54 (N.m/volt)
$K_j$	velocity constant of j-th motor	27.54 (N.m/volt)
$K_k$	velocity constant of k-th motor	0.2391 (N.m/volt)
$K_m$	velocity constant of m-th motor	0.2391 (N.m/volt)
$D_i$	Damper coefficient of i-th roller	0.002(N.m.sec)
$D_j$	Damper coefficient of j-th roller	0.002(N.m.sec)
$D_k$	Damper coefficient of k-th roller	0.002(N.m.sec)
$D_m$	Damper coefficient of m-th roller	0.002(N.m.sec)

**Table 5.27 Control Parameters**

	Case I	Case II	Case III	Case IV
Goals	T = 1N, $V_w = 1$ in/min	T = 1N, $V_w = 10$ in/min	T = 1N, $V_w = 20$ in/min	T = 10N, $V_w = 1$ in/min
Tension control gain	20	20	20	20
velocity control gain	2	2	2	2
	Case V	Case VI	Case VII	Case VIII
Goals	T = 10N, $V_w = 10$ in/min	T = 10N, $V_w = 20$ in/min	T = 20N, $V_w = 1$ in/min	T = 20N, $V_w = 20$ in/min
Tension control gain	20	20	20	20
velocity control gain	2	2	2	2

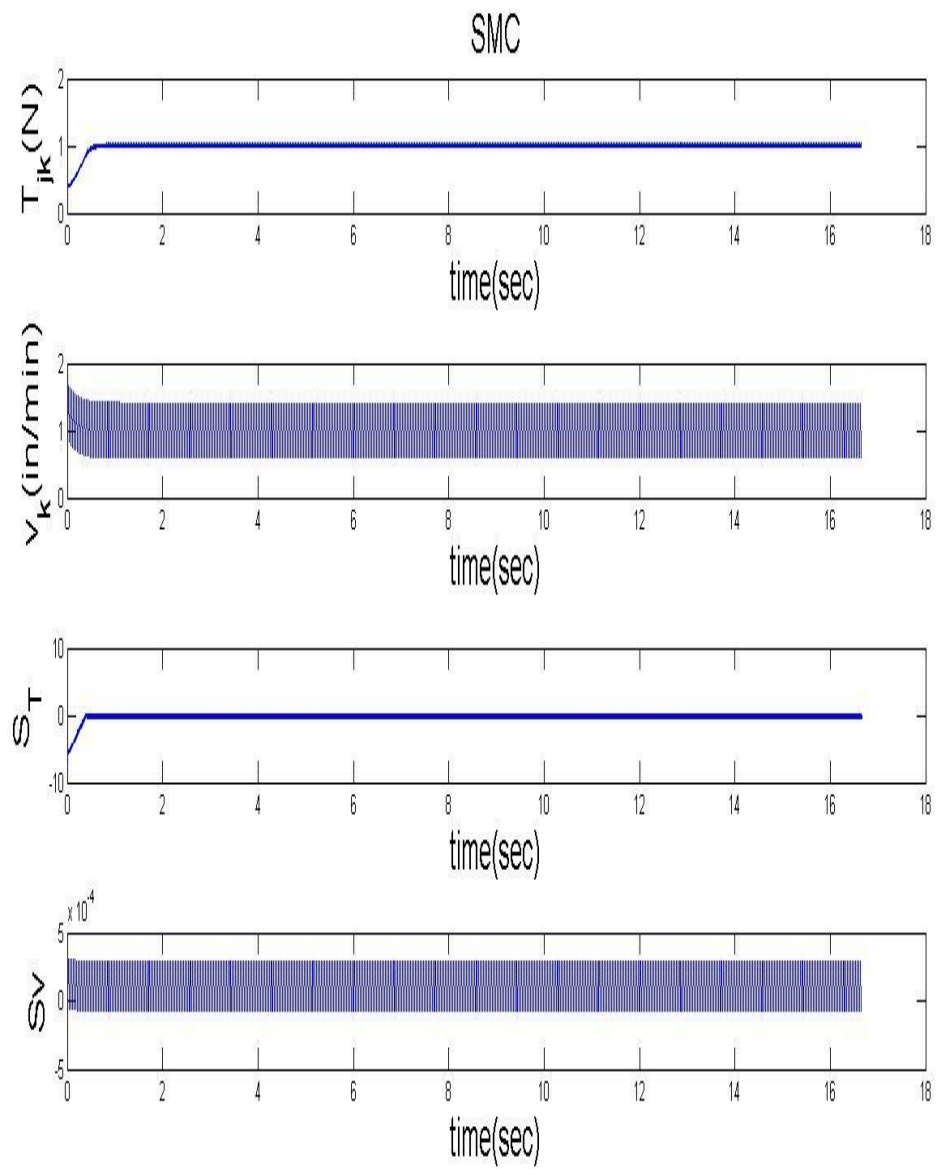


Fig .5.6 Performance of Sliding mode controller (1 N tension, 1 in/min transporting velocity)

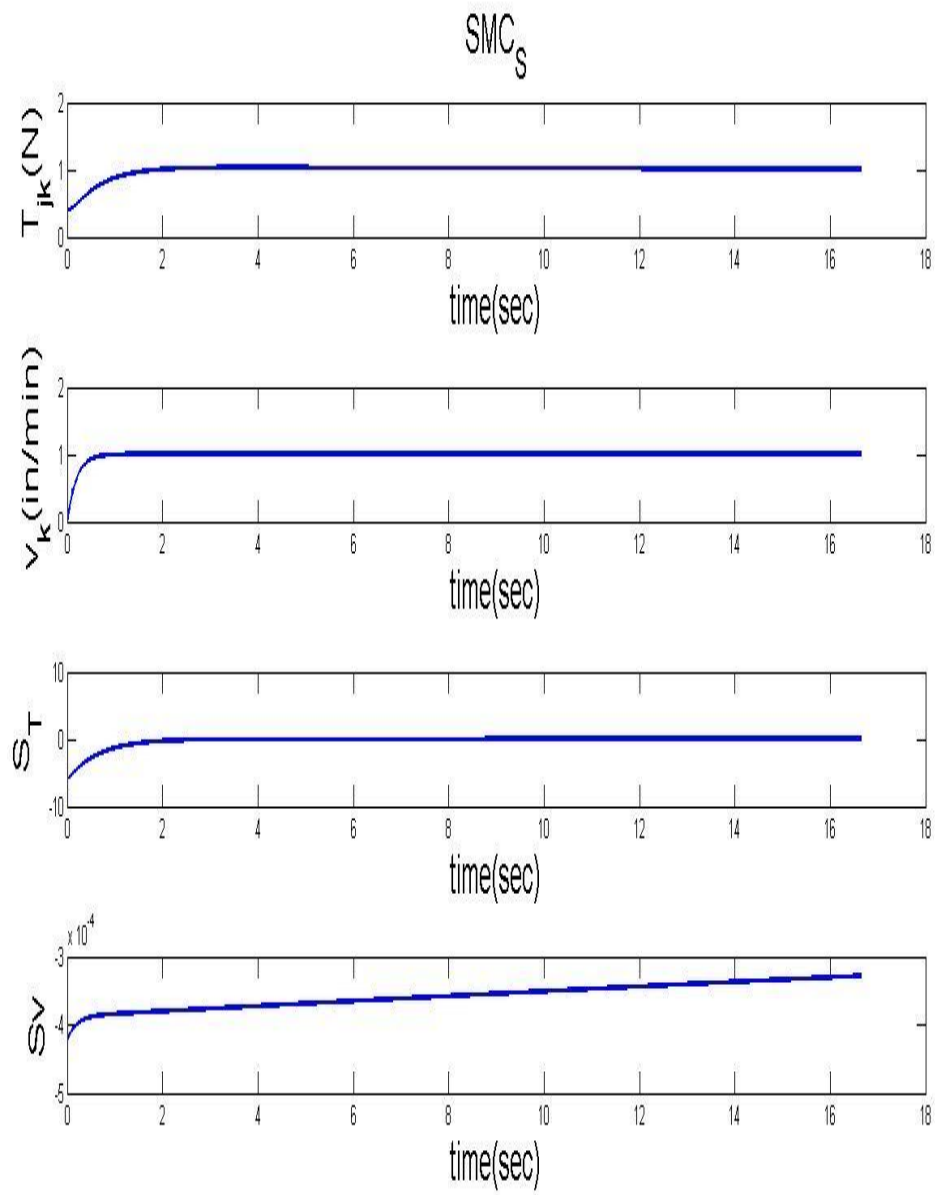


Fig. 5.7 Performance of  $SMC_S$  (1 N tension, 1 in/min transporting velocity)

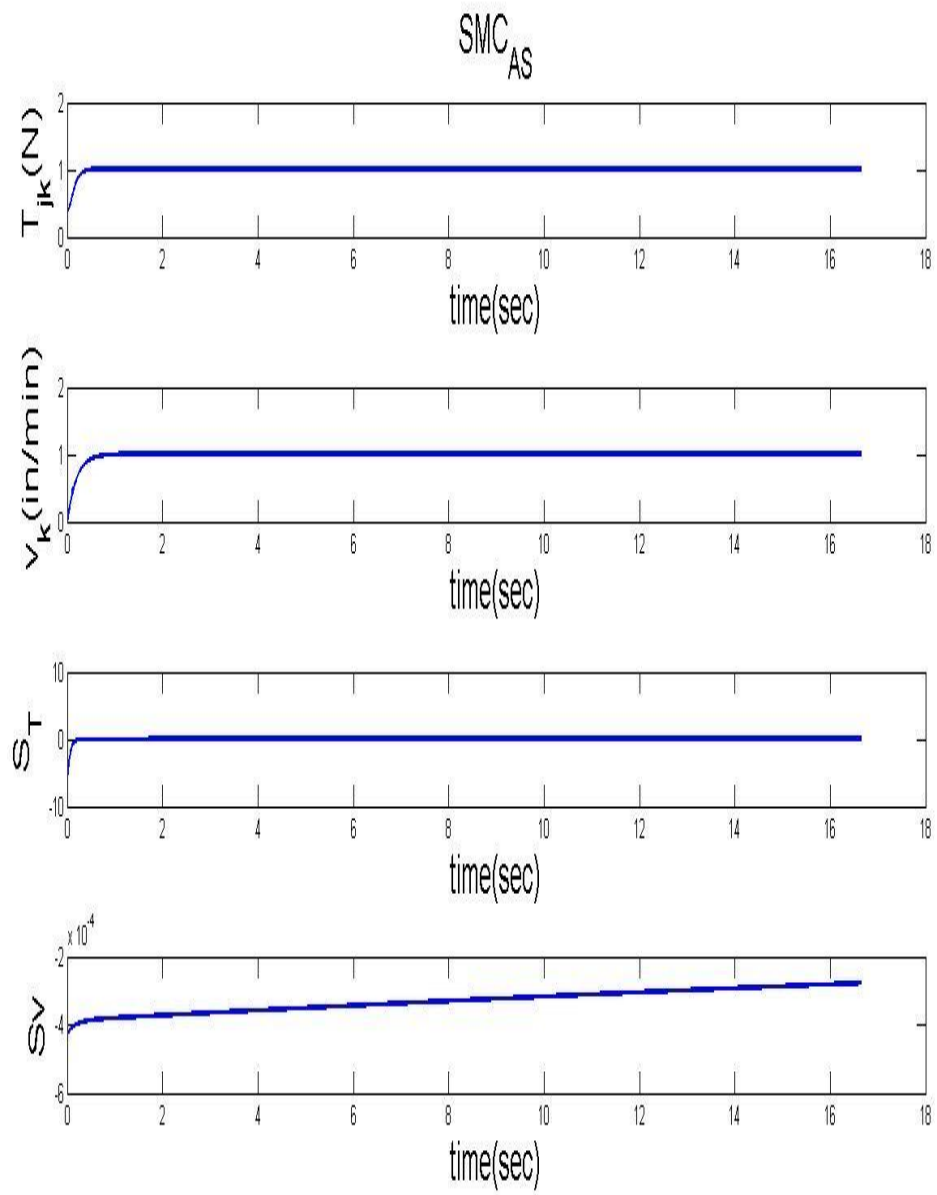


Fig. 5.8 Performance of  $SMC_{AS}$  (1 N tension, 1 in/min transporting velocity)



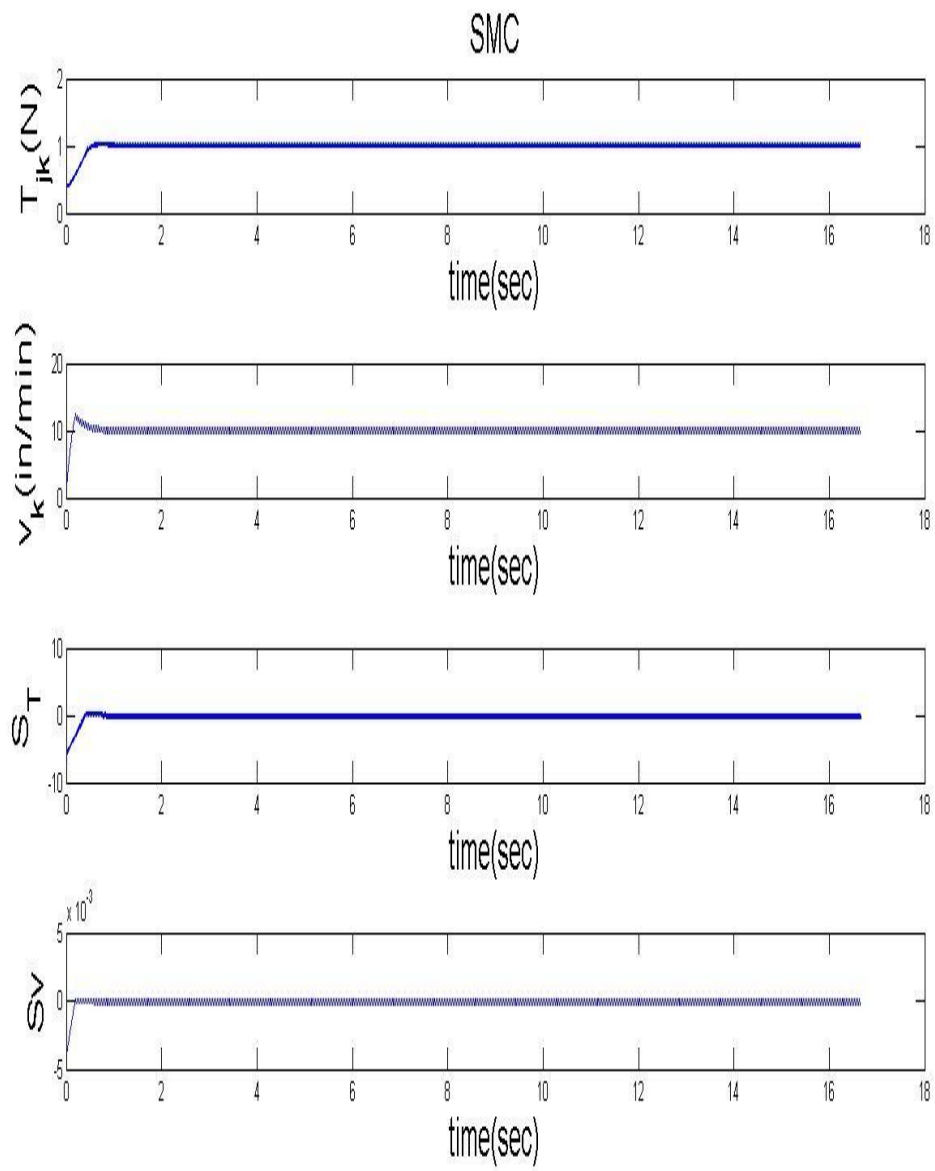


Fig. 5.9 Performance of SMC (1 N tension, 10 in/min transporting velocity)

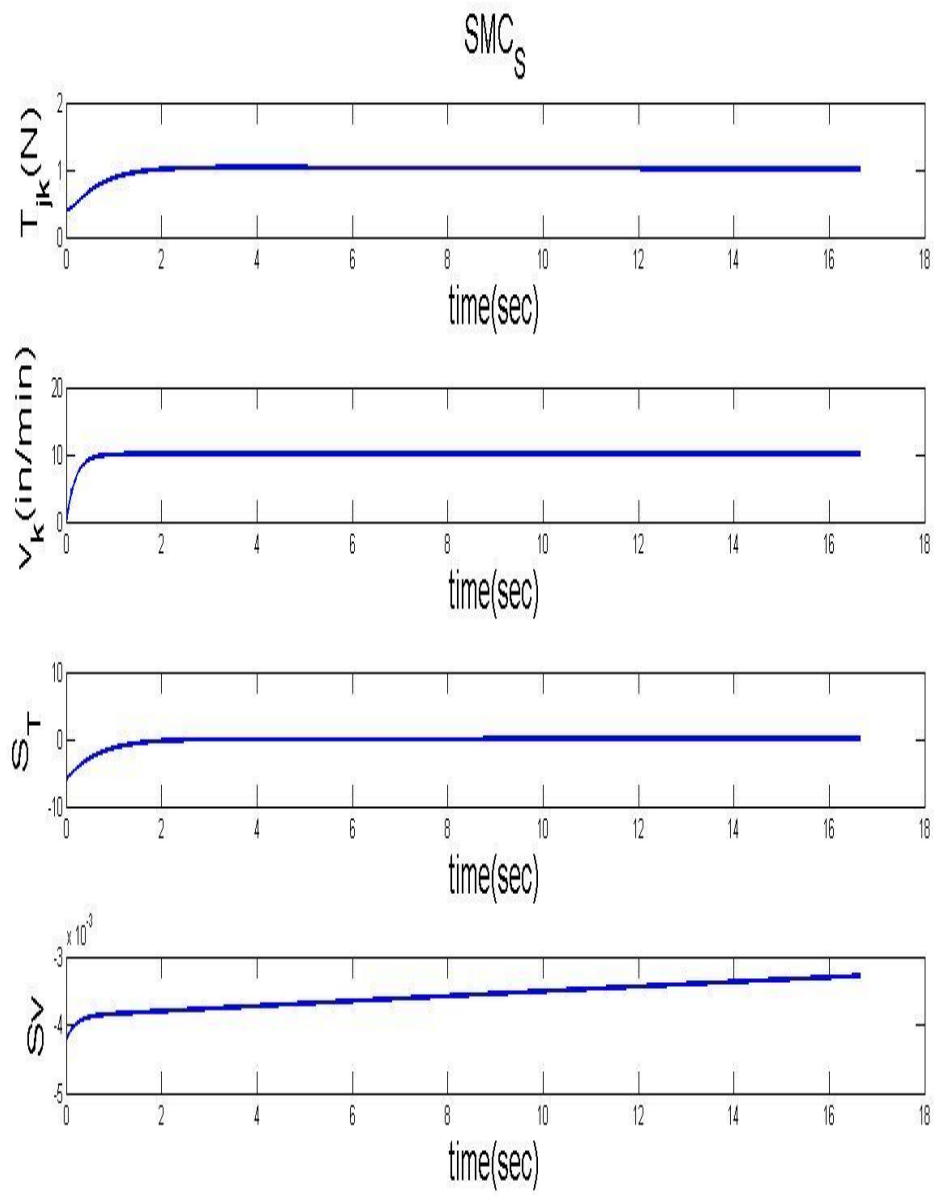


Fig. 5.10 Performance of  $SMC_S$  (1 N tension, 10 in/min transporting velocity)

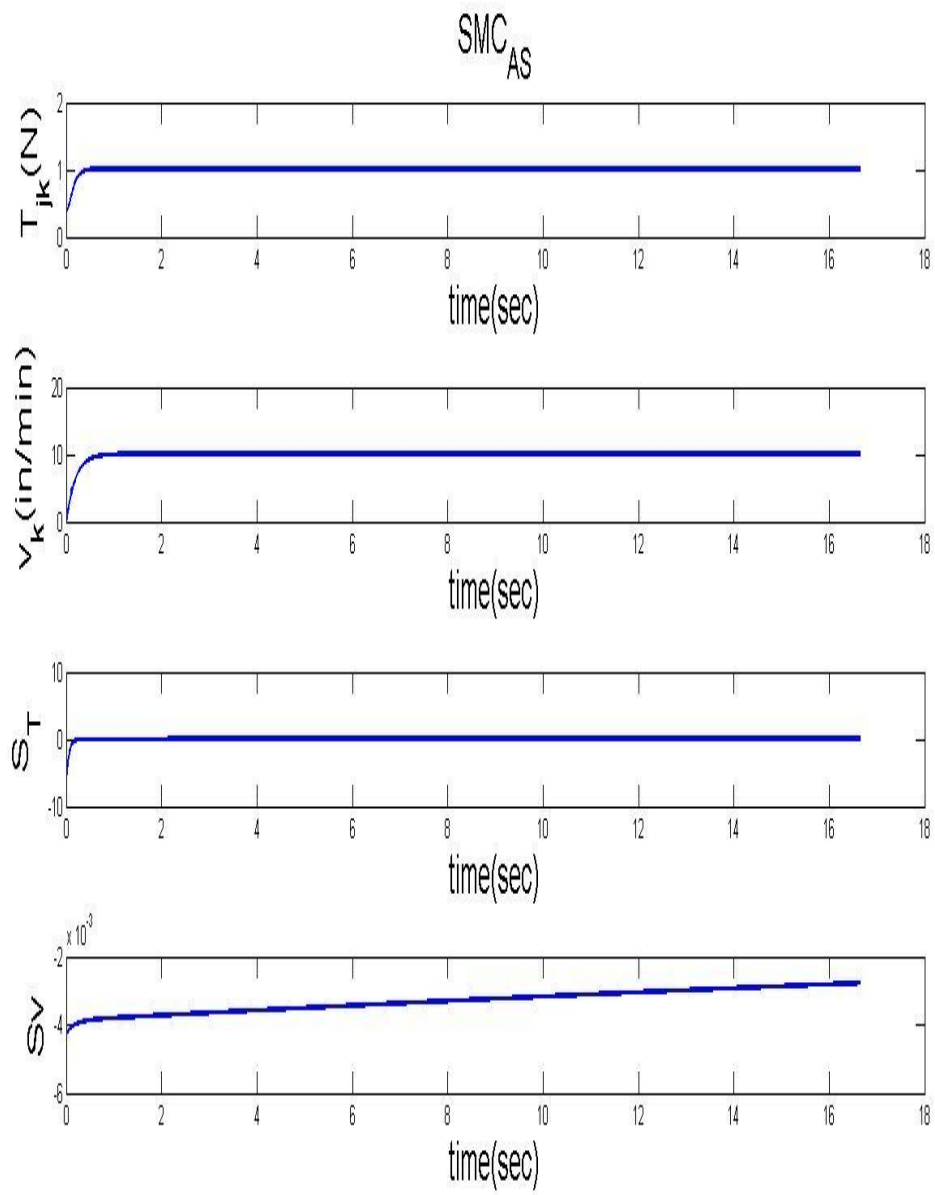


Fig. 5.11 Performance of  $SMC_{AS}$  (1 N tension, 10 in/min transporting velocity)

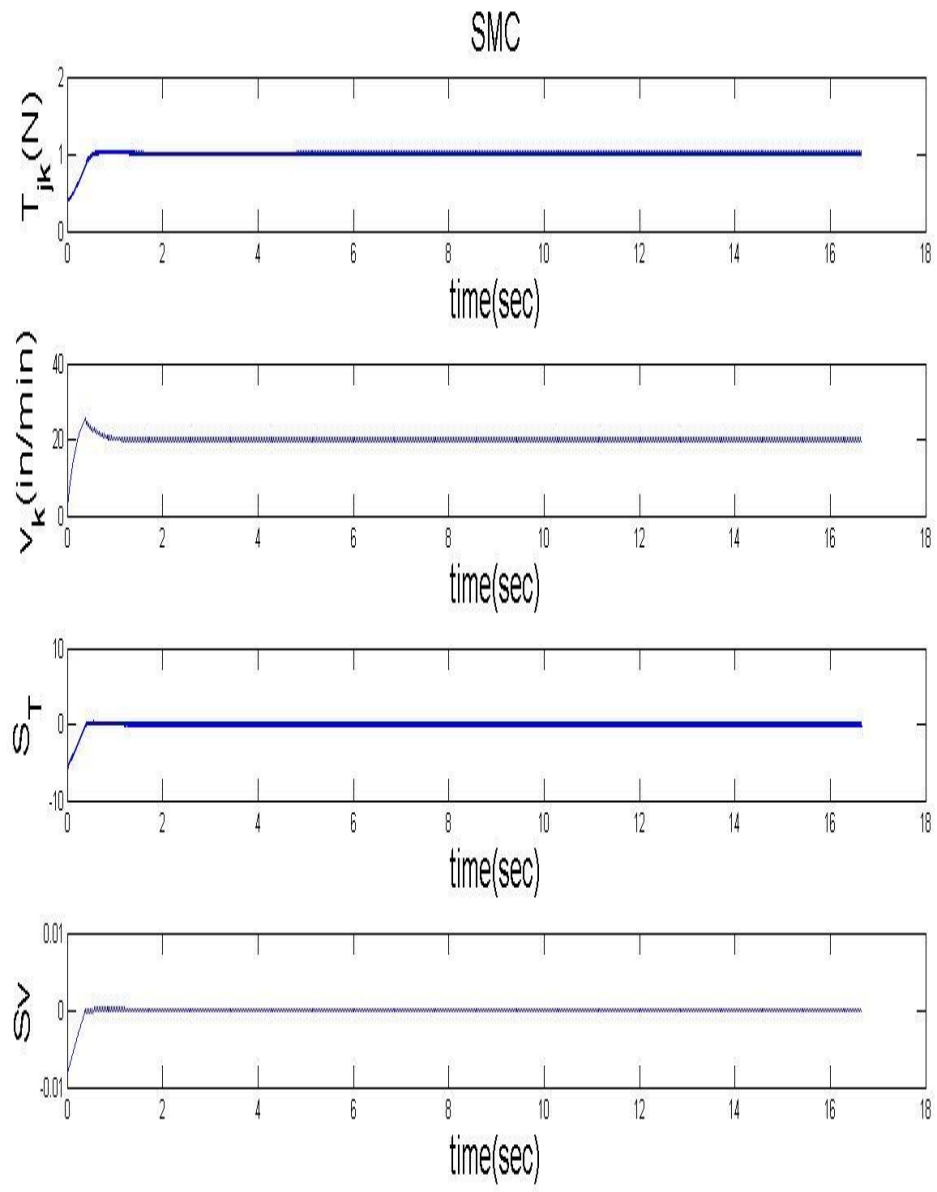


Fig. 5.12 Performance of SMC (1 N tension, 20 in/min transporting velocity)

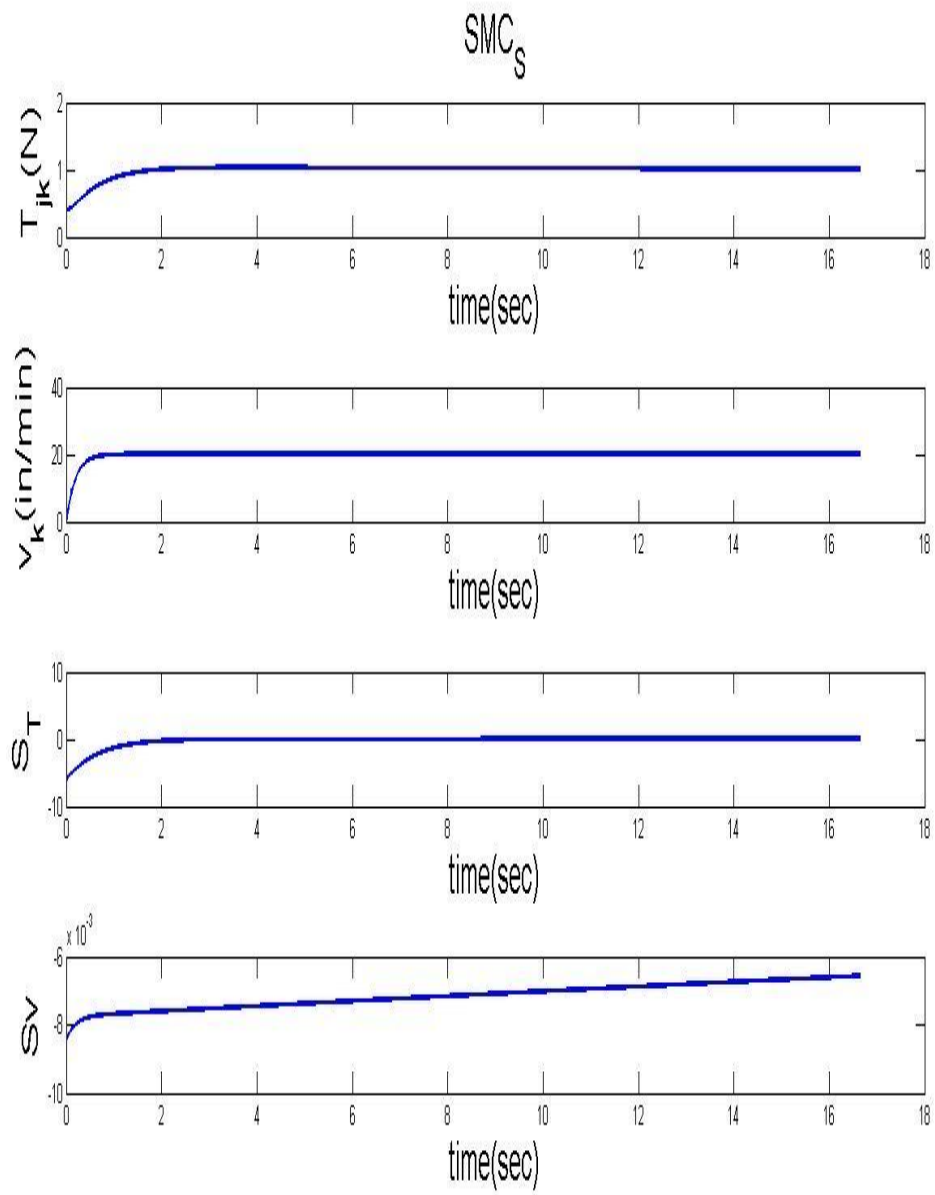


Fig. 5.13 Performance of  $SMC_S$  (1 N tension, 20 in/min transporting velocity)

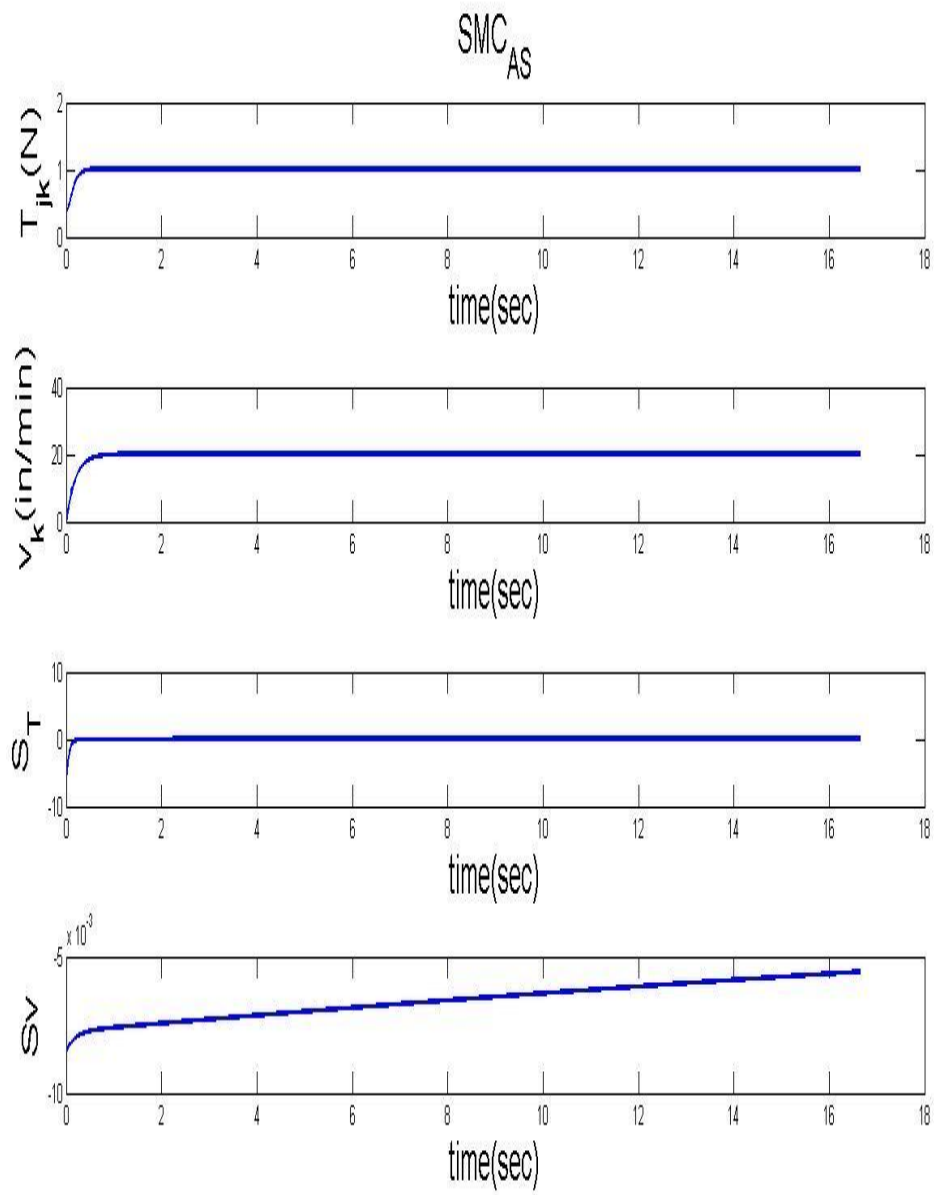


Fig. 5.14 Performance of  $SMC_{AS}$  (1 N tension, 20 in/min transporting velocity)

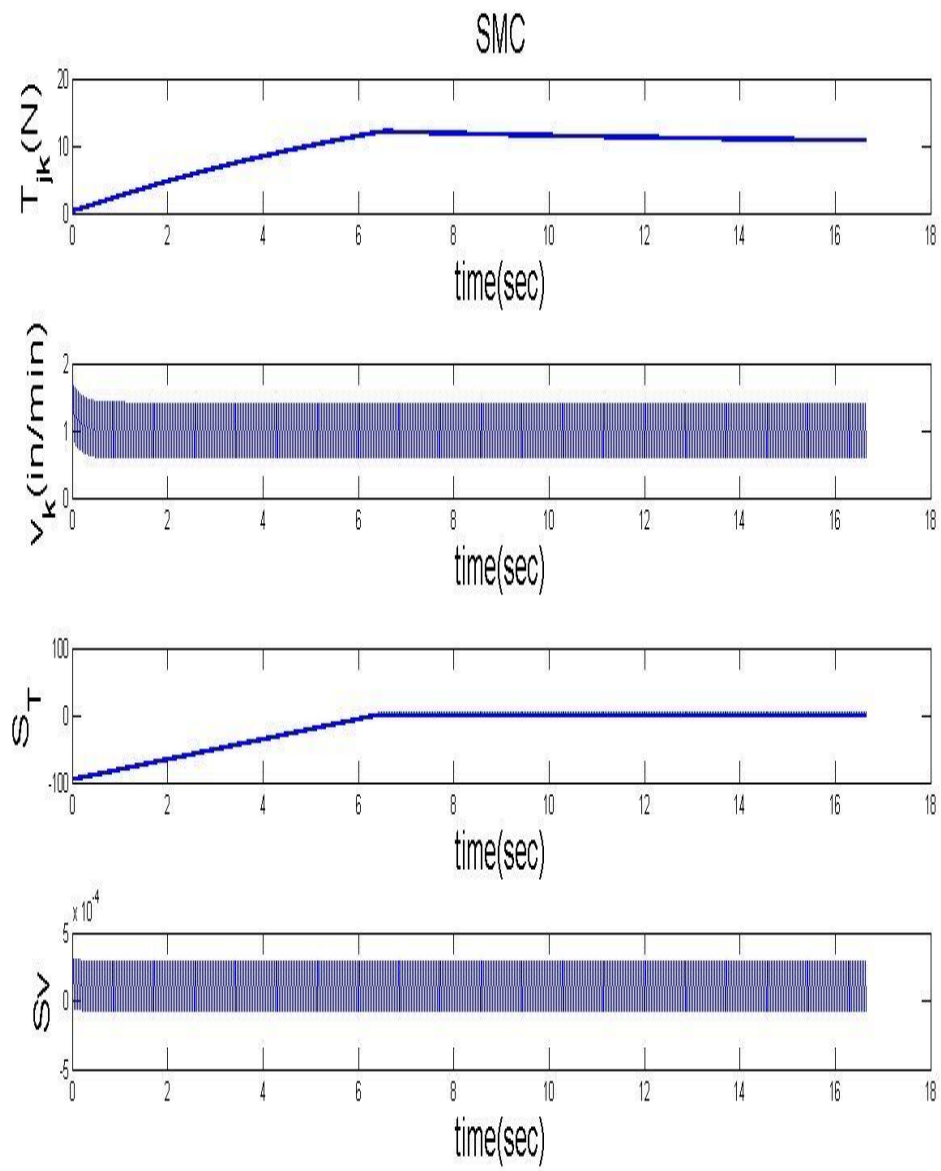


Fig. 5.15 Performance of SMC (10 N tension, 1 in/min transporting velocity)

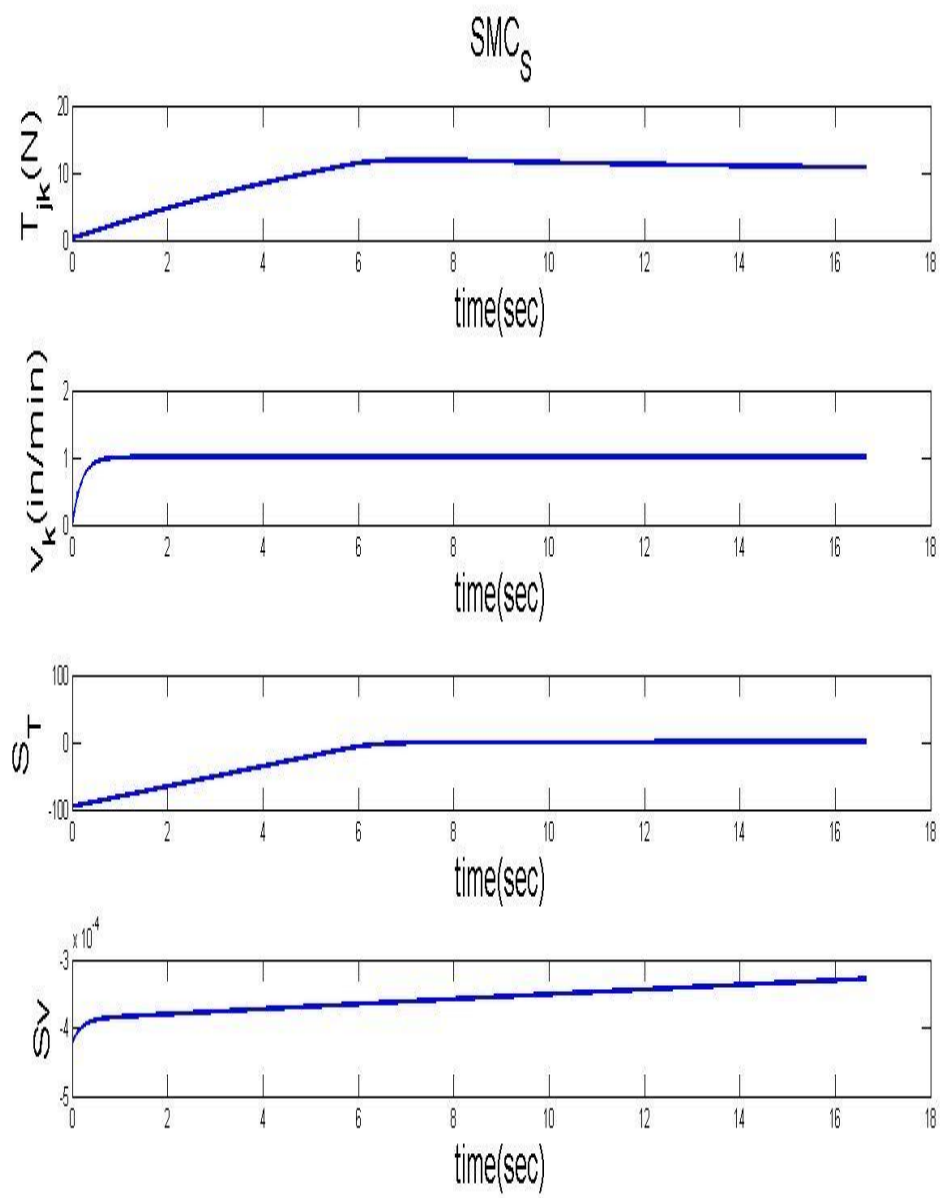


Fig. 5.16 Performance of  $SMC_S$  (10 N tension, 1 in/min transporting velocity)



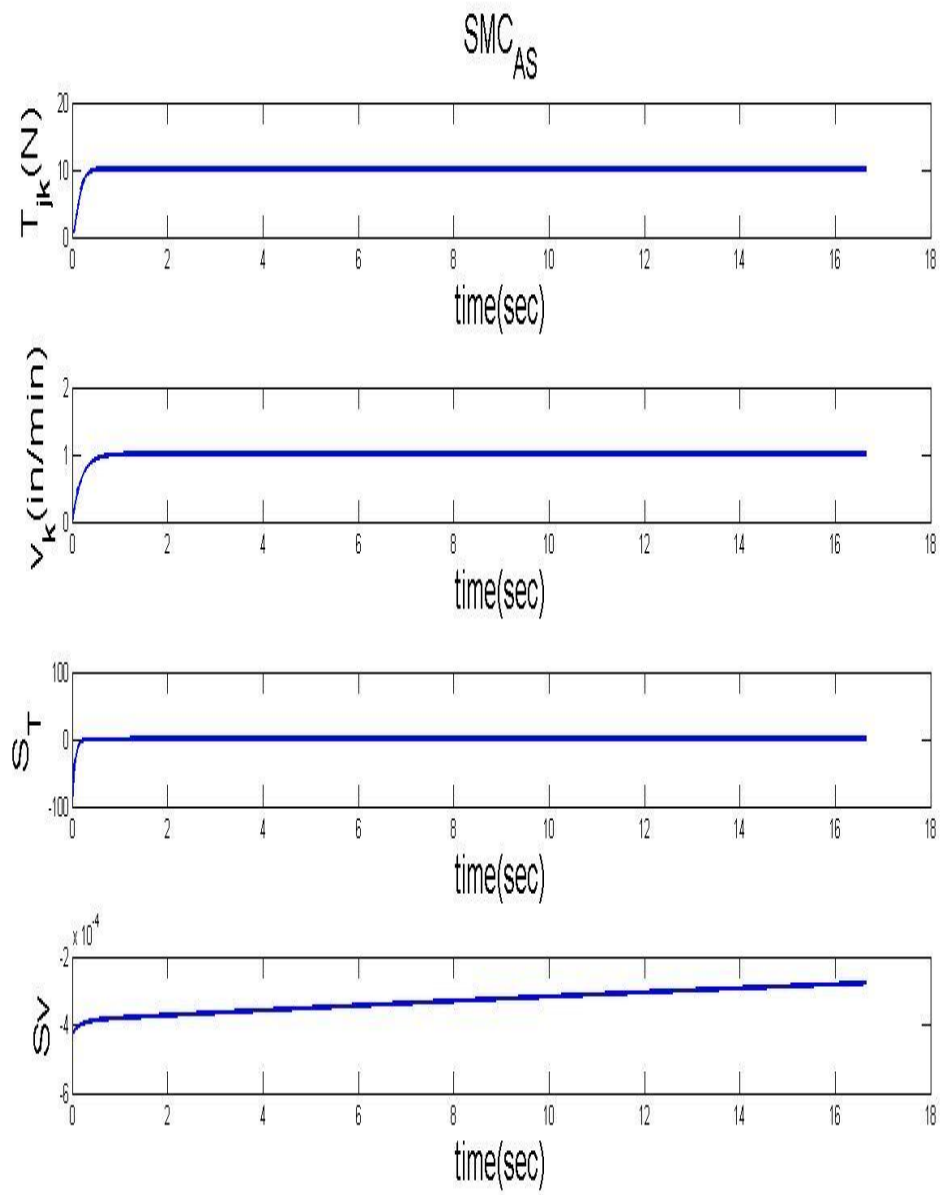


Fig. 5.17 Performance of  $SMC_{AS}$  (10 N tension, 1 in/min transporting velocity)

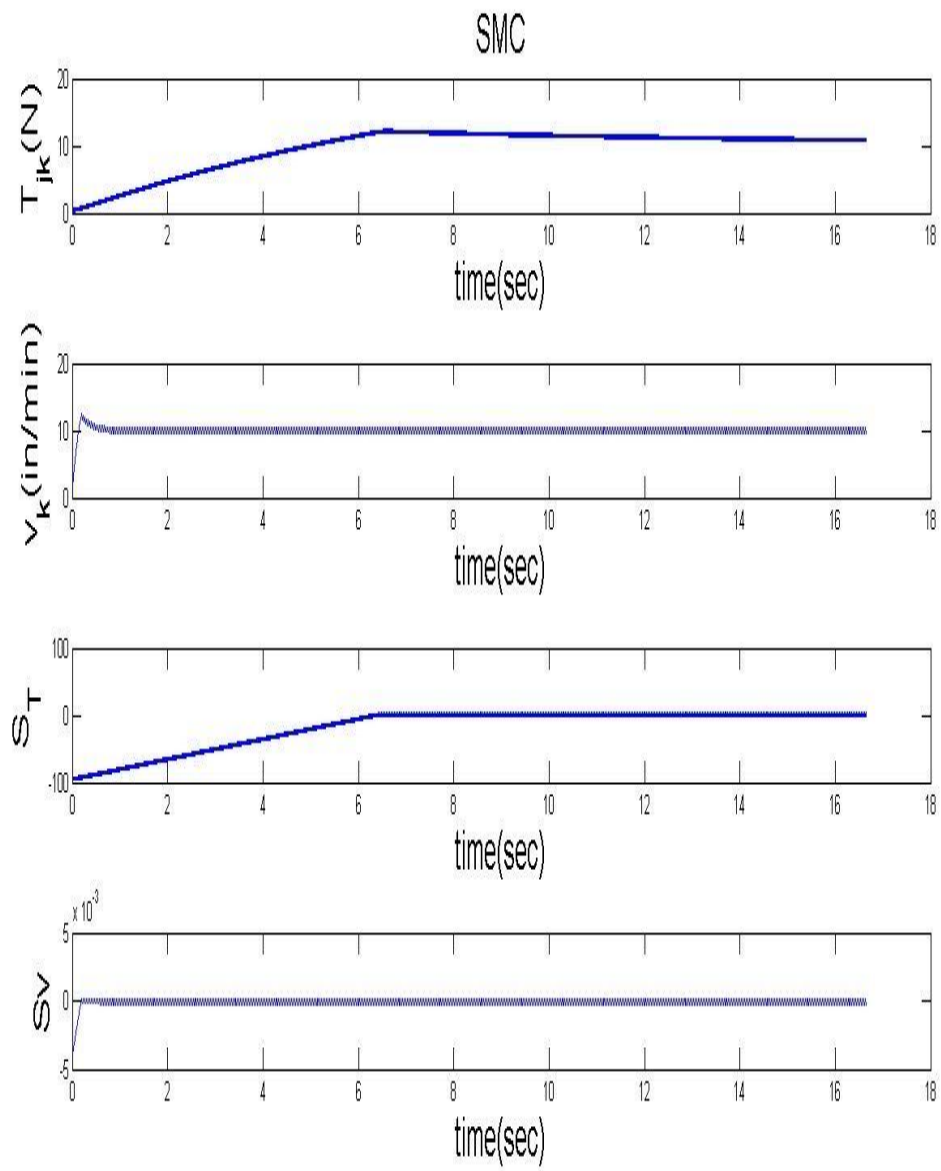


Fig. 5.18 Performance of SMC (10 N tension, 10 in/min transporting velocity)

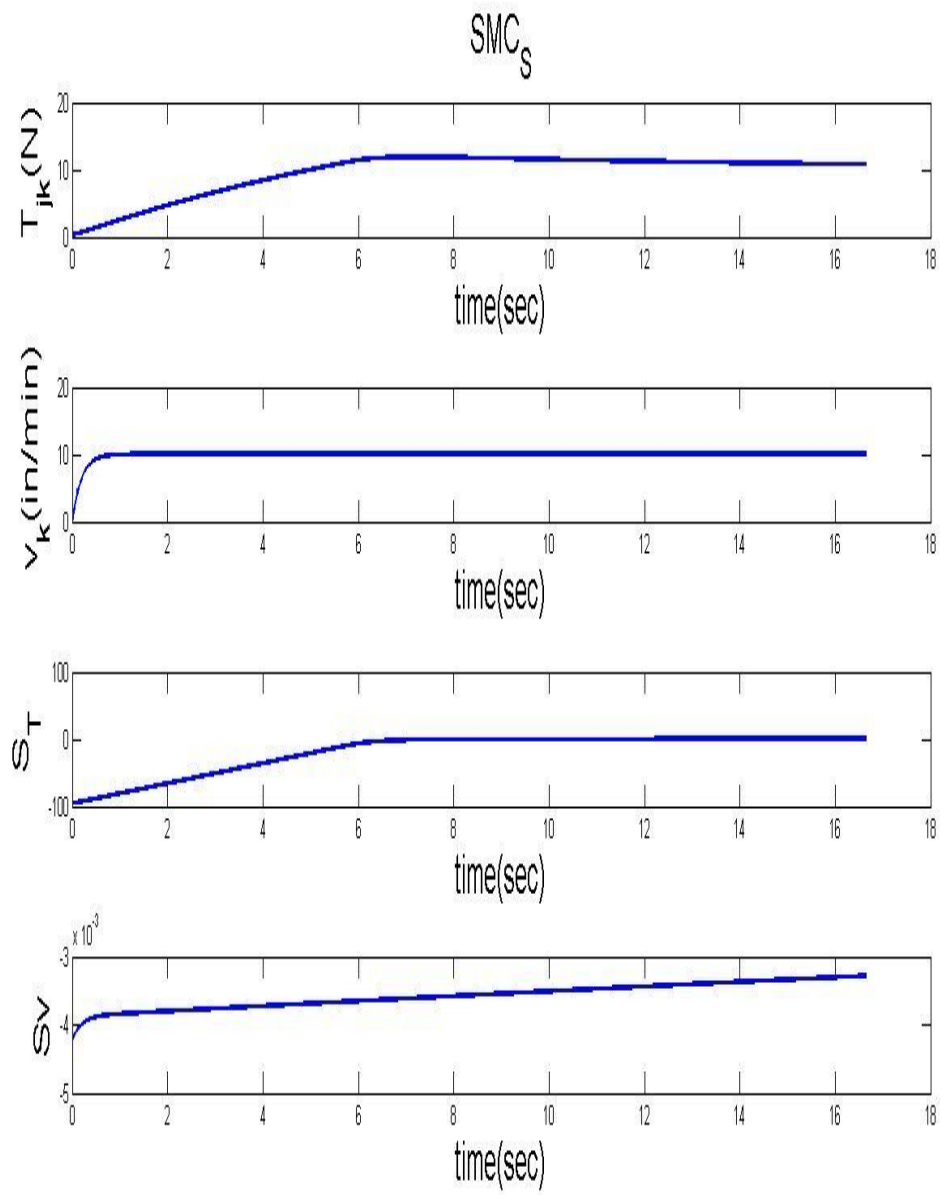


Fig. 5.19 Performance of  $SMC_S$  (10 N tension, 10 in/min transporting velocity)

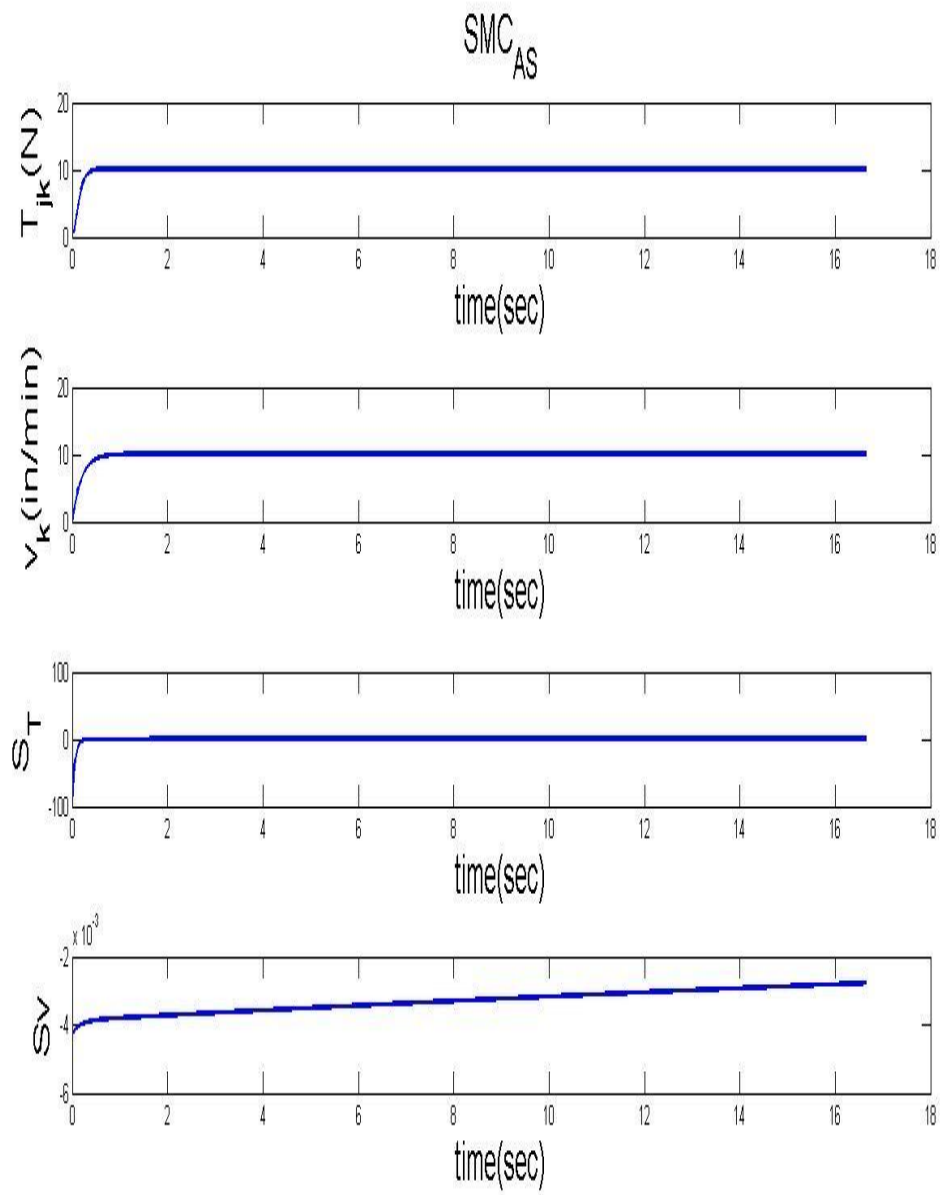


Fig. 5.20 Performance of  $SMC_{AS}$  (10 N tension, 10 in/min transporting velocity)

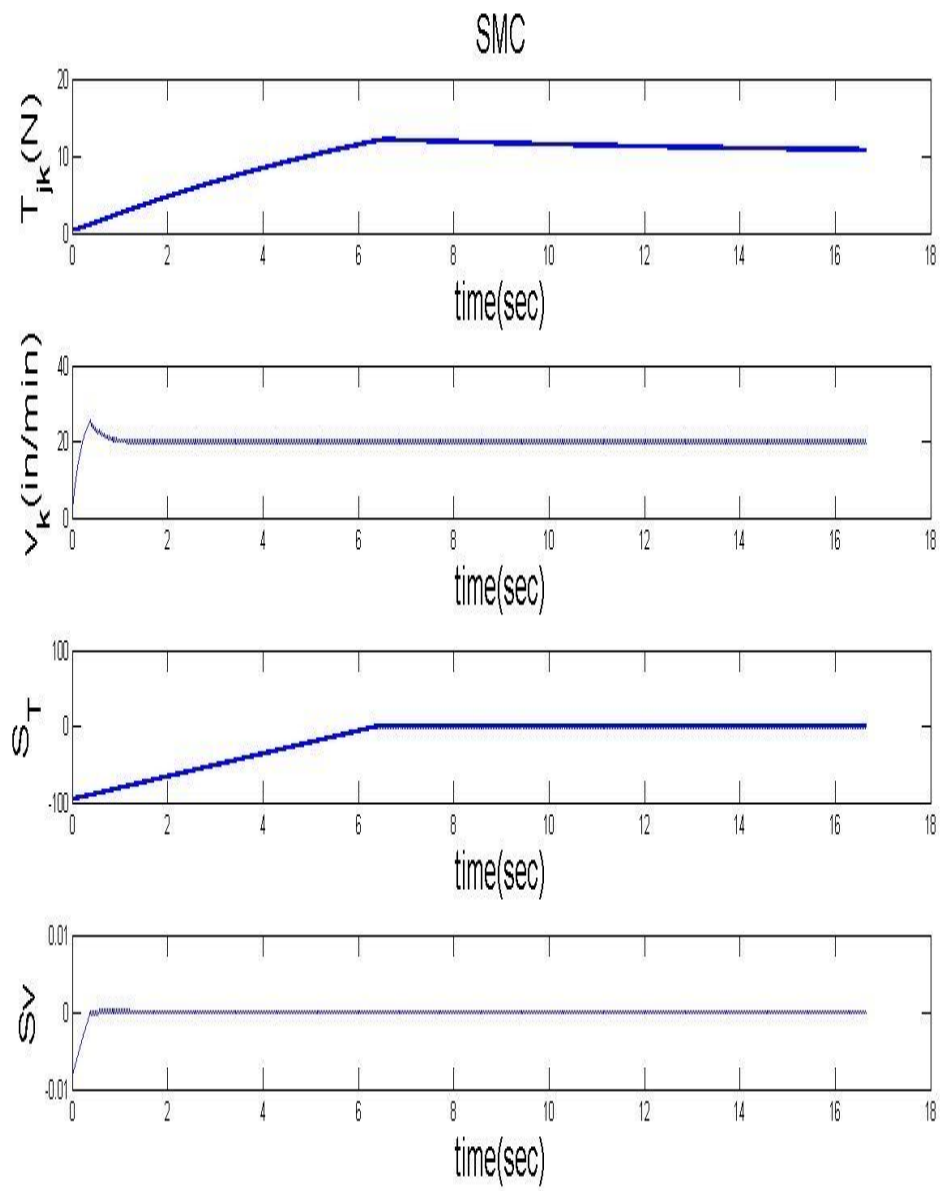


Fig. 5.21 Performance of SMC (10 N tension, 20 in/min transporting velocity)

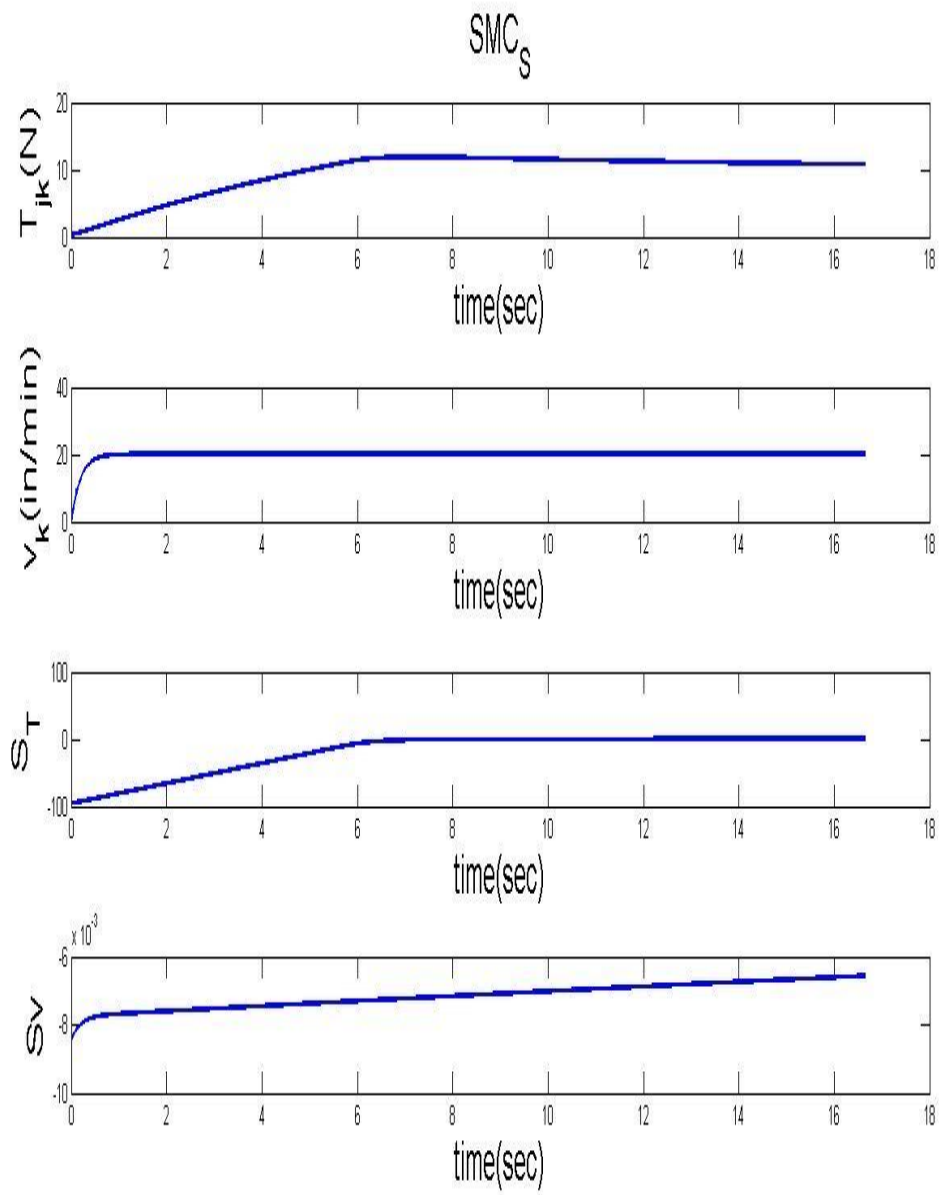


Fig. 5.22 Performance of  $SMC_S$  (10 N tension, 20 in/min transporting velocity)

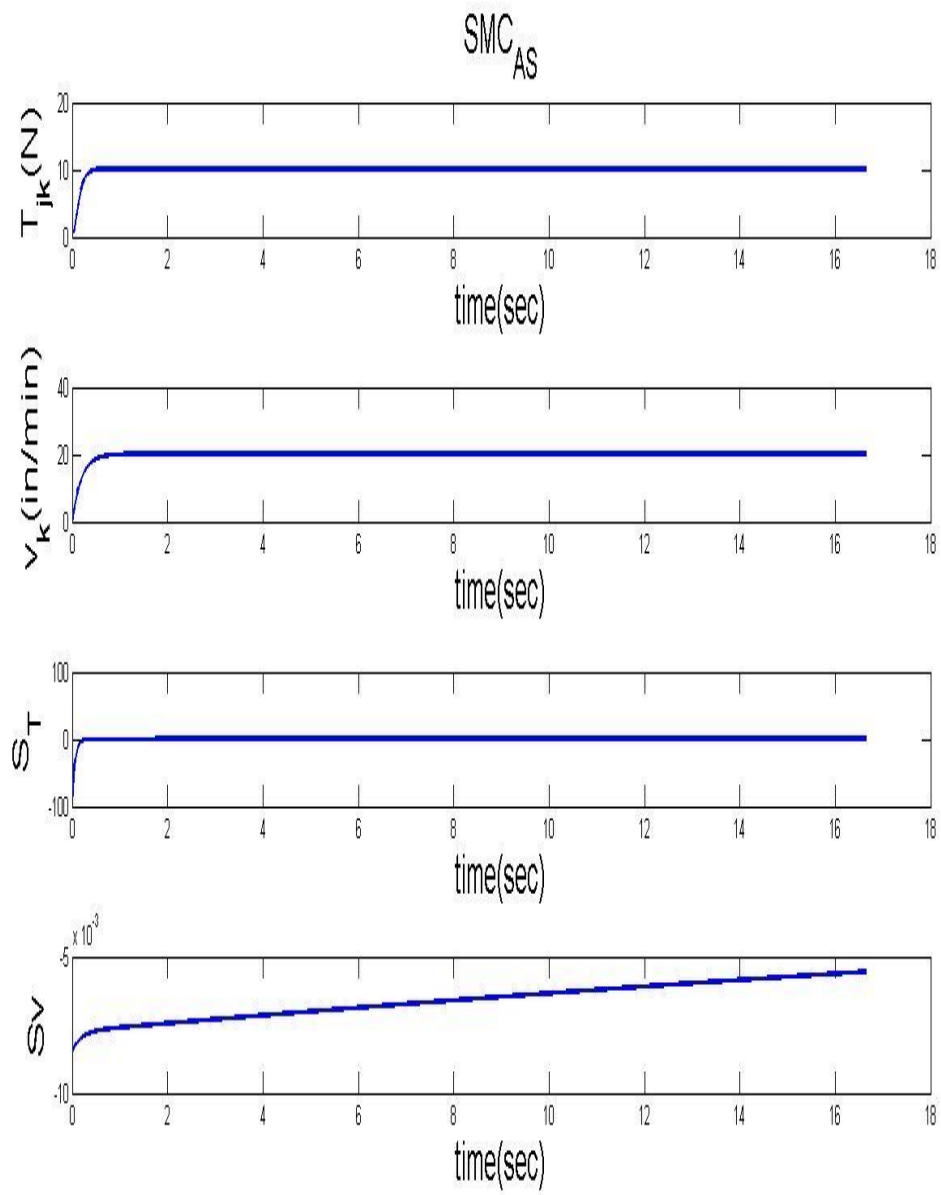


Fig. 5.23 Performance of  $SMC_{AS}$  (10 N tension, 20 in/min transporting velocity)

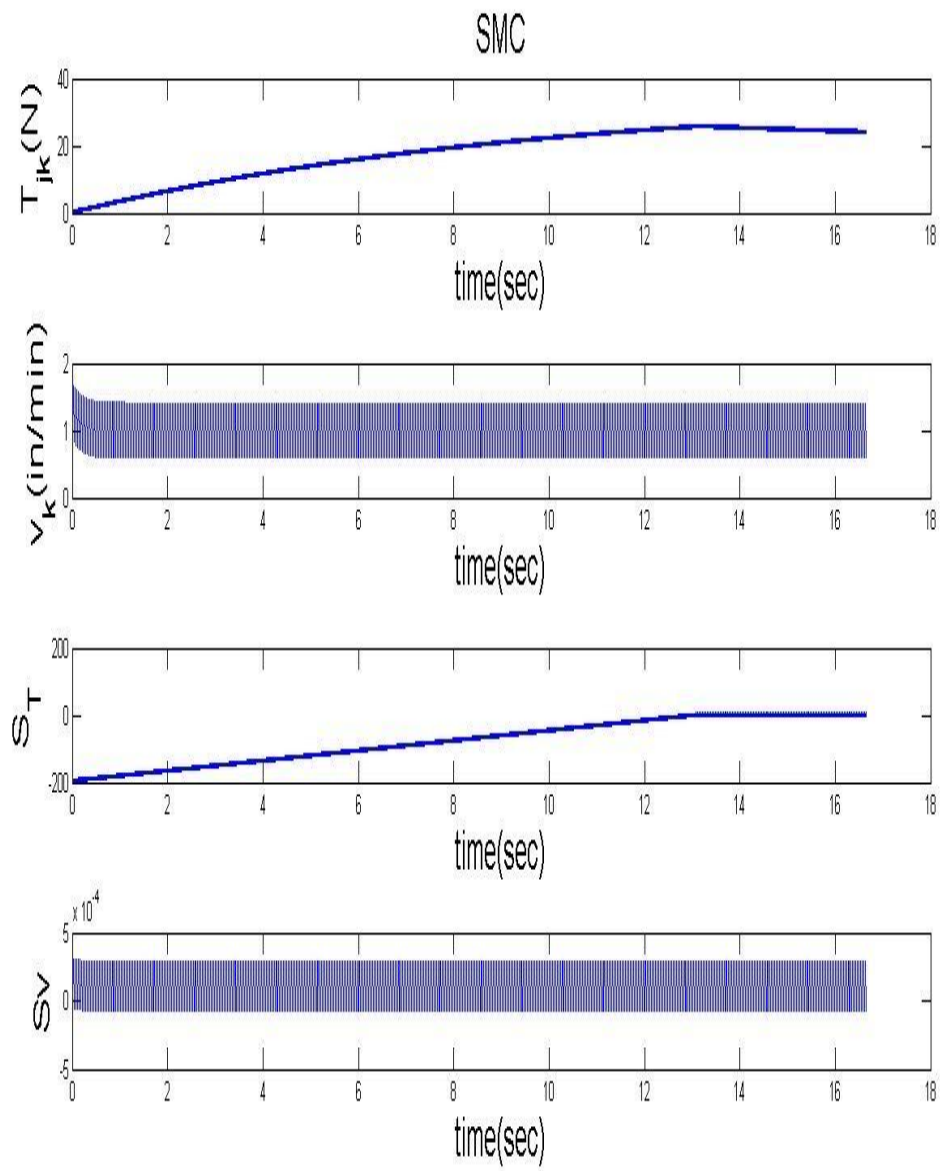


Fig. 5.24 Performance of SMC (20 N tension, 1 in/min transporting velocity)



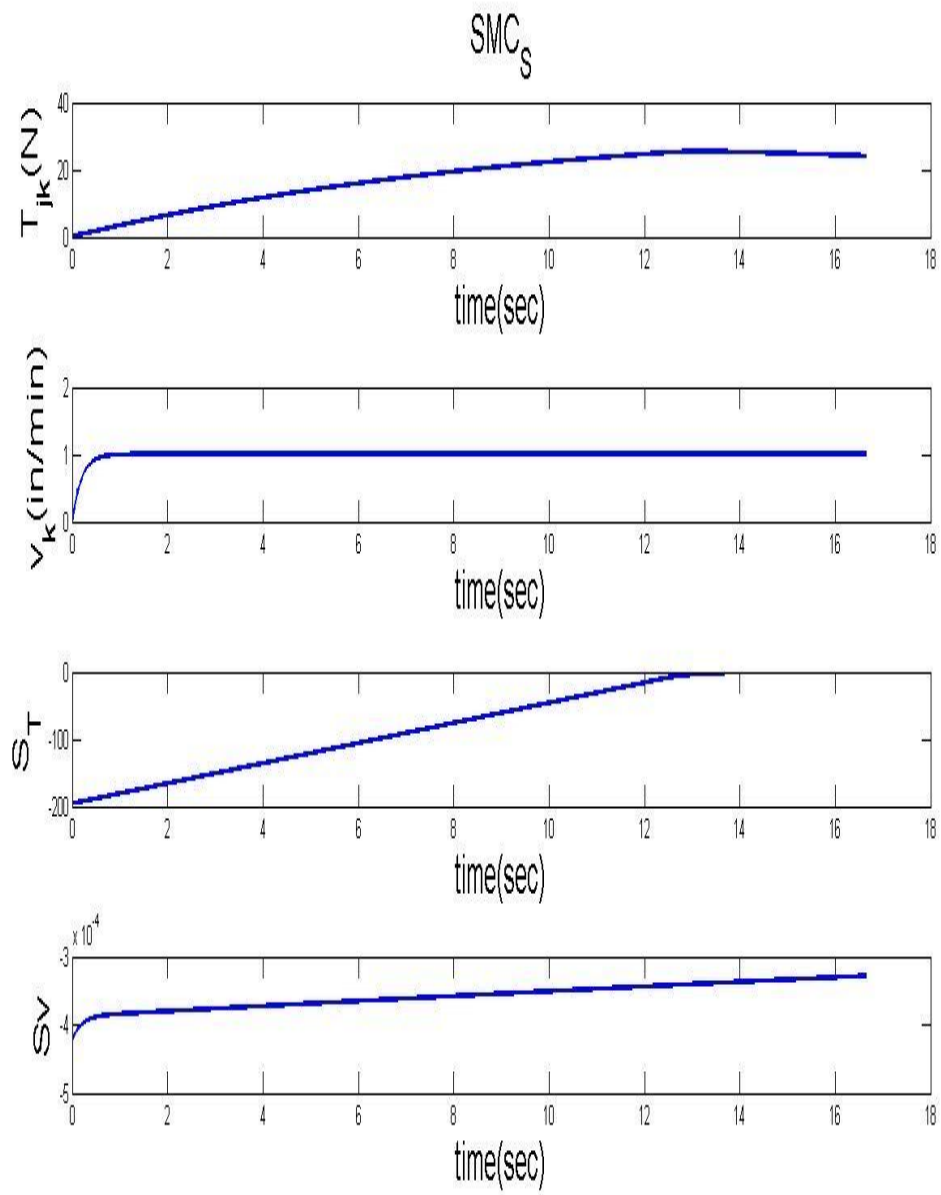


Fig. 5.25 Performance of  $SMC_S$  (20 N tension, 1 in/min transporting velocity)

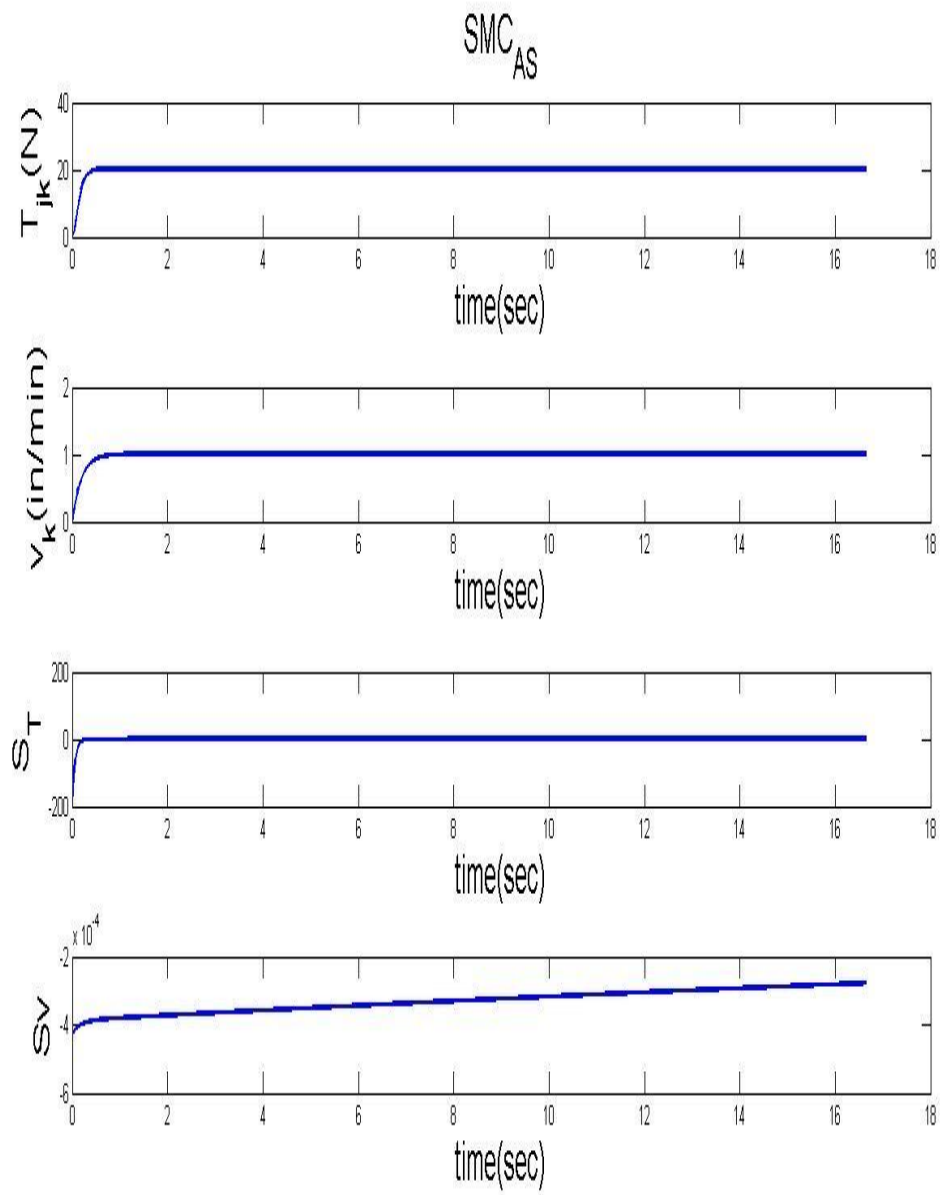


Fig. 5.26 Performance of  $SMC_{AS}$  (20 N tension, 1 in/min transporting velocity)

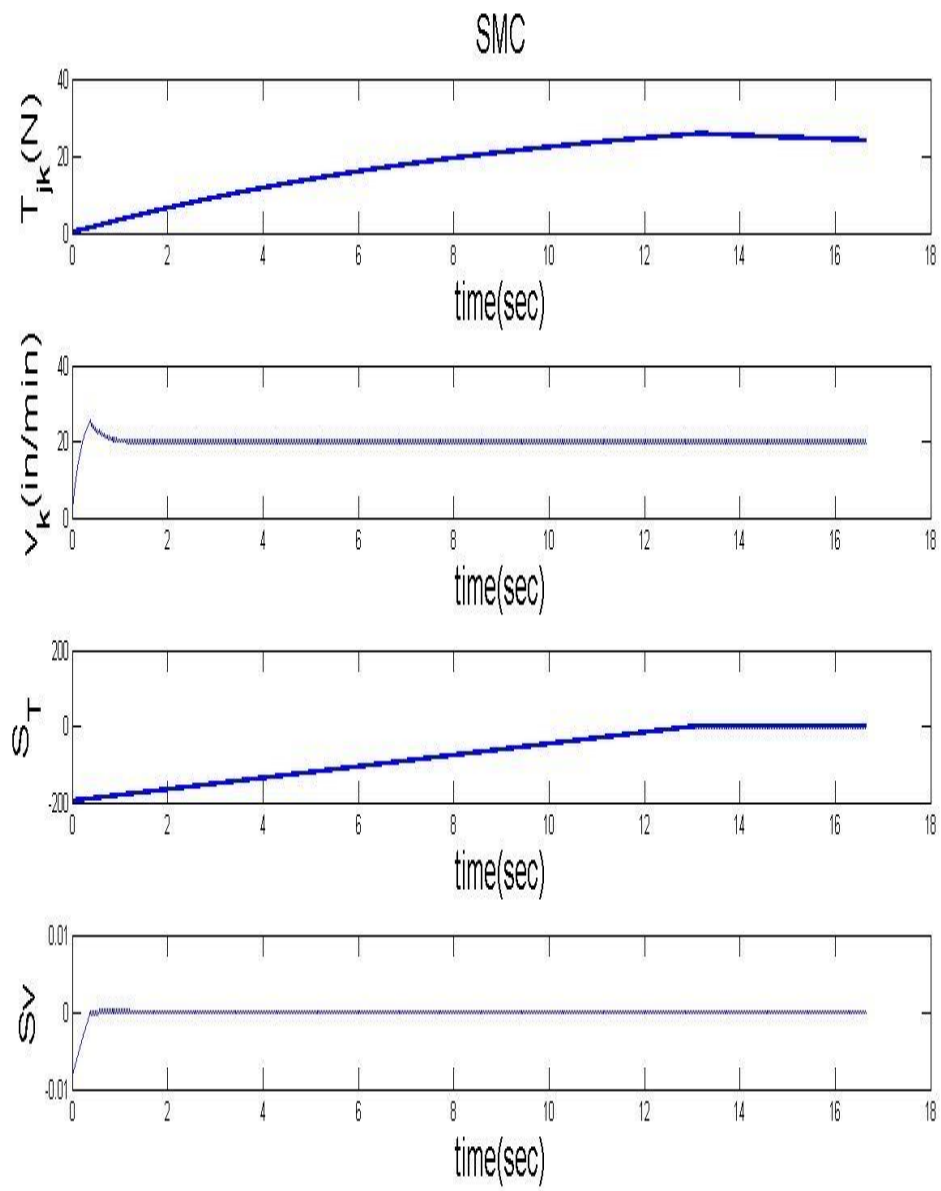


Fig. 5.27 Performance of SMC (20 N tension, 20 in/min transporting velocity)

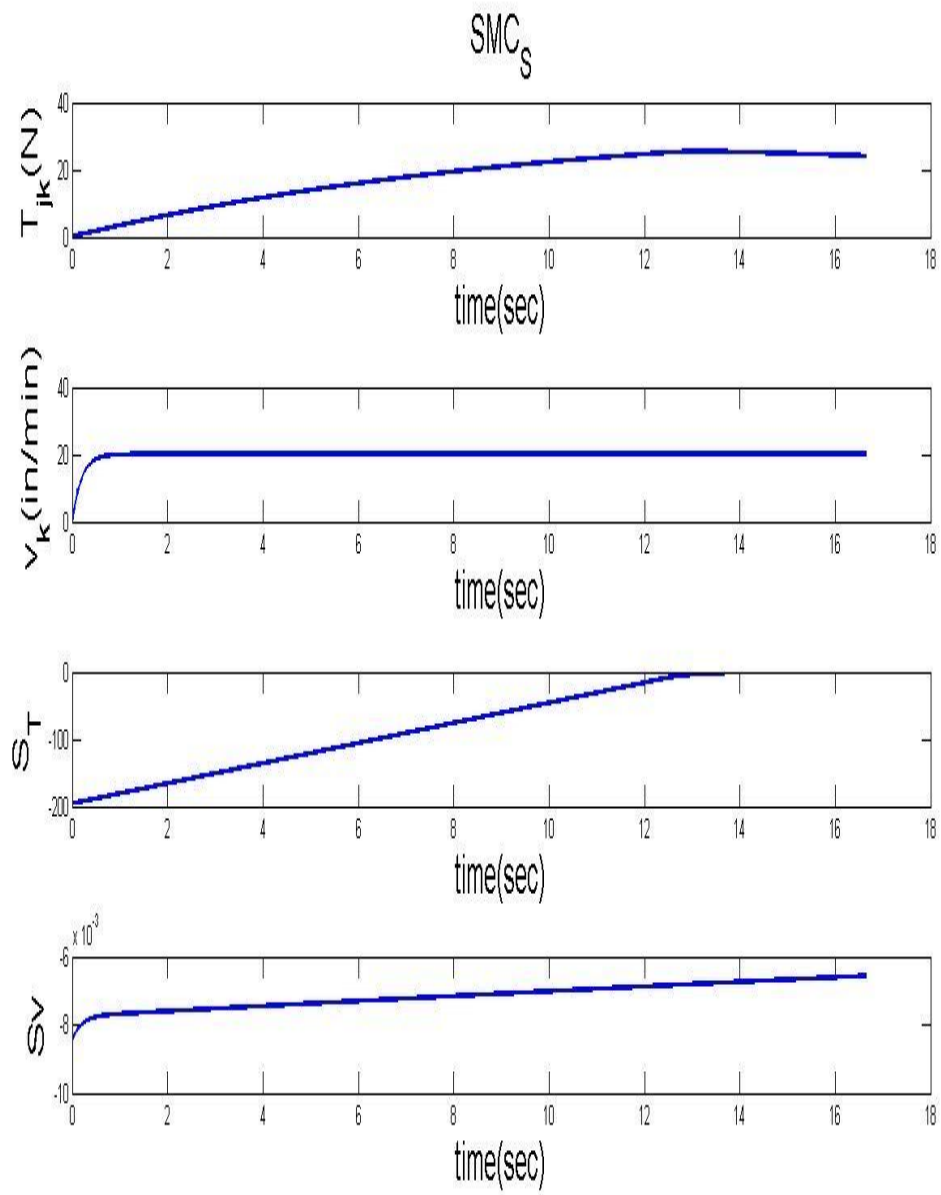


Fig. 5.28 Performance of  $SMC_S$  (20 N tension, 20 in/min transporting velocity)

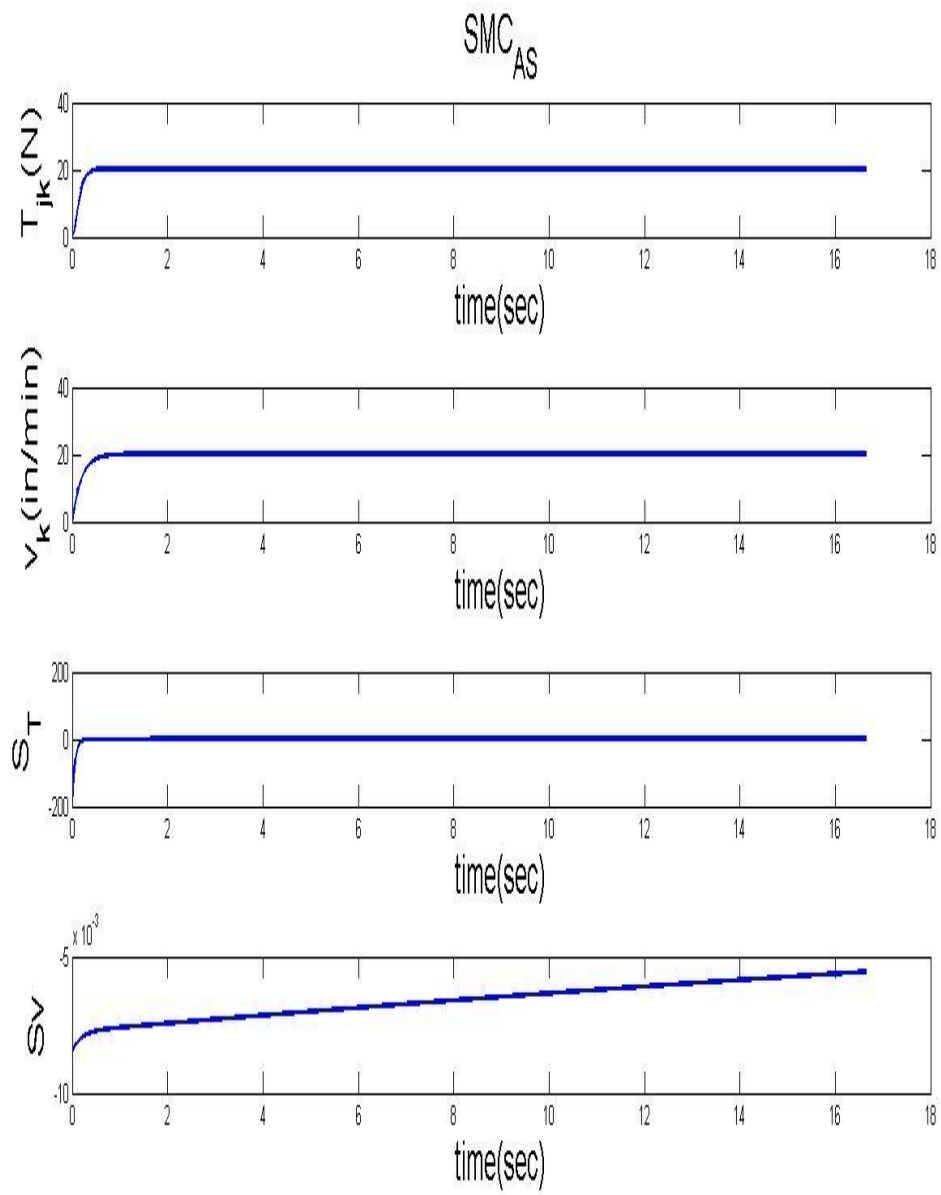


Fig. 5.29 Performance of  $SMC_{AS}$  (20 N tension, 20 in/min transporting velocity)

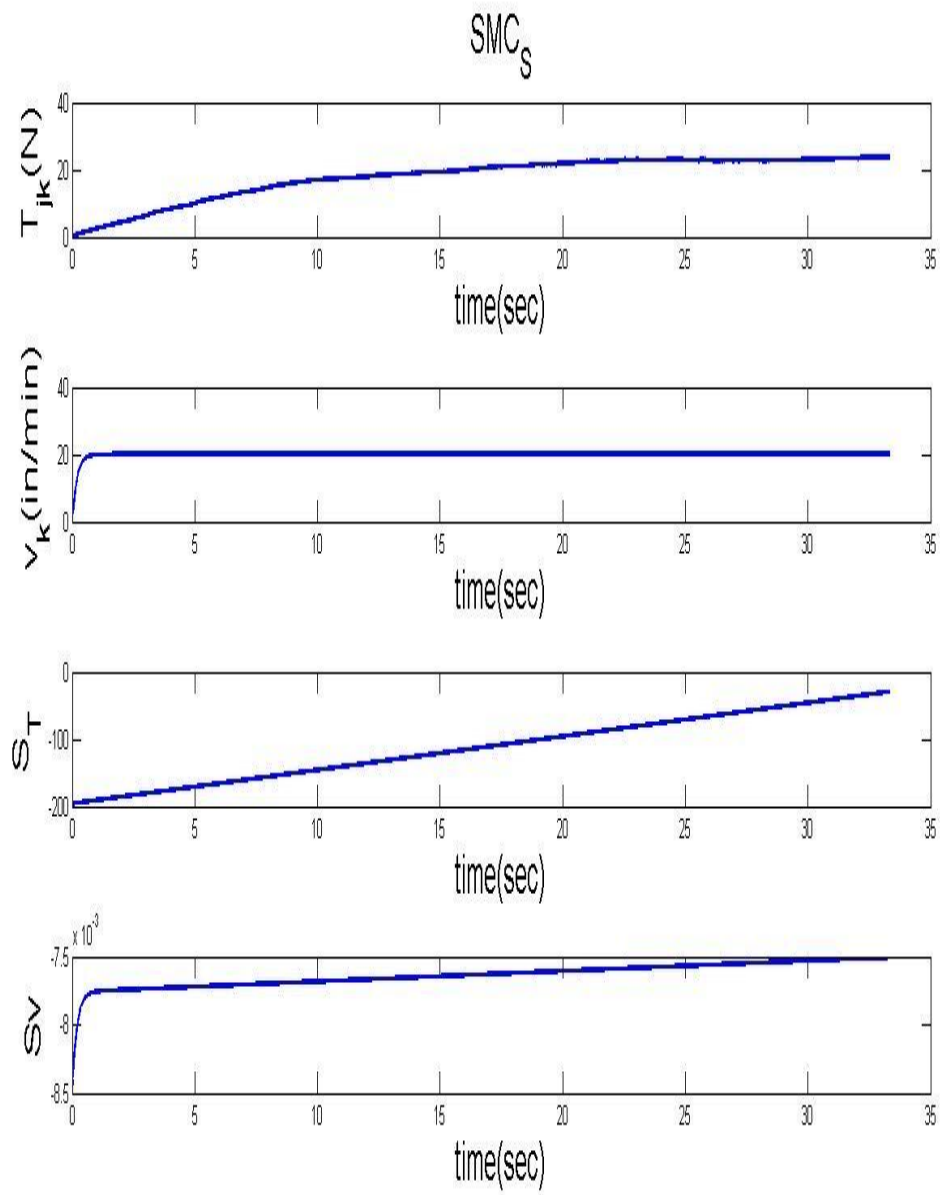


Fig. 5.30 Performance of  $SMC_S$  controller with 30 db SNR (20 N tension, 20 in/min rewinding velocity)

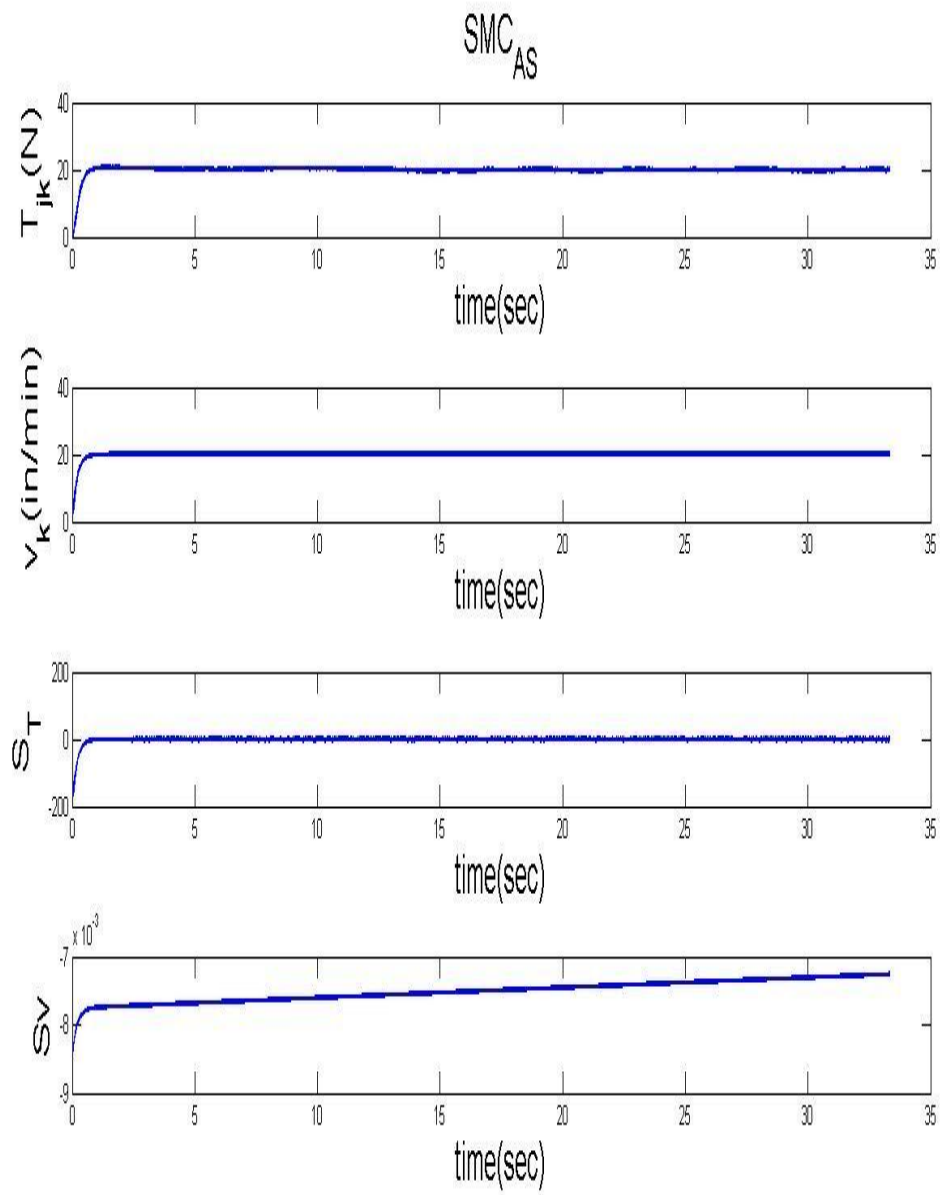


Fig. 5.31 Performance of SMC<sub>AS</sub> controller with 30 db SNR (20 N tension, 20 in/min rewinding velocity)

### 5.3 Simulation of the HDD system

As discussed previously, the main goal of the HDD system is to provide qualified products with minimum energy for the production of high quality fuel. The key for reducing energy loss is to drain as much water as possible before the wet algae enters heater. Hence, the fluid dynamics in the gravity well and capillary zone are the main concerns and key determining factors. In order to control these two factors, dominate elements such as input solution concentration, solution temperature, web tension, and web transport velocity, are required to be adjusted to achieve the goal of saving energy and providing as much dried algae as possible within the restrictions of the material, dryer system, and transport system. Fig. 5.32 is the diagram for the system, and table 5.28 provides the conditions desired for the simulation. From figs. 5.33~5.36, the simulations show that the gravity flow rate and capillary flow rate are very stable, and the energy required to produce one pound of dried algae when there exists 15 db snr white noises caused by web tension fluctuations. From the discussion earlier, the performance of the web tension controller is proven to be good, and it is proven that it can be used to effectively operate



the HDD system. Even as unknown effects caused by tension fluctuations are introduced to the system, the quality of the yield of algae can still be maintained. To sum up, energy requirement, and yield of dried algae can be maintained at desired levels even when low or high white Gaussian noise disturbances affect the process. Also, we observe that the performance is good for different web velocity and web tension control settings. Hence, we may conclude that the control method is appropriate for the HDD system.

**Table 5.28 Simulation cases**

	Case I	Case II	Case III	Case IV
Goals	Con = 10g/L, T = 10N, $V_w$ = 10 in/min	Con = 10 g/L, T = 10N, $V_w$ = 20 in/min	Con = 10g/L, T = 20N, $V_w$ = 10 in/min	Con = 20g/L, T = 20N, $V_w$ = 20 in/min
Tension control gain	20	20	20	20
velocity control gain	2	2	2	2

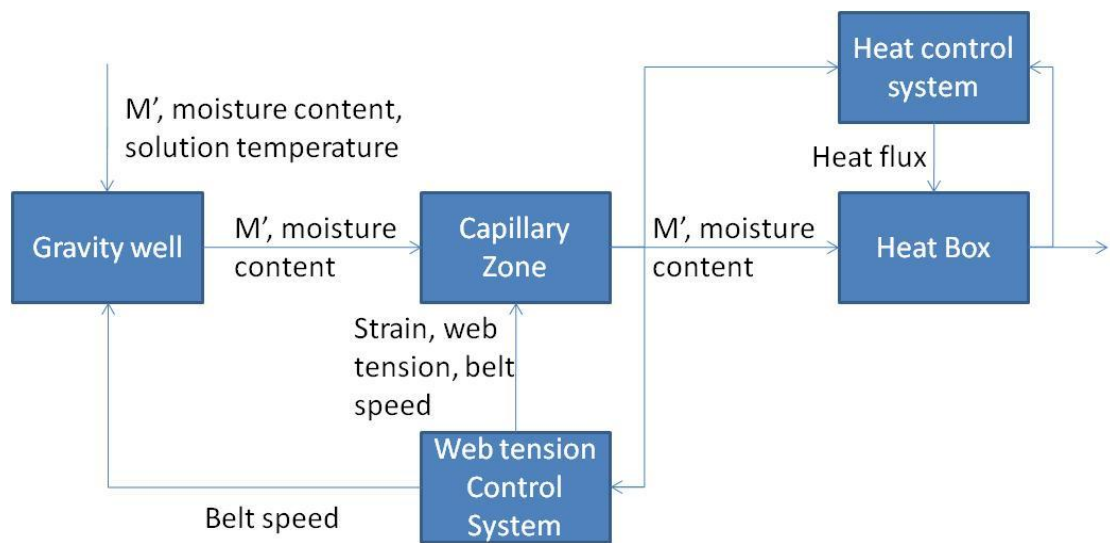


Fig. 5.32 System control module

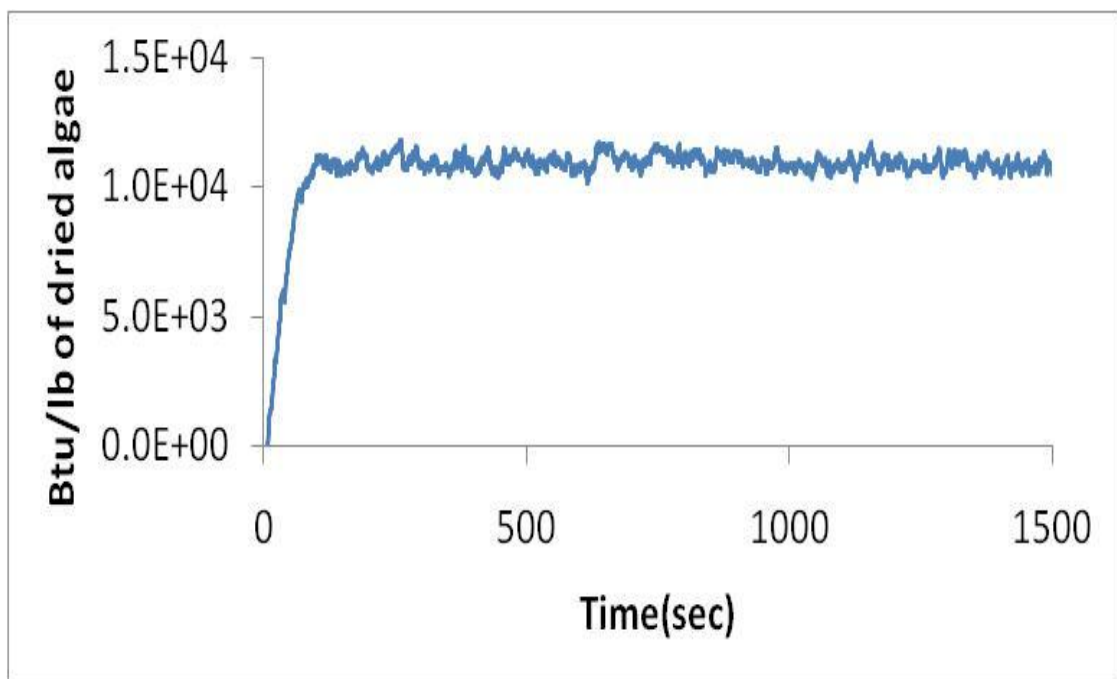


Fig. 5.33 Simulation of HDD system (10 g/L, 10 N, 10 in/min, 15 db SNR)

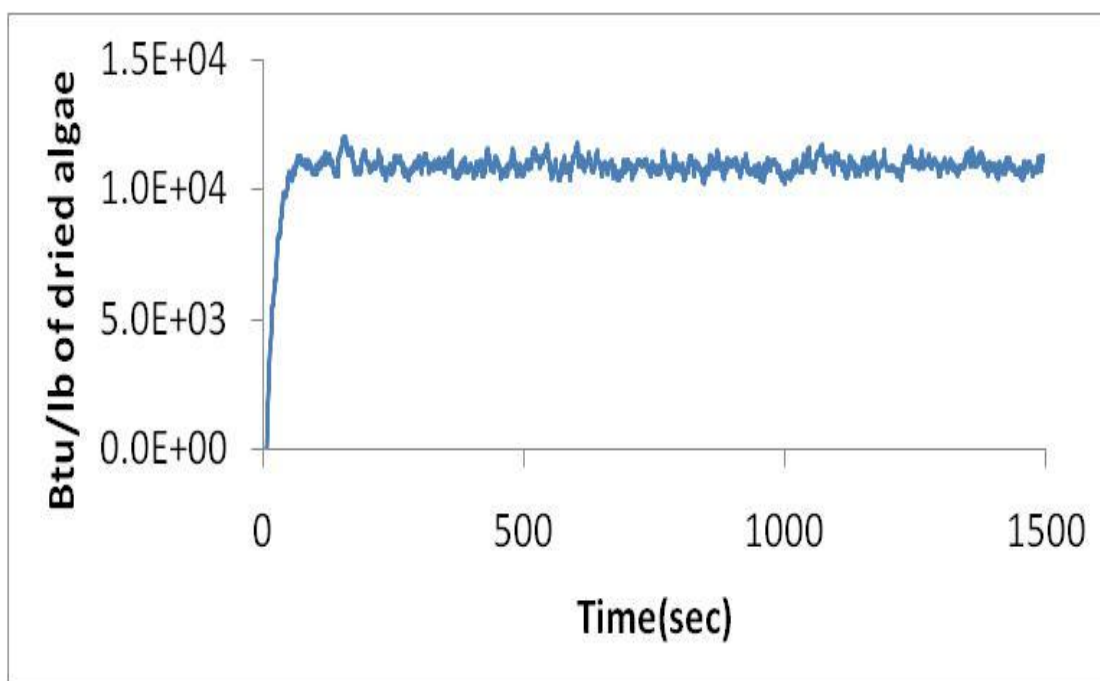


Fig. 5.34 Simulation of HDD system (10 g/L, 10N, 20 in/min, 15 db SNR)

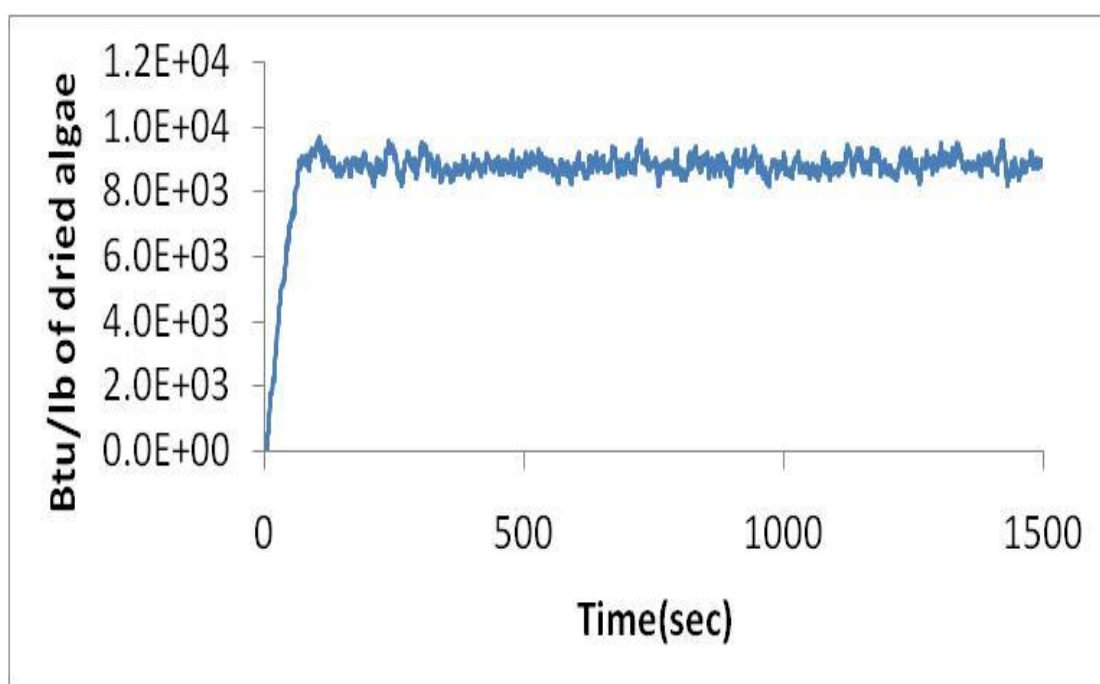


Fig. 5.35 Simulation of HDD system (10 g/L, 20N, 10 in/min, 15 db SNR)

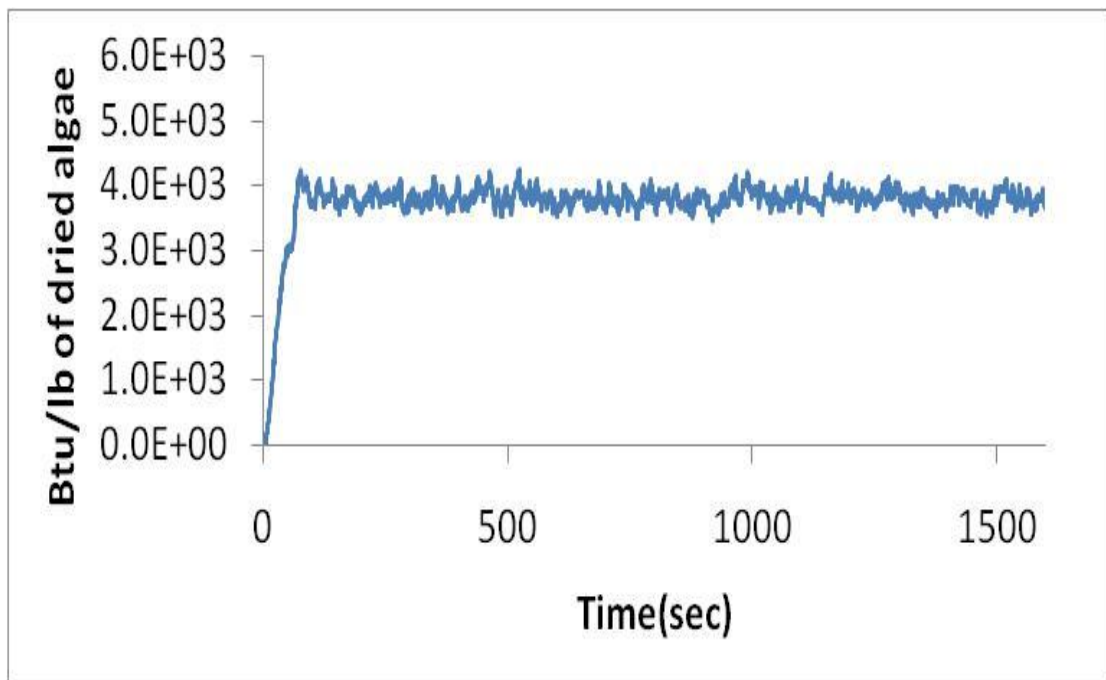


Fig. 5.36 Simulation of HDD system (20 g/L, 20N, 10 in/min, 15 db SNR)

## Chapter 6 Summary and Future work

In this thesis, a predictive model is developed for HDD system. It includes CFD modeling, roller-to-roller web tension control system, and heating control system. According to the analysis, energy efficiency and dried algae yield are highly related to the concentration of the input solution. Modulating web tension can be used to reduce the energy load of the dryer. If conditions such as dryer operating settings, web velocity limitations, restrictions on input concentration, and production cost of the input solution, and so on, can be given, the desired control settings can be determined from a lookup table. In this study, a general dryer is chosen, and the results show that the operating cost for dewatering can be reduced to around \$1.5 dollars per gallon of bio-diesel. If higher concentrations of algae can be used, the dewatering cost can be further reduced. In short, the method provided in this study offers a methodology for a company or production center to determine the most efficient operation of the harvesting system for different conditions. The lookup table for determining operating parameters of the HDD system can reduce the trial and error involved with the control of the system. In

addition, the modeling effort is an effective tool for the design, development, validation, commercialization, operation, and maintenance of the HDD system.

The predictive model has been built, and it seems that the proposed HDD system can be operated well and ride through some unexpected disturbances, although the control system has not been tested in a laboratory prototype. Hence, experiments on the HDD system prototype should be done in the future. Besides, the verification of scaling up the prototype equipment is required after a fully functional control system has been implemented and tested in the HDD prototype. Moreover, in order that algae can be a market replacement for petroleum, the efficiency of the production process has been maximized. Once a small-scale prototype is built and the HDD is ready to transition to a commercial product platform, the modeling tools developed in this work will also transition to an application engineering toolbox. This will serve to establish optimal system designs for new applications and to reliably establish the expected throughput, energy efficiency, product quality, operating cost and economic value. The core elements will form the basis for

an adaptive model-based control system that will permit the system to automatically respond to system changes such as belt wear, algae size variation, biomass dilution, contaminants, and other system disturbances while maintaining reliable and efficient production levels. In addition, information obtained from comparing the simulation model with real-world system performance will provide an effective real-time diagnostic tool that will be used to pinpoint system components or processes that are degrading or beginning to fail. If the overall production cost can be reduced to 100 USD/bbl, algae-based fuel has the potential to be a competitive alternative to fossil fuels.

## **Bibliography**

- [1] International Energy Agency. <http://www.iea.org/>
- [2] <http://images.google.com>
- [3] IPCC AR4 WG1, S. Solomon, D. Qin, M. Manning, Z. Chen, M. Marquis, K.B. Averyt, M. Tignor and H.L. Miller (eds.). Climate Change 2007: The Physical Science Basis. Contribution of Working Group I to the Fourth Assessment Report of the Intergovernmental Panel on Climate Change. Cambridge University Press, Cambridge, United Kingdom and New York, NY, USA, 2007
- [4] M.L. Parry, O.F. Canziani, J.P. Palutikof, P.J. van der Linden and C.E. Hanson, Eds. Climate Change 2007: Impacts, Adaptation and Vulnerability. Contribution of Working Group II to the Fourth Assessment Report of the Intergovernmental Panel on Climate Change. Cambridge University Press, Cambridge, United Kingdom and New York, NY, USA, 2007
- [5] Puppen, D. Environmental evaluation of biofuels. Periodica Polytechnica Ser Soc Man Sci 10:95-116 , 2002
- [6] Demirbas, A., Arin, G. An overview of biomass pyrolysis. Energy Sour 5:471–482, 2002
- [7] Ma, F., Hanna, M.A. Biodiesel production: a review. Biores Technol 70:1–15, 1999



- [8] Xu, H., Miao, X., Wu, Q. High quality biodiesel production from a microalga *Chlorella protothecoides* by heterotrophic growth in fermenters. *J Biotechnol* 126:499–507, 2006
- [9] Acièn Fernández F-G, García Camacho F, Sánchez Pérez J-A, Fernández Sevilla J-M, Molina Grima E. Modeling of biomass productivity in tubular photobioreactors for microalgal cultures: effects of dilution rate, tube diameter, and solar irradiance. *Biotechnol Bioeng* 58(6):605–616, 1998
- [10] Ben-Amotz A. Biofuel and CO<sub>2</sub> capture by algae. Paper presented at the Algae Biomass Summit, San Francisco, 15 Nov 2007
- [11] Goldman J. Outdoor algal mass cultures—II. Photosynthetic yield limitations. *Water Res* 13:119–136, 1979
- [12] Huntley M, Redalje D. CO<sub>2</sub> mitigation and renewable oil from photosynthetic microbes: a new appraisal. *Mitig Adapt Strategies Glob Chang* 12(4):573–608, 2006
- [13] Sheehan J, Dunahay T, Benemann J, Roessler P. Look back at the U.S. Department of Energy's Aquatic Species Program: biodiesel from algae; Close-Out Report. NREL Report No. TP-580-24190, 1998
- [14] Leonard BP. A stable and accurate convective modeling procedure based on quadratic upstream interpolation. *Comput Methods Appl Mech Eng* 19:59-98, 1979
- [15] Courant R, Isaacson E, Reeves M. On the solution of nonlinear hyperbolic

differential equations by finite differences. Comm Pure and Applied Mathematics 5:243-255, 1952

- [16] Fluent Inc. Fluent 6.3 user's guide. Fluent 2006
- [17] A. M. AL Jarrah. Phase Distribution of nearly equal density Solid-Liquid two phase flow in a horizontal pipe: Experimental and Modeling. Journal of Mathematics and Technology 2(1): 78-82, 2011
- [18] M. Ishii, K. Mishima. Two-fluid model and hydraulic constitutive relations. Nucl. Eng. Design 28: 107-126, 1984
- [19] M. Ishii, N. Zuber. Drag coefficient and relative velocity in bubbly, droplet or particulate flows. AIChE J. 25: 843-858, 1979
- [20] D. A. Drew, R. T. Jr Lahey. The virtual mass and lift force on a sphere in rotating and straining inviscid flow. Int. J. Multiphase Flow 13: 113-121, 1987
- [21] J. U. Brackbill, D. B. Kothe, C. Zemach, A continuum method for modeling surface tension. Journal of Computational Physics 100(2):335-354, 1992
- [22] D. Jamet, D. Torres, J. U. Brackbill, On the theory and computation of surface tension: The elimination of parasitic currents through energy conservation in the second-gradient method. Journal of Computational Physics 182(1):262-276, 2002
- [23] Van Doormal JP, Raithby GD. Enhancement of the SIMPLE Method for Predicting Incompressible Fluid Flows. Numer Heat Transfer 7:147-163, 1984

- [24] L. Hageman, D. Young, Applied iterative methods. New York: Academic Press, 1981
- [25] J. D. Anderson. Computational Fluid Dynamics: The Basics with Applications. McGraw Hill, 1995
- [26] Patankar SV. Numerical heat transfer and fluid flow. Hemisphere publishing corporation, New York, 1980
- [27] Versteeg HK, Malalasekera W. An Introduction to Computational Fluid Dynamics: The Finite Volume Method. Longman. Harlow, 1996
- [28] Versteeg HK, Malalasekera W. An Introduction to Computational Fluid Dynamics: The Finite Volume Method. Pearson Prentice Hall. Harlow, 2007
- [29] Roache PJ. Fundamentals of Computational Fluid Dynamics. Hermosa Publishers, New Mexico, 1998
- [30] Ferziger JH, Peric M. Computational Methods for Fluid Dynamics, Springer, Berlin, 1996
- [31] Schiesser WE. The Numerical Method of Lines: Integration of Partial Differential Equations. Academic Press, San Diego, 1991
- [32] Jakobsen HA. Numerical Convection Algorithms and Their Role in Eulerian CFD Reactor Simulations. International Journal of Chemical Reactor Engineering A1:1-15, 2003
- [33] Patankar SV, Spalding DB. A Calculation Procedure for Heat, Mass and

- Momentum Transfer in Three-Dimensional Parabolic Flows. *Int J Heat Mass Transfer* 15:1787-1806, 1972
- [34] Carver MB. Numerical Computation of Phase Separation in Two Fluid Flow. *J Fluids Eng* 106:147-153, 1967
- [35] Chorin AJ. A numerical method for solving incompressible viscous flow problems. *J Comput Phys* 2:12-26, 1967
- [36] Chorin AJ. Numerical solution of the Navier-Stokes equations. *Math Comp* 22:745-762, 1968
- [37] Felten FN, Lund TS. Kinetic energy conservation issues associated with the collocated mesh scheme for incompressible flow. *J Comput Phys* 215:465-484, 2006
- [38] Harlow FH, Welch JE. Numerical Calculation of Time-Dependent Viscous Incompressible Flow of Fluid with Free Surface. *Physics and Fluids* 8:2182-218, 1965
- [39] G. E. Young and K. N. Reid, Lateral and Longitude Dynamic Behavior and Control of Moving Webs. *Journal of Dynamic Systems Measurement and Control* 115:309-317, 1993
- [40] Mathur, P. D. and Messener, W. C. Controller Development for a Prototype High-Speed Low-Tension Tape Transport. *IEEE Transactions on Control Systems Technology* 6:534-542, 1998

- [41] K. C. Lin, "Observed-Based Tension Feedback control with Friction and Inertia Compensation". IEEE Transactions on Control Systems Technology 11(1): 109-118, 2003
- [42] H. Koc, D. Knittel, M. D. Mathlin, and G. Abba, Modeling and Robust Control of Winding Systems for Elastic Webs. IEEE Transactions on Control System Technology 10(2):197-208, 2002
- [43] J. J. Slotine and W. Li, Applied Nonlinear Control. Englewood Cliffs, NJ: Prentic-Hall, 1991
- [44] V.I. Utkin. Variable structure systems with sliding modes: A survey. IEEE Trans. Automatic Contr. 22:212-222, 1977